ACTA UNIVERSITATIS SZEGEDIENSIS

ACTA PHYSICA ET CHEMICA

NOVA SERIES

TOMUS XXI FASCICULI 3—4

AUSHAF 21(3—4) 85—196 (1975)

HU ISSN 0001—6721

SZEGED, HUNGARIA

1975

ACTA UNIVERSITATIS SZEGEDIENSIS

ACTA PHYSICA ET CHEMICA

NOVA SERIES

TOMUS XXI FASCICULI 3—4

AUSHAF 21 (3—4) 85—196 (1975)
HU ISSN 0001—6721

SZEGED, HUNGARIA
1975

LFMO TREATMENT OF BINUCLEAR COBALT COMPLEXES

By

V. MARÁZ

Institute of Theoretical Physics, Attila József University, Szeged

(Received July 10, 1975)

In this paper the energy levels and electron transitions of the $[(NH_3)_4Co(OH)_2Co(NH_3)_4]^{4+}$ and $[(NH_3)_3Co(OH)_3Co(NH_3)_3]^{3+}$ binuclear complex ions are calculated by the LFMO method (ligand field method combined with LCAO-MO method).

Introduction

As well known, the ligand field (LF) method (BETHE [1], VAN VLECK [2]) is a fairly good approximation for the interpretation of some important properties of complex compounds having only one central metal ion. As known, this method treats the ligands as point charges or point electric dipoles and considers the electrons of the central metal ions as if they were subjected to an electric field originating from the surrounding atoms or molecules.

Since the first application of the LF method [2] many authors dealt with this method and employed it to calculate the electronic structure, transitions, magnetic properties etc. of such complexes, and several excellent books have been published on this topic. (ILSE and HARTMANN [3], BALLHAUSEN [4], JØRGENSEN [5], GRIFFITH [6], ORGEL [7], MOFFITT [8], LIEHR [9], TANABE and SUGANO [10], KISS [11], GILDE and BÁN [12] etc.)

It is evident that the LF method cannot be applied in itself in the case of polynuclear complexes, but the basic idea of the method is applicable in this case, too, if we combine this method with other methods, for example the LCAO-MO method. In the following we call this method LFMO method and we treat the binuclear complex ions $[(NH_3)_4Co(OH)_2Co(NH_3)_4]^{4+}$ and $[(NH_3)_3Co(OH)_3Co(NH_3)_3]^{3+}$ (denoted in the following by K_1 and K_2, respectively) by this method.

Geometries and method of calculation

We assume that the geometry of the complex ions K_1 and K_2 is "bi-octahedral": the two octahedra have in the case of K_1 a common edge and in the case of K_2 a common face, and on the basis of Pauling's ions radii [13] we take the nuclear distance Co—O to be 1.88 Å, Co—N 1.92 Å and Co—Co 2.66 Å for both complexes. The symmetry of these systems is $D_{2h}(K_1)$ and $D_{3h}(K_2)$.

In the present paper we treat these complex ions by the LFMO method: (1) because of the undoubted importance of the bridges we treat the compounds $Co(OH)_2Co$ and $Co(OH)_3$ Co by the LCAO-MO method (zeroth order problems), (2) then, we take into account the NH_3 molecules as point electric dipoles (having 1.48 Debye dipole moment) setting up an electrostatic field around the central compounds. After K. Jørgensen [5] we call this field "ligand field".

Zeroth order problems

In the LCAO—MO treatment of $Co(OH)_2Co$ and $Co(OH)_3Co$ we neglect the influences of the H atoms on the compounds and we do not take into account the electrons in the closed shells of Co and O atoms. We take into account only the six valence electrons of the Co ions and the four valence electrons of the OH ions (20 electrons for K_1 and 24 electrons for K_2). For the calculation of MO-s we take into account the five 3d, one 4s and three 4p atomic orbitals of Co atoms and the three 2p orbitals of O atoms and we represent these atomic orbitals by Slater type orbitals.

Table I (K_1)

	Co	O
A_{1g}	$d_{z^2}(1)+d_{z^2}(2)$ $d_{x^2-y^2}(1)+d_{x^2-y^2}(2)$ $s(1)+s(2)$ $p_z(1)+p_z(2)$	$p_x(1)+p_y(1)+p_x(2)+p_y(2)$
A_{1u}	$d_{xy}(1)+d_{xy}(2)$	
B_{1g}	$d_{xy}(1)-d_{xy}(2)$	$p_z(1)+p_z(2)$
B_{1u}	$d_{z^2}(1)-d_{z^2}(2)$ $d_{x^2-y^2}(1)-d_{x^2-y^2}(2)$ $s(1)-s(2)$ $p_z(1)-p_z(2)$	$-p_x(1)+p_y(1)-p_x(2)+p_y(2)$
B_{2g}	$d_{xz}(1)-d_{xz}(2)$ $p_x(1)-p_x(2)$	$-p_x(1)+p_y(1)+p_x(2)-p_y(2)$
B_{2u}	$d_{yz}(1)-d_{yz}(2)$ $p_y(1)-p_y(2)$	$p_z(1)-p_z(2)$
B_{3g}	$d_{yz}(1)+d_{yz}(2)$ $p_y(1)+p_y(2)$	
B_{3u}	$d_{xz}(1)+d_{xz}(2)$ $p_x(1)+p_x(2)$	$p_x(1)+p_y(1)-p_x(2)-p_y(2)$

From these atomic orbitals we can easily construct symmetry adapted functions transforming according to the irreducible representations of D_{2h} and D_{3h} using group theoretical considerations. The reducible representations are

$$\Gamma_1 = 5A_{1g}+5B_{1u}+3B_{2g}+3B_{2u}+3B_{3u}+2B_{3g}+2B_{1g}+A_{1u}$$

$$\Gamma_2 = 5E'+4E''+4A_1'+4A_2''+A_2'.$$

The symmetry adapted functions are presented in Table I.

Table I (K_2)

	Co	O
A_1'	$d_{z^2}(1)+d_{z^2}(2)$ $s(1)+s(2)$ $p_z(1)+p_z(2)$	$p_x(1)+p_y(1)+p_x(2)+$ $+p_y(2)+p_x(3)+p_y(3)$
A_2'		$p_z(1)+p_z(2)+p_z(3)$
A_2''	$d_{z^2}(1)-d_{z^2}(2)$ $s(1)-s(2)$ $p_z(1)-p_z(2)$	$p_x(1)+p_x(2)+p_x(3)-$ $-p_y(1)-p_y(2)-p_y(3)$
E'	$d_{x^2-y^2}(1)+d_{x^2-y^2}(2)$ $d_{xz}(1)+d_{xz}(2)$ $p_x(1)+p_x(2)$	$-2p_x(1)-2p_y(1)+p_x(2)+$ $+p_y(2)+p_x(3)+p_y(3)$ $p_z(3)-p_z(2)$
	$d_{xy}(1)-d_{xy}(2)$ $d_{yz}(2)-d_{yz}(1)$ $p_y(2)-p_y(1)$	$p_x(2)+p_y(2)-p_x(3)-p_y(3)$ $p_z(2)+p_z(3)-2p_z(1)$
E''	$d_{xy}(1)+d_{xy}(2)$ $d_{yz}(1)+d_{yz}(2)$ $p_y(1)+p_y(2)$	$p_x(2)+p_y(3)-p_y(2)-p_x(3)$
	$d_{x^2-y^2}(2)-d_{x^2-y^2}(1)$ $d_{xz}(1)-d_{xz}(2)$ $p_x(1)-p_x(2)$	$2p_x(1)-2p_y(1)-$ $-p_x(2)-p_x(3)+p_y(2)+p_y(3)$

For the secular equations we calculated the group overlap integrals S_{ij} exactly, while the group integrals H_{ij} ($i \neq j$) have been determined by the approximation formula of WOLFSBERG and HELMHOLZ [14]

$$H_{ij} = 0{,}5KS_{ij}(H_{ii}+H_{jj})$$

where the empirical factor K was chosen to be 2.20 for σ bonds and 2.62 for π bonds [15]. The integrals H_{ii} were substitued by ionization potentials: in the case of Co, for 4s orbitals —7.84 eV, for 4p orbitals —4.08 eV, for 3d orbitals —9.38 eV [16] and in the case of O, for 2pσ orbitals —11.24 eV and for 2pπ orbitals —10.54 eV [17].

The energy values (in eV) and the LCAO coefficients of the normalized MO-s are summarized in Table II.

Table II (K_1)

symmetry	energy	c_1	c_2	c_3	c_4	c_5
A_{1g}	− 3.425	−0.059 138	−0.043 349	0.284 836	1.052 616	0.398 073
	− 8.208	0.665 666	0.235 770	0.522 180	0.168 007	−0.631 554
	− 9.441	−0.292 055	0.954 304	0.014 894	−0.006 985	0.057 616
	− 9.799	−0.603 264	−0.177 328	0.783 875	−0.048 049	−0.177 026
	−13.040	0.347 462	0.048 320	0.371 078	−0.119 734	0.704 611
A_{1u}	− 9.343	1				
B_{1g}	− 8.550	0.902 097	0.515 110			
	−11.843	−0.439 903	0.861 377			
B_{1u}	+40.640	−0.289 141	−0.086 190	−0.146 637	0.143 289	−0.523 670
	− 5.466	−0.108 230	0.217 003	0.485 199	0.539 337	0.357 385
	− 8.237	−0.500 138	0.741 289	−0.201 041	−0.122 941	0.409 595
	− 9.054	0.837 761	0.519 545	−0.100 773	0.033 479	0.079 291
	−12.449	0.142 542	−0.382 249	−0.160 923	−0.006 404	0.811 277
B_{2g}	+ 2.701	−0.343 684	1.023 286	0.625 703		
	− 8.175	0.873 498	0.298 007	−0.390 963		
	−12.416	0.409 138	−0.130 174	0.799 262		
B_{2u}	− 3.810	−0.075 041	0.987 295	0.468 299		
	− 8.613	0.901 800	0.202 422	−0.459 036		
	−12.432	0.439 406	−0.183 982	0.792 978		
B_{3g}	− 1.899	−0.139 556	0.999 040			
	− 9.124	0.992 223	0.076 800			
B_{3u}	− 5.264	0.148 135	0.995 703	0.014 215		
	− 7.742	0.854 178	−0.113 340	0.671 425		
	−12.230	−0.528 837	0.018 591	0.762 123		

Table II (K_2)

symmetry	energy	c_1	c_2	c_3	c_4	c_5
A_1'	− 2.470	−0.155 695	0.167 135	0.102 850	0.573 758	
	− 7.467	0.612 587	0.618 890	0.329 762	−0.617 880	
	− 9.763	0.695 179	−0.737 786	0.043 971	0.120 595	
	−13.155	0.375 006	0.394 784	−0.128 670	0.644 253	
A_2'	−11.308	1				
A_2''	+47.702	0.290 326	1.559 748	−1.492 805	−0.650 839	
	− 5.394	−0.121 404	0.491 707	0.561 751	−0.329 839	
	− 8.730	0.962 781	0.056 223	0.094 860	0.224 506	
	−12.121	−0.214 054	0.229 541	0.010 192	0.875 835	
E'	− 4.082	−0.127 224	−0.043 830	0.980 326	0.070 714	0.435 881
	− 7.772	0.150 743	0.861 337	0.162 714	−0.508 971	−0.331 774
	− 8.942	0.920 663	−0.178 292	0.155 195	0.267 924	−0.264 276
	−11.997	0.318 428	−0.121 420	−0.125 037	−0.629 115	0.623 291
	−12.491	0.137 834	0.487 715	−0.112 449	0.541 911	0.537 618
E''	+ 1.622	−0.147 161	−0.307 561	1.003 708	−0.570 871	
	− 7.856	0.544 901	0.663 596	0.304 040	0.455 551	
	− 9.250	0.775 610	−0.627 044	−0.031 295	0.044 362	
	−12.554	−0.306 432	−0.328 974	0.106 686	0.782 210	

Ligand field potentials

The electrostatic potential of the ligand fields can be written in the form

$$\Phi(\vec{r}) = -\sum_{i=1}^{n} \vec{p}_i \operatorname{grad} |\vec{r}-\vec{r}_i|^{-1},$$

where n is the number of the point dipoles, $\vec{r}_i$ and $\vec{p}_i$ is the position vector and the dipole moment of the i-th dipole. By means of the well known formula [18]

$$\frac{1}{r_{12}} = \sum_{l=0}^{\infty} \sum_{m=-l}^{l} \frac{4\pi}{2l+1} \frac{r_<^l}{r_>^{l+1}} Y_{lm}(\vartheta_1, \varphi_1) Y_{lm}^*(\vartheta_2, \varphi_2),$$

where $r_<$ is the lower and $r_>$ is the higher of r_1 and r_2, the ligand field potentials can be expressed in terms of spherical harmonics. Because of the approximations applied in the calculations it will be convenient to expand Φ in the form

$$\Phi = -\sum_{l=0}^{\infty} \sum_{m=-l}^{l} \frac{4\pi}{2l+1} \left\{ \sum_{(1)} \vec{p}_i \operatorname{grad} \left[\frac{r_<^l}{r_>^{l+1}} Y_{lm}(\vartheta, \varphi) Y_{lm}^*(\vartheta_i, \varphi_i) \right] + \right.$$

$$\left. + \sum_{(2)} \vec{p}_j \operatorname{grad} \left[\frac{r_<'^l}{r_>'^{l+1}} Y_{lm}(\vartheta', \varphi') Y_{lm}^*(\vartheta_j', \varphi_j') \right] \right\},$$

where the first summation is extended over the dipoles near Co_1, the second is extended over the dipoles near Co_2 and $\{r, \vartheta, \varphi\}$; $\{r_i, \vartheta_i, \varphi_i\}$ are coordinates referred to Co_1 as origin and $\{r', \vartheta', \varphi'\}$, $\{r_j', \vartheta_j', \varphi_j'\}$ are coordinates referred to Co_2 as origin. As the dipoles are all directed radially toward the corresponding central ion and all dipoles have the same extent (p) of dipole moment both members of the expression of Φ can be written in the form

$$\tilde{\Phi} = -\sum_{l=0}^{\infty} \sum_{m=-l}^{l} R_{lm}^{<>}(r) Y_{lm}(\vartheta, \varphi)$$

where

$$R_{lm}^{<>}(r) = \begin{cases} \dfrac{4\pi}{2l+1} lpr^{l-1} \displaystyle\sum_i r_i^{-l-1} Y_{lm}^*(\vartheta_i, \varphi_i) & \text{if} \quad 0 \leqq r \leqq r_i \\ -\dfrac{4\pi}{2l+1} (l+1) pr^{-l-2} \displaystyle\sum_i r_i^l Y_{lm}^*(\vartheta_i, \varphi_i) & \text{if} \quad r_i \leqq r \leqq \infty \end{cases}$$

In the case of K_1 and K_2 $r_i = r_0 = 1.92$ Å, and $\vartheta_1 = \vartheta_2 = 45°$, $\vartheta_5 = \vartheta_6 = 90°$, $\varphi_1 = 0$, $\varphi_2 = 180°$, $\varphi_5 = -\varphi_6 = 90°$ for K_1, and $\vartheta_1 = \vartheta_2 = \vartheta_3 = 45°$, $\varphi_1 = 180°$, $\varphi_2 = -\varphi_3 = 60°$ for K_2. The potential energy of an electron in the ligand field is of course $V = -e\Phi$.

Energy levels and transitions

According to the perturbation theory, for the calculation of the energy levels in first order the matrix elements $\langle\psi|V|\psi\rangle$ must be calculated with the zeroth order MO-s. As these MO-s are built up from Co and O atomic orbitals, these matrix elements are multicentre integrals. In the calculations we neglected all the two- and

three-centre integrals and took into account only the single-centre integrals. (For this reason the potential Φ has been written in two terms.) With this approximation we get the values for the first order energies (in eV) summarized in Table III. The wavenumbers (in cm^{-1}) of the allowed electron transitions are presented in Table IV.

*Table III**

K_1		K_2	
−5.787	− 9.415	−2.104	−11.308
−6.194	− 9.441	−2.220	−11.533
−6.828	−11.862	−6.592	−11.897
−7.190	−12.111	−7.368	−12.465
−7.798	−12.243	−7.769	−12.498
−8.315	−12.250	−8.182	−12.979
−8.629	−12.319	−9.038	
−8.830	−12.604	−9.420	
−9.111			

* In this table only the negative energies are summarized.

Table IV

K_1		K_2	
10 588	32 784	9 993	36 539
13 043	34 607	10 240	37 892
15 495	36 472	13 474	38 703
16 150	38 776	16 559	39 867
17 950	41 379	19 738	41 127
21 083	42 628	22 823	41 394
21 267	43 683	30 369	42 802
24 550	43 748	31 778	45 269
28 614	47 745	33 304	47 390
29 156	48 804	34 828	47 657
29 217	48 865		

Comparing these results with other calculations [19] and the experimental absorption spectra of the complexes [20] we can say that the results of the transitions are acceptable and they reproduce the main electronic bands of the complexes fairly well. However, this method is in consequence of his nature, incapable to reproduce many other properties, as for example the charge transfer states. These other properties can be interpreted with other methods as for example with the extended Wolfsberg—Helmholz method [21].

* * *

The author wishes to express his thanks to Dr. F. J. GILDE, Director of the Institute of Theoretical Physics, for helpful discussions and to Dr. GY. PAPP for his assistance in the computations. These computations were performed on the MINSZK—22 computer of the Attila Jozsef University.

References

[1] *Bethe, H.:* Ann. Physik **5**, 3, 135 (1929).
[2] *Van Vleck, J. H.:* The Theory of Electric and Magnetic Susceptibilities (Oxford University Press, Oxford and New York, 1932)
[3] *Ilse, F. E., H. Hartmann:* Z. physik Chem. **197**, 239 (1951).
[4] *Ballhausen, C. J.:* Introduction to Ligand Field Theory (McGraw-Hill, New York, 1962)
[5] *Jørgensen, C. K.:* Orbitals in Atoms and Molecules (Academic Press, London and New York, 1962)
[6] *Griffith, J. S.:* The Theory of Transition Metal Ions (Cambridge University Press, London, 1961)
[7] *Orgel, L. E.:* An Introduction to Transition Metal Chemistry (John Wiley and Sons, Inc., New York, 1960)
[8] *Moffith, W.:* J. Chem. Phys. **25**, 1189 (1956).
[9] *Liehr, A. D.:* J. Phys. Chem. **64**, 43 (1960).
[10] *Tanabe, Y., S. Sugano:* J. Phys. Soc. Japan **9**, 753 (1954).
[11] *Kiss, Á.:* Acta Chem. et Phys. Szeged **3**, 6 (1950).
[12] *Gilde, F. J.* and *M. I. Bán:* Acta Phys. Chem. Szeged **5**, 3 (1959)
[13] *Pauling, L.:* The Nature of the Chemical Bond (Cornell University Press, New York, 1939)
[14] *Wolfsberg, M., L. Helmholz:* J. Chem. Phys. **20**, 837 (1952).
[15] *Gilde, F.:* Dissertation, Szeged, 1958.
[16] *Landolt-Börnstein:* Zahlenwerte und Funktionen. Atom und Molekularphysik I. (Springer, Berlin, 1954)
[17] *Mulliken, R. S.:* J. Chem. Phys. **2**, 792 (1934).
[18] *Condon, E. U.* and *G. H. Shortley:* The Theory of Atomic Spectra (Cambridge University Press, London and New York, 1953)
[19] *Maráz, V.:* Acta Phys. et Chem. Szeged **20**, 5 (1974).
[20] *Császár, J.:* Private communication
[21] *Ballhausen, C. J.* and *H. B. Gray:* Inorg. Chem. **1**, 111 (1962).

ИССЛЕДОВАНИЯ ДВУХЪЯДЕРНЫХ КОМПЛЕСКОВ КОБАЛЬТА МЕТОДОМ ЛПМО

B. Мараз

В данной работе рассчитаны энергии состояний и электронных переходов двухъядерных комплексных молекул $[(NH_3)_4Co(OH)_2Co(NH_3)_4]^{4+}$ и $[(NH_3)_3Co(OH)_3Co(NH_3)_3]^{3+}$ с помощью метода ЛПМО (метод лигандного поля с ЛКАМО).

SEMI-EMPIRICAL MOLECULAR ORBITAL CALCULATIONS OF BINUCLEAR COBALT COMPLEXES, II

By

V. MARÁZ

Institute of Theoretical Physics, Attila József University, Szeged

(Received July 10, 1975)

In this paper the energy levels, molecular orbitals, orbital populations and transitions of the $[(NH_3)_4Co(OH)_2Co(NH_3)_4]^{4+}$ and of the $[(NH_3)_3Co(OH)_3Co(NH_3)_3]^{3+}$ binuclear complex ions are calculated by the LCAO-MO method using the half-empirical formula of Wolfsberg and Helmholz [1].

Introduction

In a previous paper [2] we investigated theoretically the binuclear complex compounds $[(NH_3)_4Co(OH)_2Co(NH_3)_4]^{4+}$ (denoted in the following by K_1) and $[(NH_3)_3Co(OH)_3Co(NH_3)_3]^{3+}$ (K_2), and we calculated the energy levels, molecular orbitals, orbital and bond overlap populations and transitions of these complex ions by a simple semi-empirical LCAO—MO method. In these calculations we neglected not only the influences of the H atoms and the electrons in closed shells on the complex compounds but the interactions between ligands OH and NH_3, too.

In the present paper because of undoubted importance of the bridges we take into account besides metal-metal interactions the interactions between ligands OH but we neglect the interactions between NH_3. The method of the calculations and the geometries of the complex ions are the same as in the paper [2]. The computations were performed on the MINSZK—22 computer of the Attila József University.

Results and discussion

The energy values of the MO's are summarized in Table I. These energies differ from the energies in [2] only a little (0.1—0.2 eV) with the exception of the symmetry A_2' (K_2) where the difference is 0.8 eV. In the ground state of the complexes the highest filled MO of K_1 is $2b_{2u}$ (−8.557 eV), that of K_2 is $3e''$ (−9.207 eV), the lowest empty MO-s are $1b_{1g}$ and $3e'$, respectively, as in [2].

The wavenumbers of the allowed electron transitions were calculated by means of Bohr's frequency rule the most important wavenumbers of which are summarized in Table II. In this table we give the wavenumbers of those transitions which were also taken into account in the paper [2]. The difference between the two sets of wavenumbers is not too high except the transition $2b_{1g} \leftrightarrow 2b_{3u}$ where the difference is 4500 cm^{-1}.

Table I

K_1							
A_{1g}	B_{1u}	B_{2g}	B_{3u}	B_{2u}	B_{3g}	B_{1g}	A_{1u}
− 0.272	+59.191	+ 3.963	− 3.364	− 1.705	+ 1.881	− 8.550	−9.343
− 5.998	− 1.418	− 6.014	− 7.122	− 8.557	− 9.110	−11.843	
− 6.902	− 5.908	−12.245	−11.757	−12.360	−14.136		
− 9.281	− 8.335	−14.719	−14.752	−14.111			
−12.736	−12.181						
−14.886	−14.794						
−15.334	−15.209						

K_2				
A_1'	A_2'	A_2''	E'	E''
+ 1.215	−11.308	+48.986	− 2.985	+ 2.389
− 5.533		− 0.315	− 6.779	− 5.946
− 9.465		− 8.483	− 8.760	− 9.207
−12.745		−11.961	−11.784	−12.312
−15.194		−14.924	−12.365	−14.679
			−14.679	

Table II

K_1		K_2	
7 633	26 859	5 688	24 399
13 353	27 214	5 842	26 311
17 420	38 090	7 923	36 541
20 647	39 172	19 590	40 382
25 835	46 336	20 558	47 103
25 875	46 465	21 672	48 531

Table III

atom	orbital	K_1	K_2
Co	$3d_{xy}$	1.2258	0.9688
	$3d_{xz}$	0.6419	0.7988
	$3d_{yz}$	1.9939	0.7988
	$3d_{x^2-y^2}$	0.7952	0.9688
	$3d_{z^2}$	0.8305	0.9057
	$4s$	0.5541	0.7610
	$4p_x$	0.1560	0.1679
	$4p_y$	0.2257	0.1679
	$4p_z$	0.1785	0.2638
O	$2p_x$	1.4997	1.5513
	$2p_y$	1.4997	1.5513
	$2p_z$	1.6935	1.6525
N	$2p_z$	1.6866	1.6885

The orbital populations [3] of the complexes are also similar in the two calculations (Table III.) and the resultant electron configurations of Co atoms according to the present calculations are

$$(3d)^{5.5}\ (4s)^{0.6}\ (4p)^{0.6} \text{ for } K_1 \text{ and } (3d)^{4.4}\ (4s)^{0.8}\ (4p)^{0.6} \text{ for } K_2.$$

The calculation shows that we obtain reasonable results for polinuclear complex compounds if we disregard the interactions between the ligands of the complexes.

* * *

The author wishes to express his thanks to Dr. F. J. GILDE, Director of the Institute of Theoretical Physics, for his helpful discussions and to Dr. GY. PAPP for his assistance in the computations.

References

[1] *Wolfsberg, M., L. Helmholz:* J. Chem. Phys. **20**, 837 (1952).
[2] *Maráz, V.:* Acta Phys. et Chem. Szeged **20**, 5 (1974).
[3] *Fraga, S., G. Malli:* Many-Electron Systems: Properties and Interactions (W. B. Saunders Company, Philadelphia, London and Toronto, 1968)

ПОЛУЭМПИРИЧЕСКИЕ ВЫЧИСЛЕНИЯ НА ДВУХЪЯДЕРНЫХ КОМПЛЕКСАХ КОБАЛЬТА МЕТОДОМ МОЛЕКУЛЯРНЫХ ОРБИТ II.

B. Мараз

В данной работе рассчитаны энергии, молекулярные орбиты, орбитальные популации и электронные переходы с помощью метода ЛКАО-МО с использованием полуэмпирической формулы Вольфсберга — Гельмгольца.

TRANSFER OF ELECTRONIC EXCITATION ENERGY BETWEEN TRYPTOPHANS AT THE ACTIVE SITE OF LYSOZYME

By

P. MARÓTI and L. SZALAY

Institute of Biophysics, József Attila University, Szeged

(Received July 15, 1975)

35—40% of the total fluorescence of lysozyme in aqueous solution is known to originate from the intensities I_A+I_B of fluorescence of tryptophan-62 and tryptophan-63 (TRP-62 and TRP-63). On account of their proximity I_A and I_B could not be determined separately with the chemical methods applied to date.

A kinetical model was developed which permits determination of I_A/I_B and $I_{AB}/(I_A+I_B)$, where I_{AB} is the intensity of fluorescence arising from the transfer of electronic excitation energy between TRP-62 and TRP-63. From this model $I_A/I_B=0{,}53$ and $I_{AB}/(I_A+I_B)=0{,}25$, in other words, the total intensity of the fluorescence of the *pair* originates from energy transfer, this is 9—10% of the total fluorescence of *lysozyme*, one third of the fluorescence intensity of the pair arising from TRP-63, and two thirds from TRP-62.

From the depolarization of fluorescence, using literature data, we obtained 8% of the total fluorescence of lysozyme for the intensity of the fluorescence from energy transfer within the pair, in good accordance with the model, and therefore the separation of fluorescences I_A and I_B is verified.

For the evaluation of the literature data on degrees of fluorescence polarization, the relative positions of the two indole rings of TRP-63 and TRP-62 were calculated from crystallographical data. For the calculations with the model, the total interaction energy (1,75 eV) and the transfer frequency ($3{,}7\cdot10^{12}$ sec^{-1}) were determined.

Introduction

The proteins containing luminescent amino acids can also be studied by luminescence analysis in addition to the known biochemical and *X*-ray crystallographical methods. Lysozyme is a good choice for luminescence analysis because, among others, it contains 3 phenylalanines (PHE), 3 tyrosines (TYR) and 6 tryptophans (TRP). All these are flurorescent, but only three of the TRP-s contribute to the totel flurorescence, the fluorescence of the other amino acid residues being quenched [1]. These three are TRP-62, TRP-63 and TRP-108, located at sites 62, 63 and 108 in the sequence of amino acids. These TRP-s are found at active sites of the enzyme, and therefore their fluorescence (and other properties) are very sensitive to environmental effects. This is a special reason for the extended fluorescence studies carried out with lysozyme in many laboratories.

Several authors have used chemical methods to investigate the individual contributions of the TRP-s to the total fluorescence of the enzyme. TAKAHASHI [2] pointed out that only TRP-62 and TRP-63 are oxidized by low-concentration *N*-bromosuccinimide (NBS); at higher concentrations TRP-108 is oxidized, too, as are the

other TRP-s with further increase of the concentration. This process is reflected in the fluorescence: at low NBS concentrations the fluorescences of TRP-62 and TRP—63 are quenched, as is that of TRP-108 at higher NBS concentrations. LEHRER [3] and TEICHBERG [4] studied the fluorescence quenching with iodide ion. The final conclusion of their investigations was the finding that 56% of the total fluorescence originates from TRP-108, 35—40% from the TRP-62, TRP-63 pair, and 5—10% from the other TRP-s. On account of the small distance between TRP-62 and TRP-63 chemical methods were unable to differentiate between the fluorescences of TRP-62 and TRP-63.

The differentiation of the fluorescence within this TRP-pair was attempted by using the transfer of excitation energy between the two. Since the structure of lysozyme is known with high precision from *X*-ray crystallographical investigations [1], the relative positions of the indole-rings determining the fluorescence of the TRP are also well known. The degree of polarization of the fluorescence appearing after energy transfer is influenced by the relative positions of the indole-rings. From analysis of the polarized fluorescence of lysozyme, therefore, information can be expected on the individual fluorescences of TRP-62 and TRP-63.

The possibility of energy transfer between TRP-62 and TRP-63 was suggested by LONGWORTH [5] without quantitative studies. In general, the quantitative study of energy transfer is based upon the inductive resonance transfer theory elaborated by FÖRSTER [6]. In our case this theory cannot be applied because, due to the proximity of TRP-62 and TRP-63, the interaction cannot be reduced to dipole-dipole interaction, as was stated already by WEBER [7]. Because of the small overlap integral, the Förster-type critical distance for TRP→TRP homotransfer was found to be $R_0=6$ Å [8]. This is a distance commensurable with the linear dimensions of TRP, and therefore the dipole-dipole approximation is not correct and the total interaction energy should be determined. From the total interaction energy the transfer frequency can be calculated and, using the geometrical and fluorescence data, the contributions of two amino acid residues to the total fluorescence of lysozyme can be established.

1. *The frequency of excitation transfer between TRP-62 and TRP-63*

The general relation for the frequency of energy transfer, obtained *via* time-dependent perturbation calculations [9], is:

$$k = \frac{2\pi}{\hbar} |U|^2 \int \varrho_A(E) \varrho_B(E)\, dE. \tag{1}$$

Here $\varrho_A(E)dE$ and $\varrho_B(E)dE$ are probability density functions identical with the normalized fluorescence spectrum $f_A(E)dE$ of the donor molecule A and with the normalized absorption spectrum $\varepsilon_B(E)dE$ of the acceptor molecule B, i.e. they are measurable quantities. U is the interaction energy. ($\varrho_A(E)dE=\int f_A(E)dE$, $\int f_A(E)dE=1$ and $\varrho_B(E)dE=\varepsilon_B(E)dE$, $\int \varepsilon_B(E)dE=1$.) U and the overlap integral should be given for the determination of k.

a) *The interaction energy for the pair TRP-62 and TRP-63*

The total interaction energy is the sum of the different possible interaction energies. The following interaction energies exist between two atoms with centers a and b situated on the two indole-rings.

α) Electrostatic repulsive potential between the positive nuclei at a distance R is $F_0^c = e^2/R^2$. To this an exchange potential $F_0^A = e^2 S/R$, should be added where $S = \int \chi_a \chi_b dV$ is the overlap integral of the electron clouds localized on centres a and b.

β) Transition attractive potential appears between the charge cloud and the opposite nucleus. Its coulombic term is

$$F_1 = q_a^2 e^2 \int \chi_a \frac{1}{r_b} \chi_a dV + q_b^2 e^2 \int \chi_b \frac{1}{r_a} \chi_b dV$$

and its exchange term

$$F_3 = q_a q_b e^2 S \int \chi_a \frac{1}{r_a} \chi_b dV + q_a q_b e^2 S \int \chi_b \frac{1}{r_b} \chi_a dV;$$

q_a and q_b denote the charge densities of π-electrons on the centres a and b, and χ_a and χ_b are the atomic orbits of atoms with centres a and b.

γ) The interaction between electrons has a coulombic term

$$F_2 = q_a^2 q_b^2 e^2 \iint \chi_a(1) \chi_b(2) \frac{1}{r_{12}} \chi_a(1) \chi_b(2) dV_1 dV_2$$

and an exchange term

$$F_4 = q_a^2 q_b^2 e^2 \iint \chi_a(1) \chi_b(2) \frac{1}{r_{12}} \chi_a(2) \chi_b(1) dV_1 dV_2,$$

where r_{12} is the distance between the electrons, and the functions $\chi_a(i)$ and $\chi_b(i)$ refer to the i-th electrons belonging to the atoms with centres a and b, respectively.

The *total interaction energy* is the sum of the above interaction energies:

$$U = F_0^c - F_1 + F_2 + F_0^A - F_3 + F_4.$$

For calculation, use was made of the transformed form of the atomic wave functions (given in the Appendix) depending on the relative orientations of the two indole-planes. For the next two pairs of atoms of TRP-63 and TRP-62 (*i.e.* for the pairs C_2, C_8 and C_3, C_7 in Fig. 3.) the results are included in Table I. The distances and energies are given in atomic units and 10^{-12} erg, respectively. The total interaction energy can be considered to be the sum of interaction energies of the two next-situated pairs of atoms in TRP-62 and TRP-63 and therefore

$$U = -2.81 \cdot 10^{-12} \text{ erg} = -1.75 \text{ eV}.$$

b) *The overlap integral.* For the calculation of the transfer frequency from (1), in addition to the interaction energy U the overlap integral $\left(\int \varrho_A(E) \varrho_B(E) dE = \int f_A(E) \varepsilon_B(E) dE\right)$ must also be determined. This integral is not identical with

Table I

Quantities for the calculation of the interaction energy between tryptophan-63 and tryptophan-62 in lysozyme

	C_2-C_8	C_3-C_7
R	3.4	4.4
q_a	0.78	0.96
q_b	1.01	1.02
S	− 0.18	− 0.10
F_0^e	12.8	9.8
F_0^A	0.414	0.098
F_1	22.8	18.9
F_2	8.64	7.80
F_3	1.33	0.44
F_4	0.677	0.230
C	− 1.36	− 1.10
A	− 0.24	− 0.11

the Förster overlap integral (see p. 85 in [6]), here both spectra are normalized and the dimension of the integral is energy^{-1}. From the spectra in Fig. 2. the overlap integral is of the order of 10^{-4} eV^{-1}, which is extremely small. Since, in (1) the total interaction energy must be considered; however, not only the term from dipole-dipole interaction, but also the transfer frequency between the two TRP-s becomes appreciable:

$$k = \frac{2\pi}{\hbar} U^2 \int f_A(E)\varepsilon_B(E)\,dE =$$

$$= \frac{4\pi^2}{6{,}6 \cdot 10^{-27}} (-1{,}75)^2\, 10^{-4}\,\mathrm{sec}^{-1} =$$

$$= 3{,}7 \cdot 10^{12}\,\mathrm{sec}^{-1}.$$

2. *The ratio of the fluorescence intensities from molecules in energy transfer relationship*

Let us consider molecules A and B with (radiative and radiationless) deactivation frequencies k_A and k_B, the transfer frequencies for transfer from A to B and from B to A being k_{AB} and k_{BA} (Fig. 1.). $W_A(t)$ and $W_B(t)$ are the probabilities of finding the molecules A and B in excited states at time t. Since the molecules are subject to spontaneous deactivation and energy-transfer processes, these probabilities are time-dependent according to the equations

$$\frac{dW_A(t)}{dt} = -(k_{AB}+k_A)W_A(t)+k_{BA}W_B(t), \tag{2}$$

$$\frac{dW_B(t)}{dt} = k_{AB}W_A(t)-(k_{BA}+k_B)W_B(t). \tag{3}$$

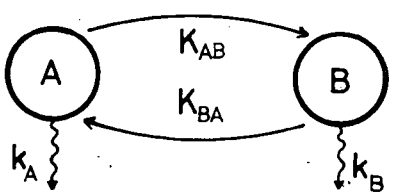

Fig. 1. Kinetics of radiationless and radiative deactivation of fluorescent molecules A and B

Taking probabilities p_A and p_B for having excited A and B molecules at time $t=0$, the solution of the system of equations is the following:

$$W_A(t) = \frac{[p_B k_{BA} - p_A(k_A+\lambda_B)]\exp\lambda_A t + [p_A(k_A+\lambda_A) - p_B k_{BA}]\exp\lambda_B t}{\lambda_A - \lambda_B}, \quad (4)$$

$$W_B(t) = \frac{[p_B(k_A+\lambda_A) + p_A k_{AB}]\exp\lambda_A t - [p_A k_{AB} + p_B(k_A+\lambda_B)]\exp\lambda_B t}{\lambda_A - \lambda_B}. \quad (5)$$

For instantaneous excitation the probabilities $W_A(t)$ and $W_B(t)$ decay biexponentially, and λ_A and λ_B are negative constants.

Within time dt after the t-th point of time the number of spontaneous deactivations of molecules A is proportional to $k_A W_A(t)dt$, and the number of radiative deactivation processes is proportional to $\eta_A k_A W_A(t)dt$, where η_A denotes the absolute quantum yield of fluorescence of molecules A. The total intensity of fluorescence $I_A = \eta_A k_A \int_0^\infty W_A(t)dt$. From the probabilities given in (4) and (5), the ratio of the intensities of fluorescence of molecules A and B is:

$$\frac{I_A}{I_B} = \frac{\eta_A k_A}{\eta_B k_B} \frac{\int_0^\infty W_A(t)\,dt}{\int_0^\infty W_B(t)\,dt} = \frac{\eta_A k_A}{\eta_B k_B} \frac{\left(1+\frac{p_A}{p_B}\right)k_{BA} + \frac{p_A}{p_B}k_B}{\left(1+\frac{p_A}{p_B}\right)k_{AB} + k_A}. \quad (6)$$

The part I_{AB} of the fluorescence of molecule B which originates from exciting energy obtained from molecule A through energy transfer can be calculated from relations (2)—(3):

$$I_{AB} = \eta_B \int_0^\infty (k_{AB} W_A(t) - k_{BA} W_B(t))\,dt = \left(\frac{p_A}{p_B}k_{AB} - \frac{k_A}{k_B}k_{BA}\right)\eta_B p_B k_B. \quad (7)$$

A useful expression is $I_{AB}/(I_A+I_B)$, the ratio of the intensity of fluorescence due to energy transfer to the total intensity of fluorescence. This expression gives information about the contributions of the members of the molecule pair to the total fluorescence of the pair.

Relations (6)—(7) can be simplified if they refer to the pair TRP-63 and TRP-62 in the lysozyme. The transfer frequency is $3.7 \cdot 10^{12}\ \mathrm{sec}^{-12}$ (see section 1), and the frequency of radiative deactivation from measurement of the decay of fluorescence is of the order of $10^9\ \mathrm{sec}^{-1}$ [11]. The terms with k_A and k_B can therefore be neglected in comparison to k_{AB} and k_{BA}. The simplified relations are:

$$\frac{I_A}{I_B} = \frac{\eta_A k_A k_{BA}}{\eta_B k_B k_{AB}}, \quad (8)$$

$$\frac{I_{AB}}{I_A+I_B} = \frac{\frac{p_A}{p_B} - \frac{k_A}{k_B}\cdot\frac{k_{BA}}{k_{AB}}}{\left(1+\frac{p_A}{p_B}\right)\left(1+\frac{\eta_A k_A k_{BA}}{\eta_B k_B k_{AB}}\right)}. \quad (9)$$

3. *The contributions of TRP-62 and TRP-63 to their total fluorescence*

a) *The ratio of the intensity of fluorescence from energy transfer to the total intensity of fluorescence.* The observed emission anisotropy of lysozyme, r, is the sum of the emission anisotropies r_A, r_B and r_C relating to the fluorescences of TRP-62 TRP-63 and TRP-108, denoted below as A, B and C. According to [7]:

$$r = \frac{r_A I_A + r_B I_B + (r_{AB} - r_B) I_{AB} + r_C I_C}{I_A + I_B + I_C}.$$

From this relation:

$$\frac{I_{AB}}{I_A + I_B} = \frac{r_A - r}{r_A - r_{AB}}. \tag{10}$$

According to the measurements of WEBER [7] the degree of polarization of fluorescence of TRP in neutral water solution excited with unpolarized light of 290 nm wavelength is $p=0.10$; consequently, $r_A = 2p/(3+p) = 0.065$. The depolarization of fluorescence appears since the absorption and emission oscillators of TRP are not parallel but form an angle ω. This angle can be calculated from the depolarization factor given in [12]: $\omega = \pm 43°$ or $\pm 137°$. Under the same conditions as above for TRP [13] the degree of polarization of the fluorescence of lysozyme, $p=0.085$ and therefore $r=0.055$. According to [13] the degree of polarization is temperature-independent in the range 0 to 60 °C, and thus the depolarization found in addition to that already obtained in TRP cannot be ascribed to Brown-rotation, but only to the energy transfer between TRP-62 and TRP-63. From the transfer depolarization factor, r_{AB} can be determined: $r_{AB} = 0.2 \left(\frac{3}{2} \langle \cos^2 \Theta_{AB} \rangle - \frac{1}{2} \right)$. Here Θ_{AB} is the angle formed by the absorption oscillator of A and the emission oscillator of B. Θ_{AB} can be calculated *via* simple geometrical relations by means of the transformation matrix T^{63-62} (see in the Appendix) and the angle ω given above. The physically meaningful single value is $r_{AB} = -0.058$.

If the values $r_A = 0.065$, $r = 0.055$ and $r_{AB} = -0.058$ are introduced into (10), $I_{AB}/(I_A + I_B) = 0.08$ is obtained. Accordingly 8% of the total fluorescence originates from indirect excitation via energy transfer.

The ratio $I_{AB}/(I_A + I_B)$ can also be determined from equation (9). Unfortunately, the exact values of the quantities in (9) cannot be given, because the environmental effects on the absorption and fluorescence of TRP-62 and TRP-63 within lysozyme are not known. LASKOWSKI [14] and HERSKOVITS [15] determined the probabilities of perturbation of different TRP-s by solvent molecules. According to these investigations TRP-62 undergoes perturbation as if it were completely surrounded by solvent molecules. Consequently, TRP-62 in water solution can be modellized with TRP in water solution. Based upon the data in [14]—[15], TRP-63 can be modelled with TRP in methanol solution. The absorption and fluorescence spectra (corrected for reabsorption) of TRP were therefore determined in water and in methanol with a Spectrophotometer Optica Milano CF—4 and with a Perkin—Elmer MPF4 Spectrofluorimeter (excitation and observation perpendicular, concentration $5 \cdot 10^{-5}$ M, exciting wavelength 290 nm). p_A/p_B was considered to be indentical with the

ratio of the absorptions in methanol and water at the exciting wavelength. This gives $p_A/p_B=1.46$. k_A/k_B was determined with the method given by STRICKLER and BERG [16]. This method has been successfully applied in the case of complex molecules [17]. Assuming that the degrees of degeneration of the ground and excited states in water and methanol are the same, $k_A/k_B=1.32$, the ratio of the transfer frequencies

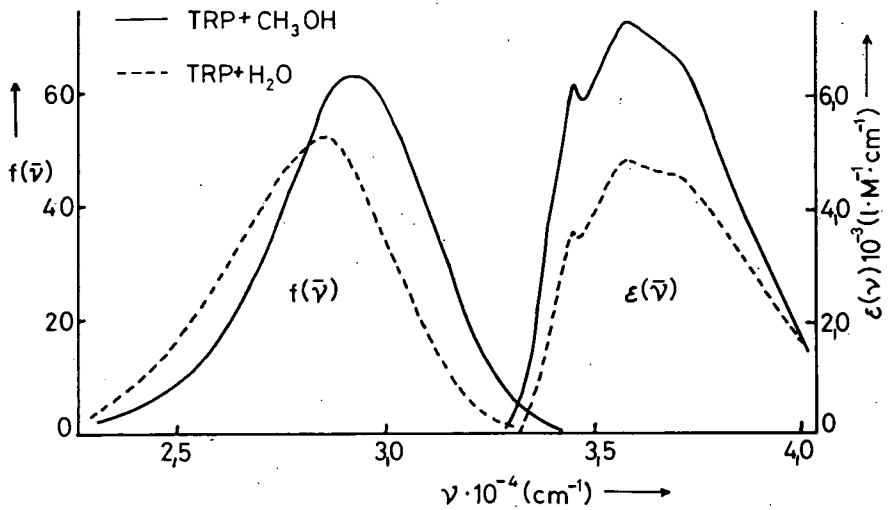

Fig. 2. Absorption and fluorescence spectra of tryptophan in methanol and water

between TRP-63 and TRP-62 was considered to be identical with the ratio of the overlap integrals: $k_{AB}/k_{BA}=2.5$. The absolute quantum yields of fluorescence from TRP-63 and TRP-62 can be taken as equal ($\eta_A=\eta_B$), because neither involves H-bonding, neither is in van der Waals interaction with any group in the pH region studied and they have approximately identical invironments [1].

If the values $p_A/p_B=1.46$, $k_A/k_B=1.32$, $k_{AB}/k_{BA}=2.5$ and $\eta_A=\eta_B$ are substituted into equation (9), we obtain $I_{AB}/(I_A+I_B)=0.25$. As mentioned earlier, the sum of the fluorescence intensities from TRP-63 and TRP-62 is 35—40% of the total fluorescence intensity of lysozyme in aqueous solution. The obtained ratio of 0.25 tells us that $35\cdot0.25$ to $40\cdot0.25=9$—10% is the intensity of fluorescence (I_{AB}) arising from energy transfer of the total fluorescence of lysozyme. This is in good aggreement with the value of 8% obtained by means of fluorescence polarization, and therefore the model outlined in section 2 can be used to distinguish between the fluorescences from TRP-63 and TRP-62. With the numerical values substituted earlier into (9), equation (8) yields $I_A/I_B=I_{TRP\text{-}62}/I_{TRP\text{-}63}=0.53$. Consequently, the total fluorescence intensity of this TRP pair in an aqueous solution of lysozyme is composed of one third weight TRP-63 and two thirds weight TRP-62 fluorescence.

Appendix

1) *The relative orientations of the indole rings of TRP-63 and TRP-62*

The scheme of the indole ring of TRP is shown in Fig. 3., together with the coordinate system (X, Y, Z) attached to the ring. The angles formed by the X and Z axes of any two TRP-s in lysozyme are known from crystallographical measurements. The relative orientations (Fig. 3.) of the indole-planes of two TRP-s have not been unambiguously determined. For an unambiguous determination the angles of all three axes should be known. However, if *three* TRP pairs are chosen, the relative orientations of *one* pair are sufficiently determined from the $3\times2=6$ angles.

Table II

Angles between axes X, X′ (upper numbers) and Z, Z′ (lower numbers) of the three indole rings of triptophans (62, 63 and 108) in lysozyme

	TRP-62	TRP-63	TRP-108
TRP-62	———	41.5 50.0	139.0 118.6
TRP-63	41.5 50.0	———	179.1 162.9
TRP-108	139.0 118.6	179.1 162.9	———

For TRP-63 and TRP-62 it is advantageous to chose TRP-108 because the angle relations promote the calculations. Let us take two coordinate systems X, Y, Z and X', Y', Z' attached to two different indole-rings with common origin. The angle relations according to [1] are shown in Table II. The upper and lower numbers denote the angles between X, X' and Z, Z', respectively. The angles (or, more conveniently, their cosines) can be obtained from the matrix equation

$$T^{62-63}\cdot T^{63-108}=T^{62-108}$$

$$\begin{vmatrix} 0.75 & \cdot & \cdot \\ \cdot & \cdot & \cdot \\ \cdot & \cdot & 0.64 \end{vmatrix} \begin{vmatrix} -1 & \cdot & \cdot \\ \cdot & \cdot & \cdot \\ \cdot & \cdot & -0.96 \end{vmatrix} = \begin{vmatrix} -0.75 & \cdot & \cdot \\ \cdot & \cdot & \cdot \\ \cdot & \cdot & -0.48 \end{vmatrix}.$$

The matrix elements to be determined are denoted by dots. Due to the normalization condition the elements to be determined in the first row, and similarly all elements of the first column of matrix T^{63-108}, disappear. The missing elements of the second and third rows are determined by the normalization condition, too (apart from their signs.). Therefore

$$T^{63-108}=\begin{vmatrix} -1 & 0 & 0 \\ 0 & \pm0.96 & \pm0.29 \\ 0 & \pm0.29 & \pm0.96 \end{vmatrix}.$$

The third element in the third row of T^{62-108} is obtained by multiplying the third row of T^{62-63} and third column of T^{63-108}. This multiplication gives a linear equation from which the middle element of the third row of T^{62-63}, and then — by using this element — all other matrix elements can be calculated. The signs of the matrix elements can be found from the atomic distances of the characteristic atoms of the two indole-rings, given in [1]. In this way T^{62-63} can be determined. Since we need T^{63-62}, T^{62-63} should be inverted (in this case, since the rotation is an orthonormalized transformation, with transposition). The final result is

$$T^{62-63}=\begin{vmatrix} 0.75 & 0.61 & 0.28 \\ -0.26 & 0.65 & -0.72 \\ -0.61 & 0.46 & 0.64 \end{vmatrix}; \quad T^{63-62}=\begin{vmatrix} 0.75 & -0.26 & -0.61 \\ 0.61 & 0.65 & 0.46 \\ 0.28 & -0.72 & 0.64 \end{vmatrix}.$$

2. *The molecular orbitals of TRP*

The calculations were carried out in π-electron approximation, according to Fig. 3. The atomic distances were taken from [10]. The molecular orbitals ψ_i were taken as linear combinations of the χ_q $(q=1, 2, \ldots, 10)$ $2p_z$ atomic orbitals:

$$\psi_i=\sum_{q=1}^{10} c_{iq}\chi_q.$$

The coefficients (c_i) and the energies (E_i) relating to the molecular orbitals were determined with a computer by the Löwdin method, from the matrix equation

$$\hat{H}\hat{c}_i = E_i\hat{S}\hat{c}_i.$$

The overlap between non-neighbouring atoms was neglected in the overlap matrix S. The p-th element in the main diagonal of the energy matrix $\hat{H}$ is the ionization energy H_{pp} of the electron of the

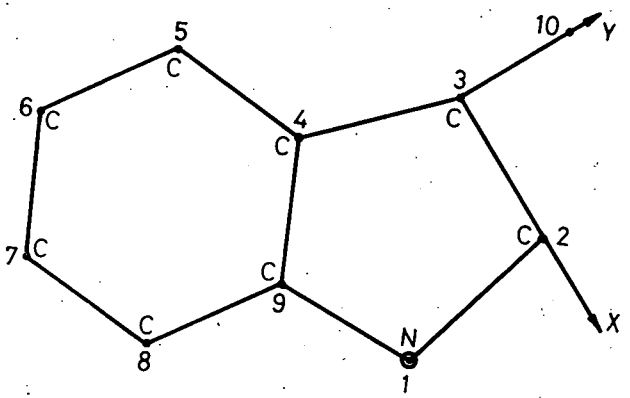

Fig. 3. Scheme of the indole-ring with the coordinate system fixed to the ring

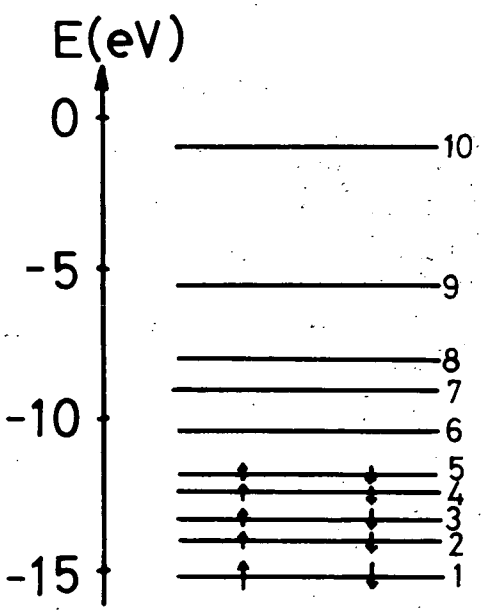

Fig. 4. Energy diagram of tryptophan

p-th atom participating in the molecular orbital. The element H_{pq} outside the main diagonal can be given for aromatic compounds according to *Hoffmann* as

$$H_{pq} = 1.75 \frac{H_{pp}+H_{qq}}{2} S_{pq}.$$

In our case $H_{11} = -14.16$, $H_{22} = \ldots = H_{10.10} = -11.31$, $H_{12} = H_{19} = -4.45$, $H_{13} = \ldots = H_{8,10} = -4.93$, $H_{3,10} = -3.78$, $H_{4,9} = -4.93$ eV.

The energy diagram is shown in Fig. 4. The excitations from the 5-th level to levels 7 and 8 give the two nearer electronic excited states of TRP (and indole derivatives), L_a and L_b, often studied experimentally.

Further the charge densities of the π-electrons localized on the atoms were calculated. The results for the ground state S_0 and excited state L_a are tabulated (Table III).

Table III

π-electron densities in the ground state S_0 and excited state ^1L_a of tryptophan around different atoms (for the notation see Fig. 3)

atomic notation	1	2	3	4	5	6	7	8	9	10
S_0	1.59	0.74	1.07	1.05	1.00	1.06	1.02	1.07	0.97	0.50
^1L_a	1.59	0.78	0.96	1.06	1.08	1.09	0.99	1.15	0.96	0.37

References

[1] *Imoto, T., L. N. Johnson, A. C. T. North, D. C. Phillips, J. A. Rupley:* The Enzymes, Vol. VII. **21**. p. 665 Acad. Press (1972).
[2] *Takahashi, T.:* J. Biochem. **58**, 385 (1965).
[3] *Lehrer, S. S.:* BBRC **29**, 767, Biochemistry **10**, 3254 (1971).
[4] *Teichberg, V. I., N. Sharon:* FEBS Letters **7**, No 2 (1970).
[5] *Longworth, J. W.:* Biopolymers **4**, 1131 (1966).
[6] *Förster, Th.:* Fluoreszenz organischer Verbindungen, Vandenhoeck und Ruprecht, Göttingen (1951).
[7] *Weber, G.:* Biochem. J. **75**, 335 (1960).
[8] *Koniev, S. V.:* Fluorescence and Phosphorescence of Proteins and Nucleic Acids, Plenum Press, New York (1967).
[9] *Lamola, A. A., N. J. Turro:* Energy Transfer and Organic Photochemistry, Interscience Publ., New York, London, Sydney, Toronto. Techniques of Organic Chemistry, Vol. XIV. Ed.: P. A. Leermaker, A. Weissberger, p. 24 (1969).
[10] *Lumbroso, H., G. Pappalardo:* Bull. Soc. Chim. France 1961, No **6**, p. 1131.
[11] *Eisinger, J.:* Molecular Luminescence 185—202 (E. C. Lim, 1968).
[12] *Eisinger, J.:* Polarized Excitation Transfer.: Concepts in Biochemical Fluorescence, Marcel Dekker, Inc., New York (1973),. p. 1—44.
[13] *Koniev, S. V.:* Dokl. Akad. Nauk Beloruss. SSR **12**, 1122 (1968).
[14] *Laskowski, M., E. J. Williams:* JBC **240**, 3580 (1965).
[15] *Herskovits, T. T.:* JBC **240**, 628 (1965).
[16] *Strickler, S. J., R. A. Berg:* J. Chem. Phys. **37**, 814 (1962).
[17] *Gáti, L.:* Acta Phys. et Chem. Szeged **15**, 5 (1969).

МИГРАЦИЯ ЭЛЕКТРОННО-ВОЗБУЖДЕННОЙ ЭНЕРГИИ МЕЖДУ ТРИПТОФАНАМИ, НАХОДЯЩИМ ИСЯ НА АКТИВНЫХ МЕСТАХ ЛИЗОЦИМА

П. Маротн и Л. Салаи

Известно, что 35—40 % от полной люминесценции водного раствора лизоцима происходит от триптофана 62 и 63. Химическими методами разделение люминесценции не осуществимо, поэтому мы установили кинетическую модель, применимость которой мы проверяли поляризационными исследованиями. Установили, что одна треть люминесценции происходит от триптофана 63, и две третих от триптофана 62. Использованием кристаллографических данных определили относительное положение индольных колец, определили полную энергию взаимодействия (1,75 эв) и частоту миграции ($3{,}7 \cdot 10^{12}$ сек$^{-1}$).

DAMAGES IN V_2O_5 SINGLE CRYSTALS DUE TO LASER LIGHT

By

L. NÁNAI, I. HEVESI and I. KETSKEMÉTY

Institute of Experimental Physics, Attila József University, Szeged

(Received, July 14, 1975)

The present paper describes our investigations into the optical stability of V_2O_5 single crystals. The energy threshold of surface demage was determined for single crystal plates of (010) orientation in the case of burst mode and *Q*-switched laser light. The interpretation for a possible mechanism of damaging is suggested.

Introduction

The development and use of lasers of increasing power made necessary to solve the problem of optical stability of the optical elements, meters of energy and power, *i.e.* to know the energy and power density at wich damages in the material occur. Most of the publications concerning this problem deal with transparent dielectrics [1—6]; considerably fewer papers are concerned with damaging of semicorductors [7—11]. The conclusions drawn from experimental results are manifold and often contradictory.

Based on the results obtained hitherto, the mechanisms of damaging can be grouped into several classes. In some cases the mechanical damages are attributed to acoustic (hyperacoustic) phonons due to forced MANDELSTAM—BRILLOUIN scattering [12—14]. According to another conception, melting and damaging is caused by intensive energy accumulation due to one and mutiphoton absorption [15]. Strong light absorption caused by surface defects and inhomogeneities of the material may also lead to damaging [16-17]. Thermal stresses due to light absorption, and ensuing shock waves may also cause damaging of the material [5].

The aim of our present work was to study the resistance against ruby laser light on vanadium pentoxide single crystal plates of (010) orientation V_2O_5 crystallizes in the rhombie system and forms optically anisotropic, birefringent biaxial crystals. From optical transmission measurements, its band gap width was found to be 2.3—2.4 eV [18]. Electrically V_2O_5 is an n-type impurity semiconductor of comparatively high thermoelectric force. In its conductivity, vanadium ions of valencies different from (lower then) the basic valency, and oxygen vacancies, both acting as donor centres, play a role.

From the V_2O_5 single crystal produced, crystal plates of different thickness and (010) orientation can be comparatively easily split off. The thickness of the crystal plates used in our experiments varied between 50 and 400 μ. The lustrous plane-parallel plates were visibly inhomogeneous owing to air inclusions formed during crystal growth.

The laser beams used for damaging were perpendicular to the samples of (010) orientation.

Experimental method

In our investigations the light transmit of V_2O_5 single crystals was measured as a function of the intensity of the incident laser light beam. The energy density at wich a sharp plasma flash was observed due to interaction of the incident laser beam with the crystal was considered as threshold for damaging the V_2O_5. The plasma flash was observed through a HELIOS—44 (LOMO) objective at the moment of the impact of the laser pulse. The plasma discharge was always accompanied by mechanical damage of the V_2O_5 surface. It is to be noted that, according to our experience, observation with unaided eye was sufficient for perceiving the plasma flashes.

The diagram of the experimental arrangement used for the measurements is shown in Fig. 1.

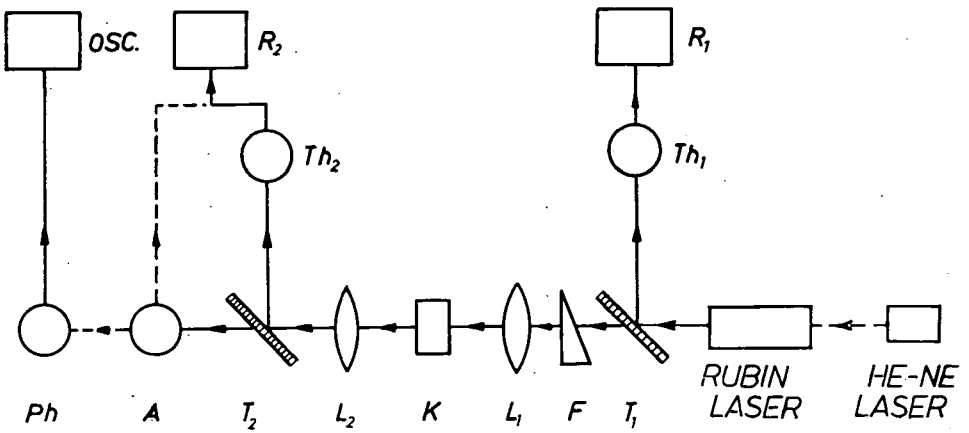

Fig. 1. Experimental arrangement: T_1, T_2: beam splitters; *F:* grey wedge; L_1, L_2: lenses; *K:* sample; Th_1, Th_2: thermoelements; R_1, R_2: compensographs; *A:* calibrated calorimeter; *Ph:* photocell; *OSC:* broad-band oscilloscope

A 0.5 mW CW He—Ne laser served to adjust the light path. A ZEISS ruby laser was used as beam source. The active element of the laser was a ruby rod doped with 0.05% Cr. The laser source was used in burst mode and Q-switched mode. For measuring the energy, part of the incident and transmitted energy was split off by the parallel glass plates T_1 and T_2, to reach the thermoelements Th_1 and Th_2. The thermovoltages of the thermoelements were recorded by the micrographs R_1 and R_2 type BD-5.The rise time $\tau=0.7$ s of KIPP&ZONEN the micrographs was much less then the cooling constant $\tau=60$—80 s; therefore the peak value of the micrograph signals could be considered to be proportional to the light energy absorbed by the thermoelements. The thermoelements were calibrated with the energy meters denoted by A in Fig. 1, developed in our institute.

The calibration curve of the thermoelements is shown in Fig. 2.

The two thermoelements were calibrated with respect to each other for both modes of operation. The intensity of the light incident on the sample was controlled by the calibrated grey wedge F. The glass lenses L_1 and L_2 ($f_1=f_2=120$ mm) served for focussing and rendering parallel the laser beams.

For the area of the light spot, $3.6 \cdot 10^{-5}$ cm^2 was obtained on the basis of the known formula. The mean duration of the pulse was determined with the photocell *Ph* (TUNGSRAM type CV-90) and the broad-band oscilloscope *OSC* (UNITRA type OS-701). On the basis of our measurements the duration of the pulses was calculated to be 0.8 ms for the burst mode and 80 ns for *Q*-switched mode.

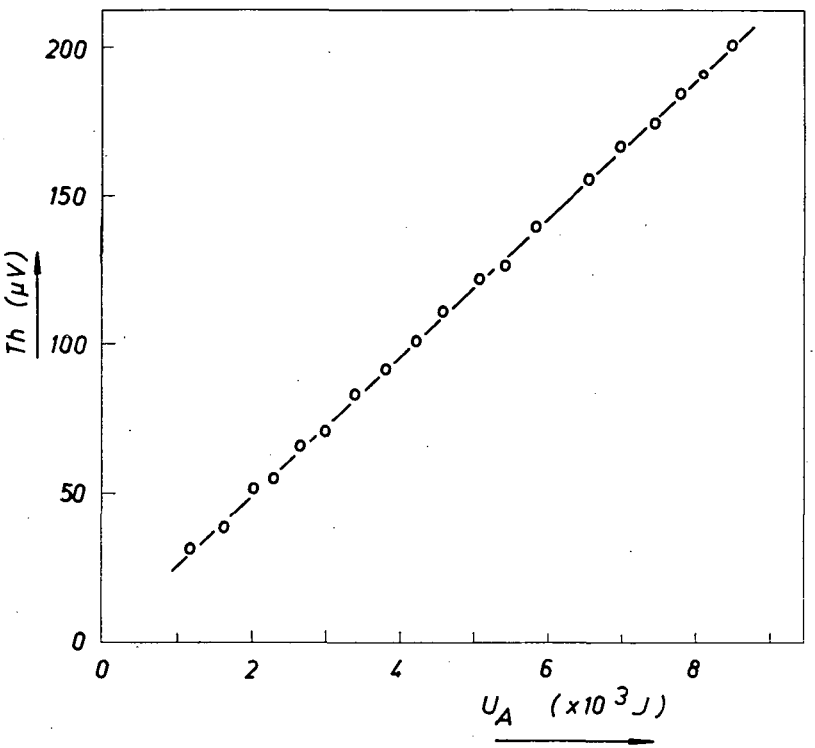

Fig. 2. Calibration curve of the thermoelement, obtained with a calibrated calorimeter for measuring the energy. The abscissa shows the flash energy, the ordinate the electric signal of the thermoelement.

Experimental results

Transmission measurements

In the transmission measurements the beam incident perpendicularly on the crystal plate was controlled, besides the grey filters, by changing the pumping energy.

Because the transmitted energy as a function of pumping energy showed high divergences, the mean of several measurements was used for calculations. In order to permit the use of the arrangement described in the broadest energy range possible, measurements were made also with laser beam focussed on the V_2O_5 surface in the case of both modes.

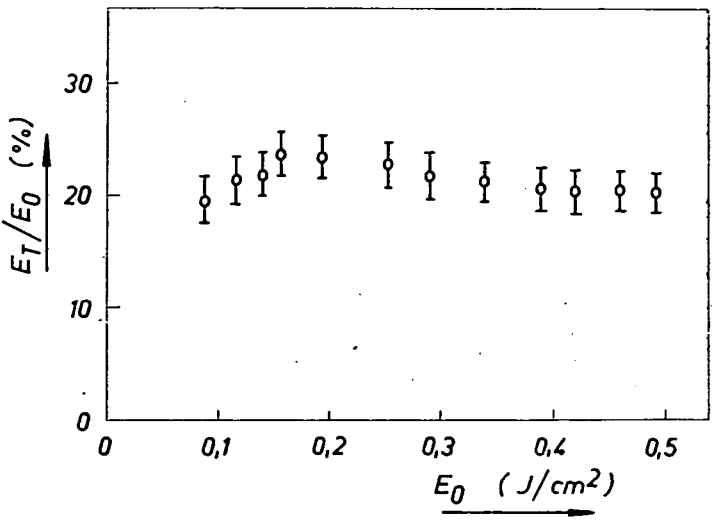

Fig. 3. Percentual transmission *vs.* incident energy density of unfocussed burst mode laser light.

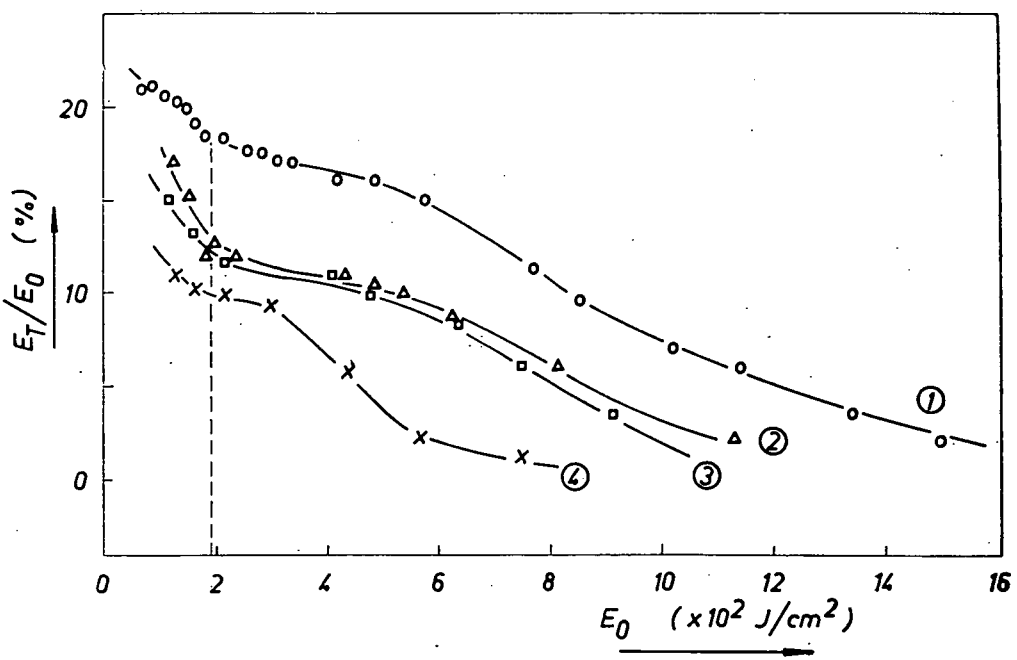

Fig. 4. Transmission of burst mode laser light focussed on the surface.

In Fig. 3 the percentual transmission of unfocussed burst mode laser light can be seen as a function of energy density.

Each point of measurement, showing also the maximum deviations, was calculated from the mean of several measurements. It can be seen that the transmission of the crystal plate studied, instead of being constant in the range of energy density investigated, is dependent on intensity. The transmission increases with higher energy densities in the energy interval 0.11—0.17 J/cm², then, after reaching a maximum, becomes constant or slowly decreases.

Fig. 4 shows the transmission of burst mode laser light focussed on the surface.

Curves (1) to (4) correspond to transmission curves of crystal plates with thicknesses increasing in the order of numeration. Curve (1) belongs to the same crystal plate as used for measuring the transmission values of Fig. 3. In the range of energy density studied, several break points can be observed in each transmission curve. The first of these pertains to the damage indicated by the plasma flash. This break point occurs in the case of all four samples at the intensity $1.9 \cdot 10^2$ J/cm² (marked by a broken vertical line in the figure). At energy densities higher then the damage threshold further decrease of the transmission can be observed.

Q-switched unfocussed laser light was used for determining the transmission curves of the three samples of different thickness shown in Figs. 5 and 6.

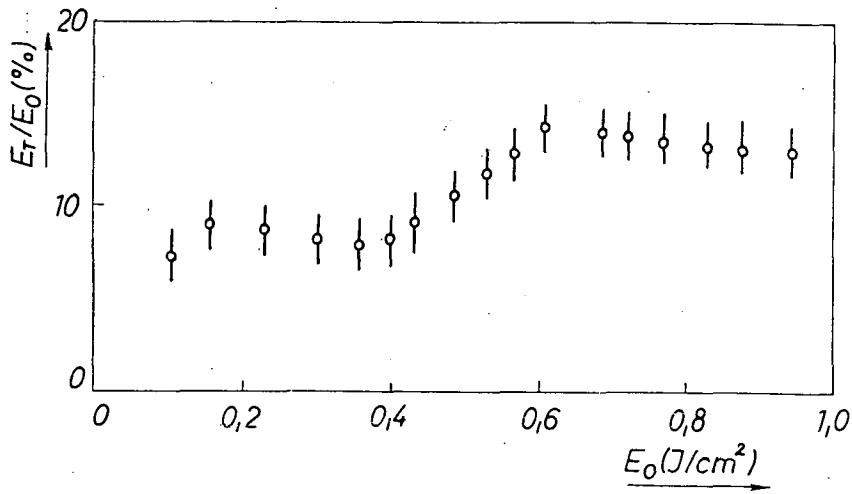

Fig. 5. Transmission of Q-switched unfocussed laser light.

It can be seen that the shape of the transmission curves is similar to that of the transmission curve obtained with unfocussed burst mode laser light, shown in Fig. 3; the transmission first increases with energy density, then after a maximum 0.6 J/cm² begins to decrease slowly. The rate of increase is the highest in the energy density interval 0.4—0.6 J/cm².

Fig. 7 shows the transmission curves measured with Q-switched focussed laser light for five samples of different thicknesses.

The energy threshold of damaging is observed at 25 J/cm² for all five samples.

It should be remarked that for samples the thickness of wich prevented transmission measurements, the damage threshold indicated by the plasma flash was the same as that given above, namely ~ 190 J/cm² for burst mode and ~ 25 J/cm² for Q-switched laser light.

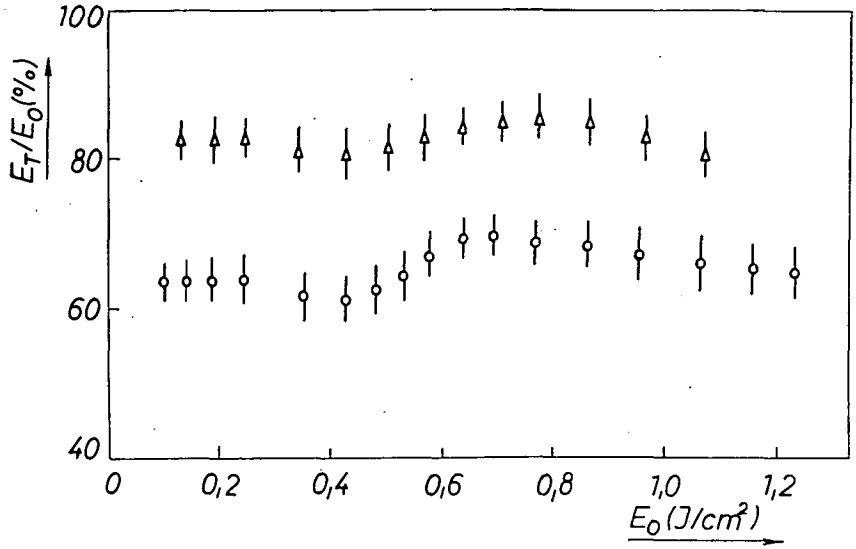

Fig. 6. Transmission of Q-switched unfocussed laser light.

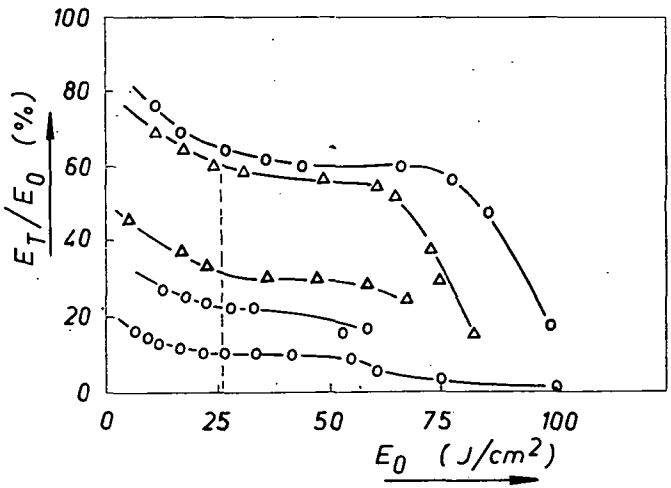

Fig. 7. Transmission of Q-switched focussed laser light.

Morphology of damages

The surface of the samples irradiated by burst mode and Q-switched laser pulses was studied with reflected light, using a microscope.

In some cases damages indicated by a circular dark spot could be observed already below the damage threshold value. Such alterations were observed on the samples and surface domains wich were less satisfactory from the optical point of view. Up to the threshold value of damaging energy or at energy densities only slightly exceeding this value the shape of the observed spot was always cicular.

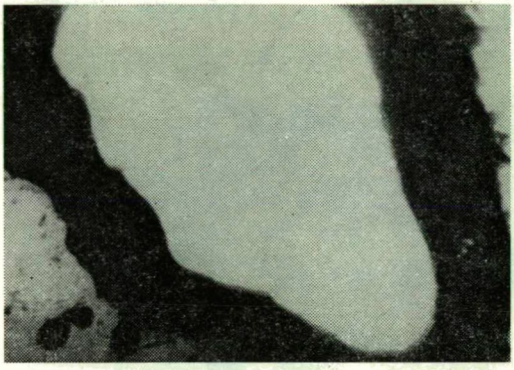

Fig. 8. Microphotograph of a crystal plate perforated by burst mode laser light at 800 J/cm² energy density.

At energy densities significantly higher then the damaging threshold the spot lost its circular form on the impact of the laser pulse of ms duration; it became elongated in the direction of the crystallographis c axis and a well observable crater formed on the surface. The diameter of the crater decreased towards the interior

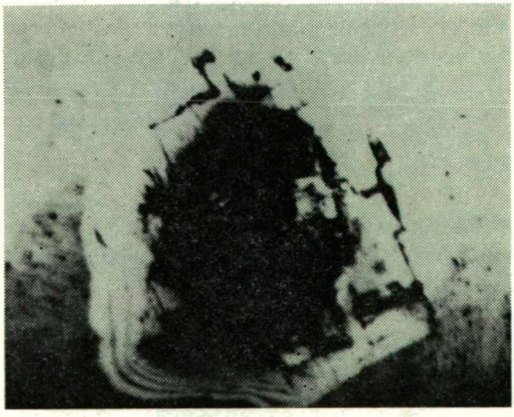

Fig. 9. Microphotograph of a crystal plate, damaged by 29 J/cm² energy density.

of the crystal. At energy densities wich caused perforation of the crystal plate, craters of decreasing diameter towards the interior of the plate were observed on both surfaces.

Fig. 8 is a microphotograph of the crystal plate perforated at 800 J/cm² energy density. The traces of the material ejected to the brim of the crater can be well observed as a dark ring.

The spots obtained with Q-switched laser pulses were always circular; elongations could never be observed.

In Fig. 9 a damage caused by a Q-switched pulse of 29 J/cm² energy density can be seen; this value exceeds only slighly the damaging threshold.

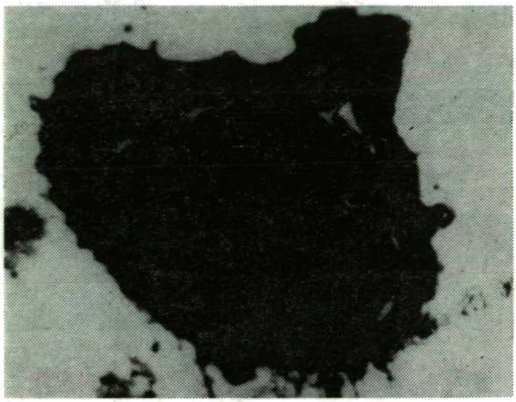

Fig. 10. Microphotograph
of a crystal surface with higher energy density (5mJ0 /c²).

The damages of the crystal are well indicated by the fractures in its lamellar structure and the appearence of interference fringes.

Fig. 10 shows the effect of irradiation with higher energy density (50 J/cm²).

Similarly as in Fig. 8, the material ejected and solidified on the brim of the crater can be well seen as a dark ring in this figure, too.

Discussion of the results

Interpretation of the transmission curves

The increases found in the transmission curves unequivocally point to non-linear effects occurring on the interaction of laser light with the material investigated. The increase in transmission observed in the energy density range 0.11—0.17 J/cm² in burst mode, similarly to that found between 0.4—0.6 J/cm² in the Q-switched mode can be explained by fading of the material, caused by the balance between the ground state and excited states of the atoms. The higher degree of fading observed in the case of Q-switched laser impulses can be explained by the circumstance that the spontaneous emission during the short pulse of $\tau=80$ ns is negligible, while in the burst

mode the spontaneous emission cannot be neglected owing to the long duration of the pulse ($\tau = 0.8$ ms), and thus the atoms returning to the ground state may repeatedly take part in the absorption. Similar results were obtained by BELIKOVA *et al.* [20, see also 21] who investigated the absorption of a ruby crystal.

The decrease in transmission observed at higher energy densities points to the increase of the absorption coefficient of the material with increasing intensity. This may be due chiefly to free electrons raised by one-electron absorption from impurities of low energy level into the conduction band. These electrons, scattered on phonons or defects, may cause further absorption and hereby increase the absorption coefficient compared to that of linear absorption. As the temperature of the material strongly increases during the interaction with laser light [15], the thermoionization caused by the high temperature contributes to the increased number of free carriers. It could be demonstrated that in V_2O_5 at 1000 °K the density of carriers may reach $7 \cdot 10^{16}$ cm^{-3}.

Interpretation of transmission curves obtained by Q-switched laser light

The absorption due to the non-linear effects discussed above leads to damages on the surface of the samples. The plasma produced in the moment of the damaging exerts a shielding effect on the incident radiation, causing further decrease in the transmission. With increasing incident energy density, the size of the damaged domain increases and the plasma formed leads to further increase in absorption. In the damaged domain the probability of light scattering also increases, the material melts and evaporates, and the light is intensely absorbed by the ion cloud formed from the molten and evaporated material; this explains the strong decrease in transmission at high energy densities.

Further remarks on the possible mechanism of damages

The difference in order of magnitude of the damage thresholds of burst mode and *Q*-switched mode laser pulses points to differences in character of the mechanism in the two cases.

Analysis of the experimental results shows that the damages caused by burst mode pulses occur in the following way. Part of the laser light is intensely absorbed on inclusions, purities and defects of microstructure. In these points the material melts and the light absorption becomes even more intensive in the liquid phase. In addition, the probability of light scattering on acoustic phonons also increases [22]. The role of strongly absorbing metallic inclusions present in the V_2O_5 is especially important [21, 23]. The strong energy absorption leads to explosion and the shock wave following the explosion causes damages in the material. The determining character of structure defects in the production of damages is shown by the elongation of the damaged domains in the direction of the crystallographic *c* axis. The duration of the pulse emitted by a *Q*-switched laser is very short, 10^{-7} s, therefore the phenomena connected with heat propagation cannot play a role. This is supported by the consistently circular shape of the damaged domain in the case of *Q*-switched laser pulses, in contrast to the elliptic form of the damaged domains of burst mode laser pulses. It seems very probable that the surface defects, dislocations, impurities have an important role also in this case. As known from the literature [24], the density of centres absorbing at 1μ in V_2O_5 reaches $1.5 \cdot 10^{18}$ cm^{-3}, and the density of surface dislocations 10^7 cm^{-2} (25). The defects in the surface layer form a quasi-continuous spectrum wich corresponds to the trap levels almost continuouly filling the upper part of the band gap. Impurity atoms and defects may be easily ionized by intense light, producing free electrons in the surface layer. The free carriers in the field of the intensive light wave are able to further light absorption through interaction with phonons and defects. Direct band-to-band one-photon absorption may contribute to the absorption, though its probability is low owing to $h\nu < \Delta E$ ($h\nu$ is the photon energy and ΔE is the band gap width 2.4 e*V*). The non-radiative recombination of the electron-hole pairs formed enhances the heating of the material.

According to GRINDBERG [7] the absorptionof non equilibrium carriers generated by the laser light becomes significant in the case of high electric fields. This absorption is ultimately responsible for the sublinearity of the transmission curves. Thus the free electrons formed by one- and multiphoton interactions transfer the excess energy to the lattice, wich evaporates due to the heating and produces a dense ionized gas layer above the surface [26]. As a result of avalanche ionization a plasma flash occurs, followed by a shock wave wich may reach the velocity of 10—15 km/s. [20]. Then the more important breaks and fractures are formed due to the shock waves. The fact that the diameter of the damaged domains, 0.2—0.5 mm, is always greater then their depth, 20—90 μ, can be explained by the cicumstance that, on the one hand, the light pulse is strongly shielded by the plasma formed at hre surface and, on the other hand, the density of defects descreases with increasing depth.

References

[1] *Wasserman, A. A.:* Appl. Phys. Lett. **10**, 132 (1967).
[2] *Giuliano, R.:* Appl. Phys. Lett. **5**, 137 (1964).
[3] *Olness, D.:* Appl. Phys. Lett. **8**, 283 (1966).
[4] *Bloembergen, N.:* Appl. Opt. **21**, 661 (1973).
[5] *Jeremenko, D. V., B. N. Morozov:* Fiz. Tver. Tela **12**, 848 (1970).
[6] *Lisicza, M. P., I. V. Fekeshazi:* Kvantovaya elektronika **6**, 61 (1972).
[7] *Grindberg, A. A., P. F. Meltiev, S. M. Rivkin, V. M. Salmanov:* Fiz. Tver. Tela **9**, 1390 (1976)
[8] *Sam, C. L.:* Appl. Opt. **12**, 878 (1973).
[9] *Vasilyevskaya, V. N., K. D. Glinchuk, L. F. Linnik, N. M. Litvochenko, O. I. Lyadskaya:* Polupr. Tech. i Microelectr. **8**, 44 (1972).
[10] *Mirkin, L. I.:* Neorg, Mat. **9**, 125 (1973).
[11] *Bertolotti, A.:* J. Appl. Phys. **38**, 4088 (1967).
[12] *Volkova, N. V., V. A. Lihachev, M. I. Stepanov, L. M. Shestopalov:* Fiz. Tver. Tela **8**, 12 (1966).
[13] *Archipov, J. P., V. A. Lihachev, V. V. Morozov, F. S. Faizullov:* Fiz. Tver. Tela **14**, 1756 (1972).
[14] *Chiao, R. Y., C. H. Townes, F. Stoicheff:* Phys. Rev. Lett. **12**, 592 (1964).
[15] *Aseev, G. I., M. L. Katz:* Fiz. Tver. Tela **14**, 1303 (1972).
[16] *Harper, G. W.:* Brit. Journ. Appl. Phys. **16**, 751 (1965).
[17] *Danileiko, J. K., A. A. Manenkov, A. M. Prochorov, V. A. Halimov-Markov:* ZHETF **58**, 31 (1970).
[18] *Bodó, Z., I. Hevesi:* pys. stat. sol. **20**, 145 (1967).
[19] *Volzhensky, S. D., M. V. Rashkovsky:* Fiz. Tver. Tela **11**, 1168 (1969).
[20] *Belikova, T. P., A. N. Savshenko, E. A. Sviridenkov:* ZHETF **54**, 37 (1968).
[21] *Abdullaev, A. A., L. M. Beliaev, T. V. Dmitrieva, G. F. Dobrzhansky, V. V. Nluchin, I. S. Liubutin:* Kristallografia **14**, 433 (1969).
[22] *Charchsan, L. (ed.)*: Lasers in industry. New York, 1972. Western Electric Co.
[23] *Patrina I. B., V. A. Joffe*: FTT **6**, 3227 (1964).
[24] *Kenny, N., C. R. Kannewurf, D. A. Whitmore*: J. Phys. Chem. Sol. **27**, 1237 (1966).
[25] *Quang N, I. Hevesi*: Acta Phys. et Chem. Szeged, **20**, 285 (1974).
[26] *Beljajev L. N., V. V. Nabatov, A. N. Golovisztikov*: Krisztallografia **18**, 334 (1973).

РАЗРУШЕНИЕ МОНОКРИСТАЛЛОВ V_2O_5 ЛАЗЕРНЫМ ЛУЧЕМ

Л. Нанаи, И. Хевеши и И. Кечкемети

В настоящей статье представлены результаты исследований оптической прочности монокристаллов V_2O_5. Определена оптическая прочность поверхности, ориентированной в направлении (010), при засветках лучем лазера, работавщего в миллисекундном и гигантском режимах излучения. Предложен механизм разрушения V_2O_5.

DEPENDENCE ON EXCITING WAVELENGTH OF EMISSION SPECTRA OF Mn^{2+} ACTIVATED MAGNESIUM METAPHOSPHATE GLASSES

By

L. SZÖLLŐSY, T. SZÖRÉNYI and K. SZANKA

Institute of Experimental Physics, Attila József University, Szeged

(Received July 1, 1975.)

The dependence on exciting wavelength of emission spectra of Mn^{2+} activated magnesium metaphosphate glasses was measured using a phosphoroscope and lock-in amplifier for four different activator concentrations at room temperature and at 100 °K. The emission spectra are very different for different exciting wavelengths. This finding seems to support the microheterogeneous structure of these glasses.

In the last years RZHEVSKII *et al.* used succesfully luminescence methods for investigating the structure of various phosphate glasses, among others insoluble magnesium metaphosphate glasses.

They mixed powders of Dy^{3+} activated glasses with different decay times and slightly different emission spectra in a given volume ratio, then measured the emission spectra and decay times of the mixtures. They were able to calculate the emission spectra and decay times of the components using a formula [1]. Later they applied the method to different Dy^{3+} activated phosphate glasses, measuring the decay times at different wavelengths of the emission spectra with a special phosphoroscope [2, 3]. On the base of the different decay times they stated the existence of two luminescence centres and calculated the spectra and decay times of both centres.

The possibility of the existence of different kinds of centres is supported by the circumstance that in most phosphate glasses the decay process of Mn^{2+} is reported to be non-exponential [4].

However, if different luminescence centres exist in the glass, then their excitabilities are expected to be different, too. This gave the idea to investigate more thoroughly the influence exerted on the emission spectra by excitation with different wavelengths.

This paper deals with the dependence on exciting wavelength of the emission spectra of Mn^{2+} activated magnesium metaphosphate glasses studied earlier [5].

Experimental

The steps of preparing the samples and their physico-chemical properties are described in detail in an earlier paper [5].

For the measurement of the emission spectra the exciting monochromator of our home-built spectrofluorimeter was substituted by a glass prism monochromator

and the apparatus was completed by a PARKER phosphoroscope [6]. The chopping frequency was 400 c/s. The signal of the multiplier was amplified by a Unipan selective nanovoltmeter type 227, rectified by a Unipan homodyne rectifier voltmeter type 202B, than recorded. The changes in intensity of the luminescence emission amounted to almost three orders of magnitude within each series of measurements. The exciting light flux was measured with a rhodamine B quantum counter [7]. This phosphoroscope arrangement was chosen in order to exclude the difficulties caused by the exciting light in measuring the weak luminescence of the samples. It was possible to apply this method and chopping frequency, because in these glasses the decay time of the manganese luminescence is of the order $\tau \approx 10^{-2}$ s [4].

Results and discussion

It was found experimentally that with the same exciting wavelength, the emission spectra measured in the "in phase" and "out of phase" position of the phosphoroscope are the same. Because of the scattering of the exciting light in the "in phase" position, the identity of the spectra could be demonstrated exactly only for excitation wavelengths pertaining to the ascending branch of the emission spectra (generally up to 520 nm).

The emission spectra of glasses containing 10^{-3}, 5.10^{-3}, 5.10^{-2} and 10^{-1} mole manganese were measured for wavelengths from 405 to 600 nm, at room temperature and at 100 °K. Between 400 and 440 nm the measurements were performed in steps of 5 nm, from 440 to 600 nm in steps of 10 nm. It was found that, for the same manganese concentration and increasing exciting wavelengths, the emission spectra shifted towards longer waves.

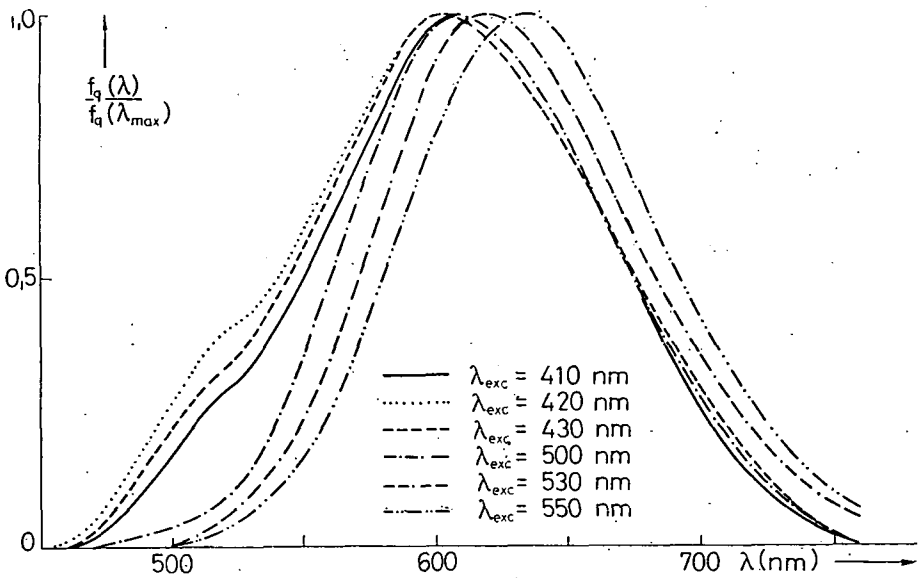

Fig. 1

Fig. 1 and 2 show the emission spectra of glasses containing 5.10^{-2} mole Mn^{2+} measured with different exciting wavelengths at room temperature and 100 °K respectively. For the sake of clearness, some of the measured spectra are not plotted in the figures. It can be seen that with exciting wavelengths generally used for these glasses (405—420 nm), the location of the red band remains essentially unchanged.

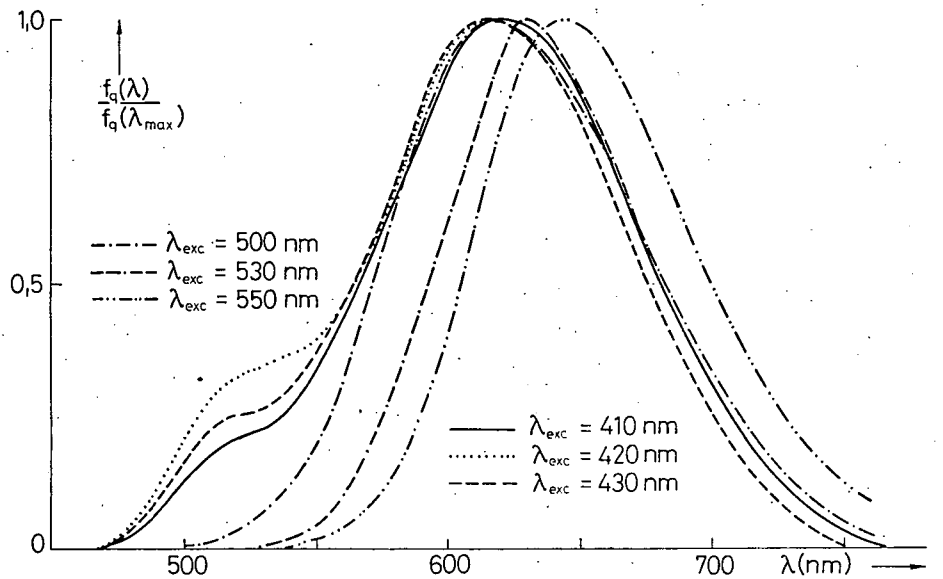

Fig. 2

The dependence on exciting wavelength of the green band is more interesting. By increasing the exciting wavelength, up to 420—425 nm, the relative intensity of the green band gradually increases; with higher exciting wavelengths it decreases again and practically disappears for about 490 nm. Dramatical changes in the red emission can be observed from 470 nm exciting wavelengths on. It seems remarkable that, with increasing activator concentration, the shift of the red band gradually decreases and the spectra converge to a "limiting" emission spectrum independent of concentration. Comparing Figs. 1 and 2, it can be seen that the above statements are valid for both temperatures, with the only difference that at 100 °K the emission spectra are more red for all exciting wavelengths than those measured at room temperature, and consequently a shift of about 20 nm can be observed also in the position of the maximum of the "limiting" spectrum. This is true for all concentrations.

The results of our measurements proved unequivocally that the influence of the exciting wavelength on the quantum distribution of the emission spectra is highly important; therefore the excitation spectra of these glasses are to be measured with special care. It is evident that the excitation spectra determined by monitoring only one wavelength or waveband of the emission spectrum are only approximatively valid for the whole range of excitation [8, 9].

The quantitative interpretation of the dependence on exciting wavelength seems to be complicated, though it appears reasonable to explain the shift of the emission spectra by supposing the existence of manganese centres of different absorptivity at different places of the glass.

* * *

The authors express their thanks to Prof. I. KETSKEMÉTY, Director of the Institute of Experimental Physics for his interest in the research work.

References

[1] *Ржевский, М. Б., В. П. Грибковский:* ЖПС, **16**, 76 (1972).
[2] *Ржевский, М. Б., М. И. Кузьменков, В. В. Печковский, С. В. Плышевский:* ЖПС, **17**, 1032 (1972).
[3] *Ржевский, М. Б., М. И. Кузьменков, В. В. Печковский, С. В. Плышевский:* ЖПС, **19**, 846 (1973).
[4] *Parke, S., A. I. Watson, R. S. Webb:* J. Phys. D: Appl. Phys. **3**, 763 (1970).
[5] *Szöllősy, L., T. Szörényi, K. Szanka:* Acta Phys. et Chem. Szeged **20**, 299 (1974).
[6] *Parker, C. A., C. G. Hatchard:* Analyst **87**, 664 (1962).
[7] *Melhuish, W. H.:* J. Opt. Soc. Am. **52**, 1256 (1962).
[8] *Szöllősy, L., T. Szörényi:* Acta Phys. et Chem. Szeged **17**, 135 (1971).
[9] *Bingham, K., S. Parke:* Phys. Chem. Glasses **6**, 224 (1965).

ЗАВИСИМОСТЬ СПЕКТРОВ ИЗЛУЧЕНИЯ МАГНИЙ-МЕТАФОСФАТНЫХ СТЕКОЛ, АКТИВИРОВАННЫХ Mn^{2+}, ОТ ДЛИНЫ ВОЛНЫ ВОЗБУЖДАЮЩЕГО СВЕТА

Л. Селлеши, Т. Сереньи, К. Санка

С помощью фосфороскопа и синхронного усилителя исследованы спектры люминесценции двухвалентного марганца в магний-метафосфатных стеклах для 4-х концентраций активатора при комнатной температуре и 100 °К при разных длинах волн возбуждающего света. Спекры излученя существенно отличаются друг от друга. Эти результаты, повидимому, подтверждают микрогетерогенное строение этих стекол.

HERSTELLUNG VON CdS-PHOTOWIDERSTANDEN AUS SAUREM MEDIUM DURCH SINTERN

Von

M. ZÖLLEI

Institut für Experimentalphysik der Attila—József-Universität, Szeged

(Eingegangen am 12. April. 1975)

In früheren Arbeiten berichteten wir über die Herstellung von CdS-Photowiderständen aus kolloidaler CdS-Lösung und aus wässeringer Suspension von CdS-Pulver sowie deren Sensibilisierung auf chemischem Wege. Um den Kreis der Aktivierungsstoffe zu erweitern, haben wir ein neues Sensibilisierungsverfahren ausgearbeitet, wodurch auch in Wasser schlecht, oder überhaupt nicht lösliche Aktivierungsstoffe in die CdS-Photowiderstände eingebaut werden können. Durch Suspendieren des CdS-Pulvers in einer sauren Lösung der Aktivierungsstoffe wurden Suspensionen erhalten, aus denen sich durch entsprechende Wahl der Dotierungskonzentration CdS-Photowidestände von hoher Lichtempfindlichkeit herstellen liessen.

Herstellung von CdS-Photowiderständen

Die in Wasser schlecht, oder überhaupt nicht lösbaren Aktivierungsstoffe wurden in 0,01—0,001 n HCl gelöst. Das CdS-Pulver (Schuchardt, 99,999% Reinheitsgerad) wurde in dieser Lösung suspendiert. Dadurch wurde, da das CdS-Pulver in verdünnten Säuren unlöslich ist, eine fein verteilte Suspension erhalten. Die gewünschte Dotierung wurde in die CdS-Schichten in zwei Schritten eingebaut: zuerst wurde die Suspension einige Tage stehen gelassen, damit die in der Lösung befindlichen Aktivierungsstoffe teilweise in die CdS-Teilchen eindiffundieren (dies läßt sich durch Erwärmen beschleunigen), dann wurde die Suspension auf mit Elektroden versehene Glasplatten aufgetragen und eingetrocknet. Um die gewünschte Dotierung endgültig einzubauen und die Lichtempfindlichkeit zu erreichen, wurden die eingetrockneten Schichten einer Wärmebehandlung unterworfen. Die Dauer der Wärmebehandlung und die angewandte optimale Temperatur sind von der Art der Dotierung abhängig.

Meßergebnisse und deren Diskussion

Die folgenden Daten beziehen sich auf mit Kupfer, bzw. mit Kupfer und Chlor sensibilisierte CdS-Photowiderstände.

Der „Dunkelwiderstand" der mit dem erwähnten Verfahren hergestellten CdS-Photowiderstände läßt sich, in Abhängigkeit von der Konzentration, der Dotierung und der Dauer der Wärmebehandlung, zwischen den Werten 10^{10} und $10^5\ \Omega$ ohne bedeutendere Änderung der Lichtempfindlichkeit der Präparate

ändern. Die Lichtempfindlichkeit der Präparate, deren Dunkelwiderstand niedriger als $10^5\,\Omega$ ist, wird durch die Wärmebehandlung stark verringert, und kann sogar ganz verschwinden. Bei Anwendung der experimentell bestimmten optimalen Temperatur konnten Präparate hergestellt werden, die in Abhängigkeit vom Abstand der Elektroden und von der Schichtdicke, bei 1—500 V Spannung mit stromstärken von einigen μA bis 10 mA belastet werden konnten.

Im folgenden teilen wir die spektrale Verteilung einiger mit in Wasser unlöslichen (oder nur in sehr geringem Masse löslichen) Kupferverbindungen hergestellten CdS-Photowiderstände mit.

Wie aus Abb. 1. (Kurve *a*) ersichtlich, verschwindet das für „reine" CdS-Photowiderstände charakteristische Maximum um 510 nm [3—5] infolge der CuS-Dotierung fast ganz und es erscheint ein neues Maximum bei etwa 660 nm. Die

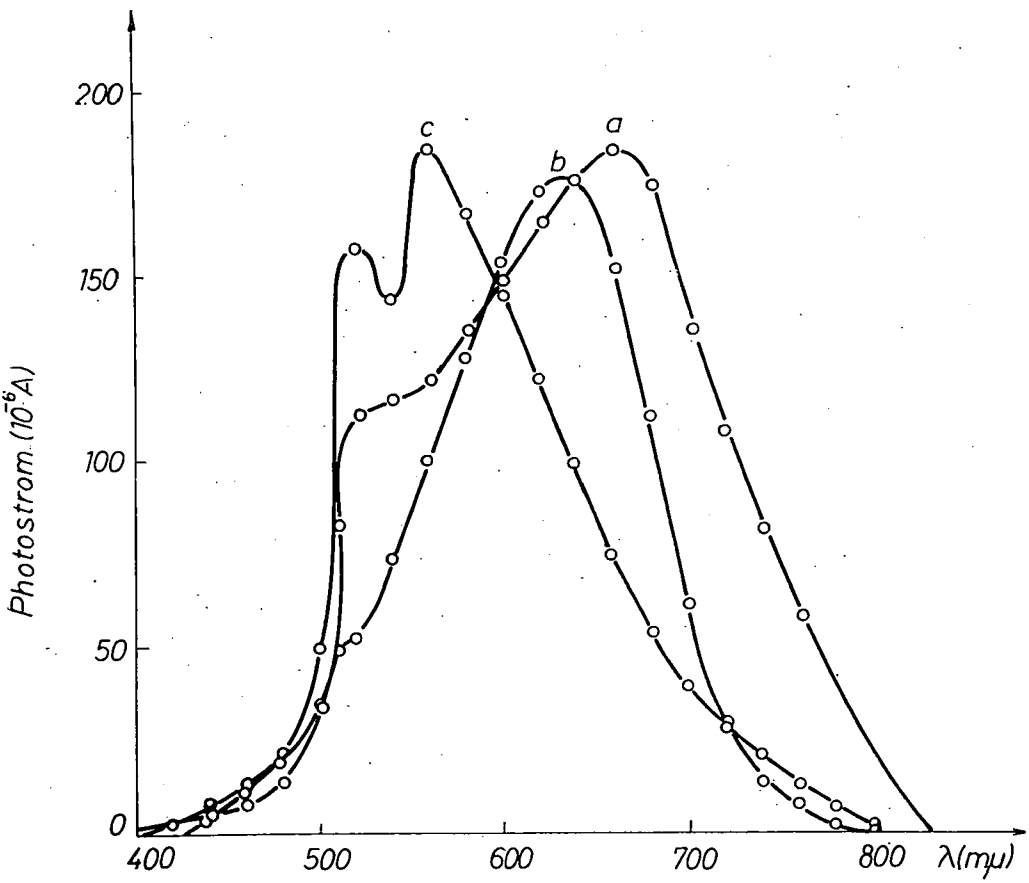

Abb. 1. Spektrale Verteilung der Lichtempfindlichkeit von *a)* mit Kupfersulfid, *b)* mit Kupferzyanid, *c)* mit Kupferazetat sensibilisierten CdS-Photowiderständen

maximale Lichtempfindlichkeit läßt sich auf zweierlei Wegen erreichen: durch längeres Ausglühen (1—2 Stunden) bei einer mäßigeren Temperatur oder durch kürzeres Ausglühen (1—10 Minuten) bei höherer Temperatur.

Das für „reine" CdS-Photowiderstände charakteristische Maximum verschwindet auch im Falle einer Kupferzyanid-Dotierung; es erscheint nur eine kleine Schulter zwischen 515—520 nm (Kurve *b*). Das neue Maximum liegt bei 640 nm. Ein Vergleich der beiden Kurven zeigt, daß die Kurve der spektralen Verteilung des mit Kupfercyanid dotierten Präparates steiler ansteigt als diejenige des mit CuS aktivierten Präparates.

Die spektrale Verteilung der Lichtempfindlichkeit der mit Kupferazetat aktivierten Präparate zeigt zwei Maxima bei 520 und 540 nm.

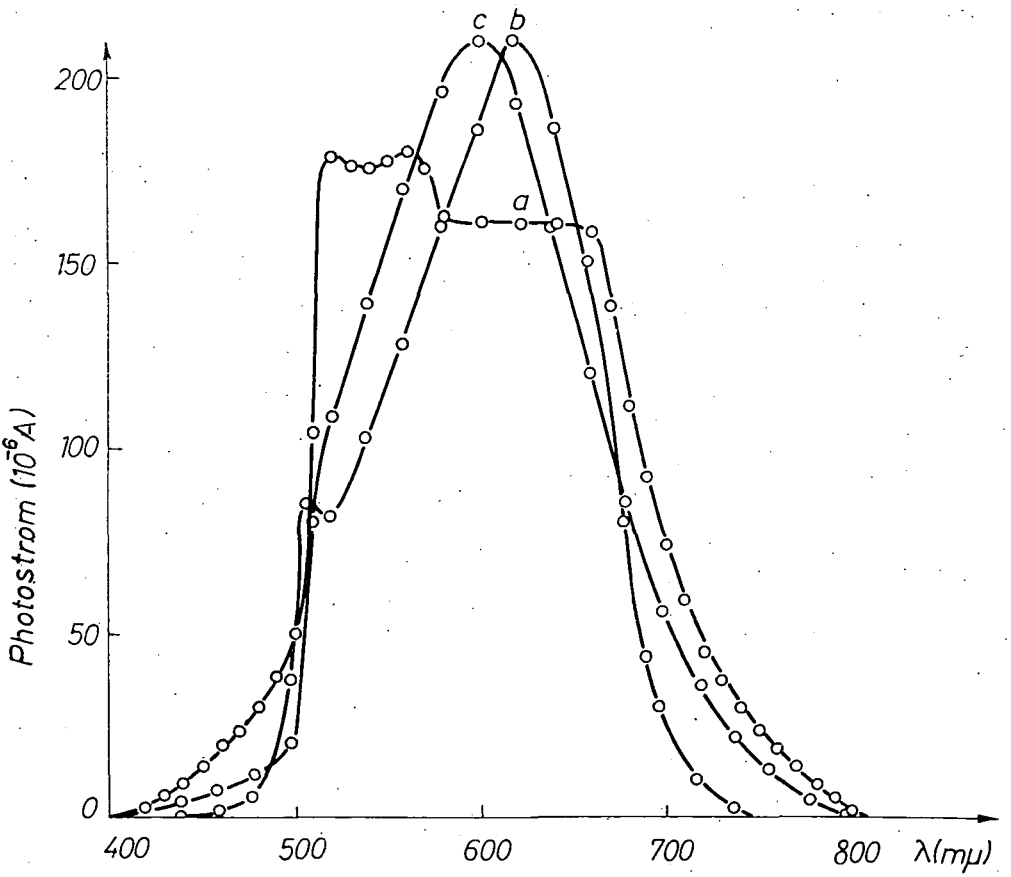

Abb. 2. Spektrale Verteilung der Lichtempfindlichkeit von *a)* mit Kupferkarbonat und Ammoniumchlorid, *b)* mit Kupferazetat und Kadmiumklorid, *c)* mit Kupferazetat und Ammoniumchlorid sensibilisierten CdS-Photowiderständen

Wir untersuchten die aktivierende Wirkung von zahlreichen Kupferverbindungen; die hier angeführten Beispiele zeigen, daß sich mit verschiedenen Kupferverbindungen CdS-Photowiderstände von verschiedener spektraler Lichtempfindlichkeit herstellen lassen. Durch Einbau einer doppelten Dotierung ist es möglich, die spektrale Empfindlichkeit der CdS-Photowiderstände weiter zu variieren. Es ist zu bemerken, daß durch doppelte Dotierung außer der Änderung der spektralen Empfindlichkeit auch eine bedeutende Steigerung der Lichtempfindlichkeit erreicht werden kann.

Um doppelte Dotierung mit Kupfer und Chlor zu erhalten, wurde in den erwähnten Kupfersuspensionen NH_4Cl und $CdCl_2$ in entsprechenden Mengen gelöst. Im folgenden zeigen wir die spektrale Verteilung der Lichtempfindlichkeit einiger aus solchen Suspensionen hergestellten CdS-Photowiderstände.

Aus Abb. 2. (Kurve *a*) ist die spektrale Verteilung der Lichtenpfindlichkeit des mit Kupferkarbonat und Ammoniumchlorid aktivierten Präparates ersichtlich, die von den vorerwähnten bedeutend Abweicht. Die Lichtempfindlichkeit ist zwischen 580—600 nm fast konstant, was für die praktische Anwendung interessant sein kann.

Die spektrale Verteilung der Lichtempfindlichkeit der mit Kupferazetat und Kadmiumchlorid, bzw. der mit Kupferazetat und Ammoniumchlorid sensibilisierten Präparate zeigen Kurven *b* und *c* der Abb. 2. An Kurve *b* ist das charakteristische Maximum noch gut sichtbar, aber das zweite Maximum ist bedeutend höher und der Anstieg der Kurve ist sehr steil. Kurve *c* zeigt nur ein Maximum. Infolge der kombinierten Wirkung von Kupfer und Chlor nimmt die Lichtempfindlichkeit so stark zu, daß das charakteristische Maximum auch ganz verschwinden kann. Die Stelle des zweiten Maximums ist in beiden Fällen von der Konzentration der Dotierung abhängig. Durch kombinierte Anwendung der Kupfer- und Chlor-Dotierung kann die Lichtempfindlichkeit der schichten in Richtung der längeren Wellen verschoben werden.

Mit der mittels Kupfer durchgefürten Aktivierung von mit verschiedenen Verfahren (Aufdampfen, Einkristallzüchlung, Pressen, usw.) hergestellen CdS-Photowiderstände haben sich zahlreiche Forscher beschäftigt. Mit den früheren, nur teilweise beschrieberen technischen Verfahren erwies sich aber der Einbau der gewünschten Dotierung und die Einstellung der entsprechenden Konzentration in vielen Fällen als sehr schwierig. Der Vorteil des von uns beschriebenen Verfahrens besteht darin, daß alle Aktivierungsstoffe in beliebiger Konzentration in das Präparat eingebaut werden können, und daß die spektrale Verteilung der Lichtempfindlichkeit der Präparate sich durch Änderung der Konzentration, der Temperatur und der Dauer der Wärmebehandlung in einem ziemlich breiten Intervall der Wellenlängen ändern läßt. Durch die Wirkung der eingebauten Aktivierungsstoffe kann die Stelle der sich ausbildenden Maxima von 520 nm bis zu 660—680 nm geändert werden; durch kombinierte Anwendung von Kupfer und Chlor läßt sich sogar erreichen, daß die Lichtempfindlichkeit in einem gewissen Gebiet des sichtbaren Spektrums konstant bleibt. Wie bereits erwähnt, kann es mit Hinsicht auf praktische Anwendungen nützlich sein, daß sich der „Dunkelwiderstand" um mehrere Größenordnungen ändern läßt.

Ein weitere Vorteil der Verfahrens besteht darin, daß es nicht nur zur Herstellung und Sensibilisierung von CdS-Photowiderständen, sondern auch im Falle anderer Sulfide und Selenide anwendbar ist.

* * *

Der Verfasser ist Herrn Professor Dr. I. KETSKEMÉTY, Direktor des Institutes für Experimentalphysik und Herrn Professor Dr. L. SZALAY, Direktor des Institutes für Biophysik für die Unterstützung der Arbeit zu aufrichtigem Dank verppfichtet.

Literatur

[1] *Zöllei, M.:* Acta Phys. et Chem. Szeged **3**, 21 (1957).
[2] *Zöllei, M.:* Acta Phys. et Chem. Szeged **17**, 29 (1971).
[3] *Weith, W.:* Z. angew. Physik **7**, 1 (1955).
[4] *Bube, R. H., S. M. Thomsen:* J. Chem. Phys. **23**, 1, (1955).
[5] *Avinor, M.:* Thesis, University of Amsterdam (1959).

ПОВЫШЕНИЕ ЧУВСТВИТЕЛЬНОСТИ СПЕЧЁННЫХ CdS-ФОТОСОПРОТИВЛЕНИЙ ПУТЁМ ОБРАБОТКИ ИХ В КИСЛОЙ СРЕДЕ

М. Зёллеи

В предыдущих работах сообщалось об изготовлении и улучшении чувствительности путём химической обработки CdS-фотосопротивлений, полученных из коллоидного раствора CdS и из водной суспензии порошка сульфида кадмия. С целью повышения чувствительности разработан новый способ и предложено решение проблемы внедрения нерастворимых или частично растворимых материалов в объём CdS-фотосопротивлении.

Размешиванием активирующего материала в порошке CdS, получена суспензия, из которой, подобрав соответствующую концентрацию активатора, изготовлены высоко фоточувствительные CdS-фотосопротивления.

PHYSICO-CHEMICAL STUDIES ON THE METHACYCLINE-TRIS[HYDROXYMETHYL]-AMINOMETHANE SYSTEM

By

G. L. SZEPESY and I. L. KAHÁN

Central Laboratory and Department of Ophthalmology, University Medical School, Szeged

(Received September 22, 1975)

The MOTC-TRIS system was studied potentiometrically, cryoscopically and photometrically.

Potentiometric titration of MOTC with TRIS revealed one larger and seven smaller potential changes in the mV *vs.* 10^C curves. These changes occurred at identical TRIS:MOTC molar ratios, whatever the MOTC or TRIS concentration was. Accordingly, it may be supposed that one MOTC molecule may bind a maximum of five TRIS molecules.

As to the nature of the bond between MOTC and TRIS, the experimental and calculated cryoscopic data suggest it to be ionic.

Spectroscopic investigation gave some evidence that the binding of MOTC to protein was not hindered by the presence of TRIS. According to the increase in $d\varepsilon_{max}$, TRIS may enhance the ionization of MOTC.

As well known, tetracyclines are a group of broad-spectrum antibiotics, widely employed in medical practice. The tetracyclines are amphoteric compounds and therefore tend to be soluble in aqueous acid or aqueous base, but they exhibit extremely low solubility near their isoelectric points. The requirement for general medical employment, especially for injections, is a sufficiently high concentration and neutral pH. One way of meeting this requirement is to form derivatives with higher solubility in near-neutral or slightly-basic solution. For this purpose either the complex-forming ability [1, 2] or the chemical reactions of the amide group of the tetracyclines [3] was utilized. These derivatives showed increased solubility at pH 4.0—8.0, enhanced stability against alkalis, and reduced acute toxicity, tissue irritation and rapid tissue diffusion.

The methacycline (MOTC) prepared by Blackwood *et al.* [4] has come into increasing therapeutical use because of its high antibiotic activity. Kahán and Hammer [5, 6] have given an account of observations that the concentration of tetracyclines in aqueous solution of tris[hydroxymethyl]-aminomethane (TRIS) could be as high as 10 per cent at ph 7.4—7.8; this mixed solution exhibited high antibiotic activity when examined *in vitro* or *in vivo* [7].

In the present paper this MOTC—TRIS system was studied to obtain information about the interaction between MOTC and TRIS. For this purpose potentiometric, cryoscopic and photometric experiments were carried out on the MOTC—TRIS system.

Materials and methods

The 6-methylene-5-hydroxytetracycline hydrochloride (methacycline hydrochloride, MOTC) was kindly supplied by the Pfizer Corporation, Eastern Europe Division, Belgium. The tris[hydroxymethyl]-aminomethane (TRIS), A grade, Lot No. 100909 and bovine plasma albumin, A grade, Lot No. 64761 were obtained from Calbiochem. These chemicals were used without further purification.

The potentiometric experiments were carried out with a RADIOMETER pH-Meter 26, together with a TITRATOR 11, an ABU 12 autoburette and an SBR 2 titrigraph.

The freezing point depressions were measured with a KNAUER Electronic Temperature Measuring Instrument, using a KNAUER Thermoelectric Cooling Unit equipped with a precision thermistor as temperature sensor. Throughout these experiments care was taken to use the same measuring vessel and identical sample volume. The spectra were determined with a BECKMAN DU Spectrophotometer, using 1 cm silica cells.

Results and discussion

Potentiometric experiments

To investigate the effect of TRIS on the MOTC molecules, two pH-titrations were carried out, using a glass electrode, with almost the same concentrations of MOTC, 0.1216 g/25 ml and 0.1291 g/25 ml, respectively. 0.5 M TRIS was used as titrant in both cases, and the recorder sensitivity was adjusted to 0.5 and 0.2 pH units/cm, respectively. The change in potential with volume of titrant added is small, except in the region of titration where some binding between the two molecules can be expected and a relatively great change in potential takes place. This means that the number of greater changes in the potential corresponds to the number of TRIS molecules bound to the MOTC molecule. The titration curves obtained are very similar to the common acid-base titration curves (Fig. 1), with one equivalence point. Accordingly, the molar rations of MOTC and TRIS were 0.99 and 0.98, respectively. No other pH jump was observed on the titration curves, and therefore a series of potentiometric titrations were run, using a plain platinum electrode against a calomel electrode as reference. In these experiments MOTC solutions

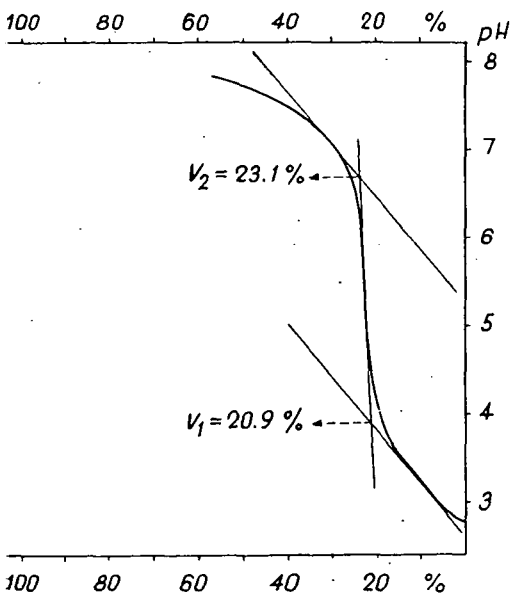

Fig. 1. pH-metric titration of MOTC; capacity of autoburette 2.5 ml (1 % = 0.025 ml)

of increasing concentration were titrated with 0.05, 0.1, and 0.5 M solutions of TRIS. Since the curves obtained were of similar type, it is sufficient to show only one (Fig. 2). Each curve consists of steep and mildly curving sections. This means that only one greater change in the potential took place due to the reaction of one molecule of TRIS with one molecule of MOTC, in agreement with the pH-titration results. Analysis of the region of small potential change was attempted *via* the first differential of the titration curve, but we failed to locate any other equivalence point owing to the extremely small potential change. Therefore, another method of analysis was used. The function between the potential and the logarithm of concentration being linear, a straightline plot is expected from exponential transformation. Thus, the potential data of the original curves were plotted against 10^C where C is the concentration, and the line of best fit was drawn using the least squares technique. All calculations were carried out with a type CII—10010 computer. As the same pattern was always obtained, only one plot is demonstrated (Fig. 3). Assuming that every change in the slope indicates further reaction of TRIS and calculating the corresponding concentrations, some information as to the number of bound TRIS molecules and the molar ratio of TRIS: MOTC may be expected. The results can be seen in Table 1. The greater change in the potential is caused when the quantities of TRIS and MOTC are equivalent, again in agreement with the results of pH-titration. These results show striking similarity to common acid-base titration, *i.e.* MOTC as an acid is titrated with TRIS as a base, and one molecule of MOTC forms a salt with one molecule of TRIS.

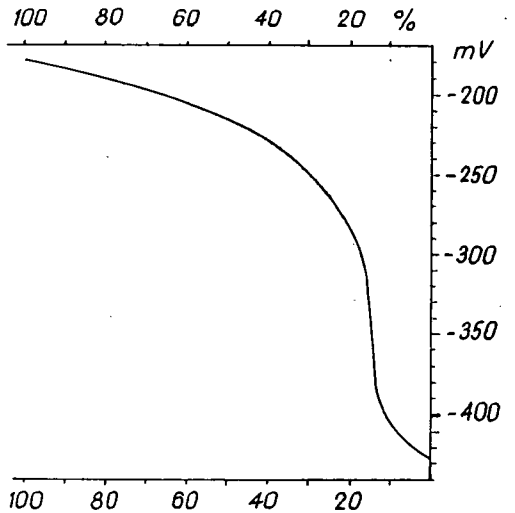

Fig. 2. Methacycline titrated with 0.1 M tris[hydroxymethyl]-aminomethane. Measured quantity 0.0172 g in distilled water Starting potential 430 mV; capcity of autoburette 2.5 ml (1 % = 0.025 ml)

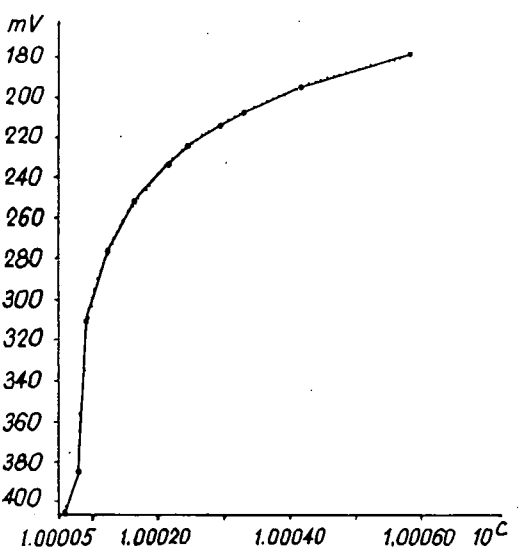

Fig. 3. 0.0172 g of MOTC (0.0000359 Mol) titrated with 0.1 M TRIS, plotted in mV *vs.* 10^C

The other changes in the potential, and accordingly in the slope, are much smaller but well discernible. The TRIS: MOTC molar ratios evaluated from the corresponding concentration of TRIS at these smaller changes of slope were 1.5, 2.0, 2.5, 30. 3.5, 4.0 and 5.0, respectively.

Cryoscopic experiments

From the potential *vs.* 10^C curves, the changes in the slopes were found to be increasingly smaller, which means that the bond between the MOTC and TRIS becomes weaker up to the fifth molecule of TRIS, whatever the nature of the bond itself. To throw light on this nature, a series of cryoscopic experiments were carried out. In these experiments first the freezing point depression of the pure solution of MOTC was measured at a given concentration. Then, increasing quantities of TRIS were added to the MOTC solution of the same concentration as before, so that the total TRIS concentration was twice, 2.5 times, 3.0 times, 3.5 times and 4.0 times that of the MOTC, keeping the volume and the concentration of MOTC constant. The freezing point depression was measured again. It should be noted that molality was used throughout these epxeriments. In addition the freezing point depressions were calculated theoretically, using the molecular freezing point depression value of 1.86 for water and the molal concentrations of all the molecular species separately. The values thus obtained were summed for each solution. The results can be seen in Table 2. Comparing the experimental and the calculated values in the case of a pure solution of MOTC, it was found that the former is twice the latter. This means that even in medium dilution the molecule undergoes complete dissociation to two ions, very probably $(MOTC)^+$ and Cl^-. In the further calculations, therefoer this dissociation was taken into consideration and the value for the Cl^- ion was added to the others. Comparison of the measured and calculated values now revealed good agreement for the MOTC—TRIS systems. This seems interesting because it means that in aqueous solution all of the bound TRIS molecules may dissociate and a highly ionized molecule of MOTC is formed. However, the possibility may arise that the TRIS molecules remain bound and their ionic dissociation contributes to the freezing point depression. This was settled in a separate experiment in which the freezing point depressions of pure TRIS solutions in various concentrations were determined. The experimentally found and calculated freezing point depression values are shown in Table 3, together with the increments in mole percent due to the ionic dissociation of the TRIS molecule. The increments were calculated by taking the given molality as one hundred percent and comparing this with the molality obtained from the measured depression of the freezing point. From the good agreement between the calculated and experimental freezing point depressions of the MOTC—TRIS system seen in Table 2, however, the conclusion may be drawn that the ionic dissociation of the TRIS molecule itself contributes little or not at all to the depression of the freezing point.

Spectroscopic experiments

Some spectroscopic experiments were carried out, partly to see the effect of TRIS on the light absorption of MOTC, and partly to obtain some information as to whether the TRIS exerts any influence on the bond between MOTC and protein. In these experiments care was taken that the pH's of the solutions to be

investigated should be practically identical. All of the solutions were therefore made in 0.02 M phosphate buffer, with a final pH 7.3—7.4. At such a phosphate concentration it was found that TRIS in a concentration of $2.5 \cdot 10^{-4}$ M did not have a substantial effect on the pH. This precaution was deemed necessary owing to the pH-dependence of the spectra of tetracyclines. Neither was any substantial change in pH found in the presence of MOTC at a concentration of $2.5 \cdot 10^{5}$ M. This MOTC concentration was used throughout all spectroscopic experiments. Thus the TRIS concentration, if present, was ten times that of the MOTC. Under these conditions, after determining the spectra of MOTC without and with TRIS, no change was found between 400 and 290 nm (wavelengths of maxima: 359 and 353 nm, with the optical density, $\varepsilon = 0.315$ at both wavelengths).

For the investigation of the bond between MOTC and protein, the best method seemed to be the evaluation of difference spectra [8]. The phosphate, MOTC and TRIS concentrations, and also the pH's were the same as before. The following spectra were determined separately: MOTC in phosphate buffer with and without TRIS, and the same with and without added albumin. The albumin concentration was $5 \cdot 10^{-5}$ M, *i.e.* twice that of the MOTC. Finally the absorption spectrum of albumin in the same concentration was also determined in phosphate buffer with and without TRIS. The given concentrations were kept constant in all solutions. The difference spectra themselves were obtained in the following way. First the values of the optical densities of the spectra of albumin with and without TRIS were subtracted from those of the spectra of MOTC with and without TRIS containing albumin at identical wavelengths. The differences thus obtained were again subtracted from the values of the optical densities of the spectra of MOTC in phosphate buffer with and without TRIS containing no albumin at all at the same wavelengths as before. These differences were plotted against wavelength (Fig. 4). The wavelengths of the maxima proved to be identical, but $d\varepsilon_{max}$ increased somewhat in the presence of TRIS. We may thus draw the conclusion that the presence of TRIS does not inhibit the binding of MOTC to protein. The higher $d\varepsilon_{max}$ may be attributed to the somewhat higher ionization of MOTC.

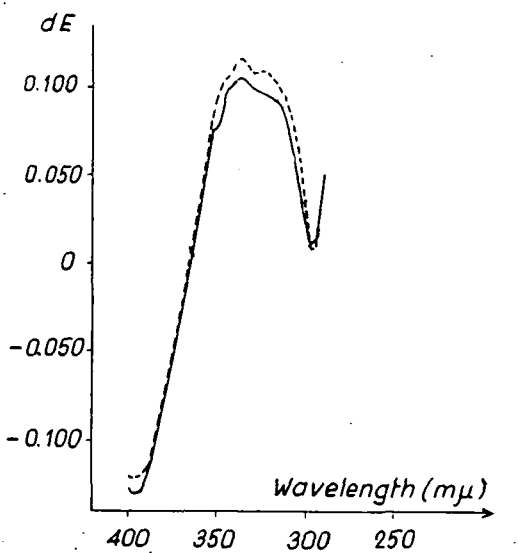

Fig. 4. Difference spectra of MOTC-albumine system: ——— without TRIS; ------- with TRIS

Table I

TRIS:MOTC molar ratios calculated from the mV vs. 10^c curves

TRIS molarity	0.05	0.05	0.1	0.1	0.1*	0.5	0.5	0.5
Grams of MOTC·10^{-3}	9.78	11.3	17.2	23.5	34.5	96.1	94.0	100.8
MOTC molarity·10^{-5}	2.04	2.36	3.59	4.9	7.2	20.0	19.63	21.05
Molar ratios	1.051	1.016	1.072	1.080	0.992	1.045	1.090	1.045
	1.418	1.546	1.489	1.487	1.485	1.432	1.548	1.520
	2.054	2.033	1.999	1.976	1.985	2.057	1.959	1.995
	2.495	2.500	2.589	2.567	2.471	2.507	2.427	2.446
	3.106	2.923	2.979	3.077	3.026	3.070	3.026	2.992
	3.473	3.432	3.508	3.545		3.470	3.530	3.553
	3.962	3.995	3.968	3.953		3.970	4.126	3.957
	4.867	5.000	4.998	4.809		4.970	5.114	4.973

* The measured quantity of MOTC turned out to be too large in relation to the concentration of TRIS, so the capacity (2.5 ml) of the autoburette ran out before the end of the titration.

Table II

Values of freezing point depression

$(MOTC)^+$ Molality	Cl^- Molality	TRIS Molality	Depression of freezing point in °C	
			Calculated	Found
0.0120	0.0120	—	0.0447	0.0435
0.0120	0.0120	0.0240	0.0894	0.0892
0.0120	0.0120	0.0301	0.1007	0.0988
0.0120	0.0120	0.0361	0.1119	0.1101
0.0120	0.0120	0.0422	0.1232	0.1216
0.0120	0.0120	0.0482	0.1344	0.1343

Table III

Values of freezing point depression

Depression of freezing point in °C		Concentration of TRIS in molality		Mole precent increment
Found	Calculated	Measured	Calculated	
0.1049	0.0950	0.0511	0.0564	10.4
0.0876	0.0782	0.0420	0.0471	12.0
0.0814	0.0670	0.0360	0.0438	21.5
0.0395	0.0223	0.0120	0.0212	76.8

References

[1] *Neumann, H., P. Viehmann:* Arzneim.-Forsch. **9**, 711 (1959).
[2] *Remmers, E. G., W. C. Barringer, G. M. Sieger, A. P. Doerschuk:* J. of Pharmaceutical Sciences, **53**, 1452, 1534 (1964).
[3] *Siedel, W., A. Soder, F. Liner:* Muench. Med. Wochschr., **17**, 661 (1958).
[4] *Blackwood, R. K., J. J. Beereboom, H. H. Rennhard, M. Schach v. Wittenau, C. R. Stephans:* J. Am. Chem. Soc. **83**, 2773 (1961).
[5] *Kahán, I. L., H. Hammer:* Chemotherapy **20**, 148 (1974).
[6] *Kahán, I. L., H. Hammer:* Arzneim.-Forsch. **25**, 234 (1975).
[7] *Kahán, I. L., I. Pápai, H. Hammer:* Graefes Arch. klin. exp. Ophthal., **190**, 257 (1974).
[8] *Perényi, T., L. Biró, M. Arr:* 7th FEBS Meeting, Madrid (1969).

ФИЗИКО-ХИМИЧЕСКОЕ ИЗУЧЕНИЕ СИСТЕМЫ МЕТАЦИКЛИН—ТРИС(ГИДРОКСИМЕТИЛ) АМИНОМЕТАН

Г. Л. Сепеши, И. Л. Кахан

Проведено потенциометрическое, криоскопическое и фотометрическое изучение системы МОТЦ-ТРИС.

Потенциометрическое титрование МОТЦ-а ТРИС-ом дало один большой и семь менее значительных скачков потенциала на кривых мв. -10^{c}. Эти изменения наблюдались при одинаковых мольных соотношениях МОТЦ-а и ТРИС-а, независимо от их концентрации. На основании этих данных предположено, что одна молекула МОТЦ-а может связывать максимально пять молекул ТРИС-а.

Полученные экспериментальные и расчетные криоскопические данные позволяют предположить наличие ионной связи между молекулами МОТЦ-а ТРИС-а.

Спектроскопическими измерениями показано, что связывание МОТЦ-а к белку не затрудняется присутствием ТРИС-а. Увеличение значений $d\varepsilon_{\text{макс}}$ указывает на вероятность того, что в присутствии ТРИС-а степень ионизации МОТЦ-а возрастает.

THE MASS SPECTRUM OF CH_3CDO

By

I. SZILÁGYI, T. BÉRCES and I. BÁRDI

Gas Kinetics Research Group of the Hungarian Academy of Sciences, Szeged

(Received 26 June, 1975)

A mixture of deuterated acetaldehydes containing CH_3CDO in a high percentage was prepared and the mass spectrum of the sample was investigated. After correcting for the contributions of the various isotopic impurities, the spectrum of CH_3CDO was obtained, and on this basis important fragmentation processes are discussed.

Introduction

The use of isotopes may supply valuable information in the solution of various chemical problems. Methods like isotope labelling, the kinetic isotope method [1], the isotope dilution method, etc., prove to be especially useful in the elucidation of the mechanisms of complex chemical reactions and in the determination of important kinetic data.

The investigation of the kinetics of the acetaldehyde pyrolysis [2] drew our attention to certain problems of the mechanism which could be studied by the deuterium labelling technique. These experiments required the preparation of CH_3CDO, determination of the isotopic composition of the labelled sample and detailed knowledge of the mass spectrum of CH_3CDO.

The mass spectrum of CH_3CDO had been studied previously [3] using a sample which consisted of various deuterated and undeuterated aldehyde species. The reinvestigation of the spectrum with aldehyde of better isotopic purity seemed to be desirable in order to minimize the corrections permitting to take into account the contributions from aldehyde species of different deuterium content.

In this paper the mass spectrometric study of a mixture of deuterated acetaldehydes containing CH_3CDO in a high percentage is described, and the spectrum of CH_3CDO obtained from the analysis of the experimental data is given.

Experimental

The labelled acetaldehyde sample was prepared by the method of LEITCH [4], *i.e.*

$$CH_3CH_2NO_2 \underset{}{\overset{D_2O}{\rightleftharpoons}} CH_3CD_2NO_2$$

$$CH_3CD_2NO_2 \underset{273\,K}{\overset{H_2SO_4}{\rightleftharpoons}} CH_3CDO + HDO + N_2O$$

Some modification of the original procedure was found to improve the isotopic purity of the CH_3CDO prepared. This is described below.

The nitroethane (FLUKA, ≧95%) was distilled prior to use. The main fraction (b.p. 385.5—386.5 °K) was only used. Equal amounts of $CH_3CH_2NO_2$ and D_2O (FLUKA, p.a., ≧99.8%) with some sodium acetate added were placed in a three-necked flask equipped with a stirrer and a reflux condenser. The system was carefully protected from moisture. H—D exchange was carried out at 363 °K under vigorous stirring. The extent of the exchange was checked from time to time by mass spectrometric analysis. The heavy water sample was replaced by a fresh one when the process seemed to approach equilibrium. This was done three times during the procedure which lasted altogether about 250 hours. Thereafter the organic phase was dried over sodium sulfate and distilled. The labelled aldehyde was obtained from $CH_3CD_2NO_2$ in the same way as described in LEITCH's paper. After drying over sodium sulfate, the sample was purified by bulb-to-bulb vacuum distillation. No chemical impurities could be detected by gas chromatography.

Acetaldehyde (FLUKA, p.a., ≧99.8%) was purified by bulb-to-bulb distillation.

Mass spectra were obtained on a FINNIGAN 1015 S/L quadrupole instrument. All spectra were taken at an ionizing voltage of 70 eV, the electron current was 250 μA. The instrument was equipped with an electron multiplier detector. Spectra were recorded in the mass range of 1—55 by a three-channel light beam oscillograph (relative sensitivities being 1:10:100), with a scanning-time of 10 s per mass range.

The spectra of labelled and normal acetaldehyde were taken shortly one after the other in order to obtain well comparable results.

Results and discussion

Corrections and pressure dependence. The recorded spectra were corrected for (*i*) the background, (*ii*) the natural abundances of isotopes, and (*iii*) for the pressure-dependent character of certain ions.

The background was negligible, except for measurements made at low aldehyde pressures in the ion-source. In these cases the spectra had to be corrected for the presence of traces of air and water. All spectra were corrected for the natural abundances of ^{13}C and ^{18}O.

The results given below were obtained under conditions where the pressure in the ion-source was fixed at a value of $6 \cdot 10^{-6}$ torr. In a few measurements, however, the pressure was varied between $7 \cdot 10^{-7}$ and $1 \cdot 10^{-5}$ torr. It was found that the relative intensities (compared to the intensity of the parent ion) of ions at m/e 48 and 47 in the spectra of the labelled aldehyde sample and those at m/e 45 in the spectra of normal acetaldehyde increased with increasing pressure. It is to be noted that the parent or molecular ions (designated as p^+) of acetaldehyde-d_2, acetaldehyde-d_1 and acetaldehyde-d_0 give peaks at m/e 46, 45, and 44, respectively, while the pressure-dependent ions were observed at masses $(p+D)^+$ and $(p+H)^+$ in the spectra of the labelled and the normal aldehyde, resp., *i.e.* at m/e 48, 47, and 45. Therefore it was concluded that the ions showing pressure-dependence are formed in ion-molecule reactions. The intensities measured for these ions at $6 \cdot 10^{-6}$ torr were corrected by multiplying with the ratio (I_{p+D}/I_p) and (I_{p+H}/I_p), respectively, obtained at the lowest pressures studied.

Isotopic composition of the labelled acetaldehyde sample. Determination of the isotopic composition of the labelled acetaldehyde sample was based on the assumption that the specific intensity (the intensity observed at a fixed pressure in the ion-source) of the molecular ion is the same for CH_3CHO and different deuterated acetaldehyde species. This assumption was shown by BRINTON and BLACET [3] to be applicable in case of various acetaldehyde species.

In the spectrum of the labelled acetaldehyde sample, contributions to ion intensities at m/e 48 to 44 are expected from the parent ions of normal and deuterated acetaldehyde species as well as from fragment ions of the deuterated aldehydes. In order to obtain the relative abundance of the various acetaldehyde species, the measured intensities have to be corrected by substracting the contributions of the fragment ions. However, the spectra of the deuterated aldehydes are not readily available, therefore assumed relative abundances for compounds of higher deuterium content were used (Table I). While this approximation is accurate enough for acetaldehyde-d_2, acetaldehyde-d_3 and acetaldehyde-d_4 present in small quantities in the labelled sample, a different treatment is required for acetaldehyde-d_1 which is the major component (see below).

Table I

Assumed[a]) relative intensities for acetaldehyde-d_2, acetaldehyde-d_3 and acetaldehyde-d_4 in the m/e range 48—44

m/e	aldehyde-d_2	aldehyde-d_3	aldehyde-d_4
48			1000
47		1000	—
46	1000	34	400
45	68	400	—
44	400	36	100

[a] Obtained by extrapolation from known spectra of CH_3CHO and the labelled aldehyde sample

In the second column of Table II intensities of ions measured at m/e 48 to 44 of the labelled acetaldehyde spectrum are given. After correction for fragment ion contributions originating from the acetaldehyde-d_2, acetaldehyde-d_3 and acetaldehyde-d_4 present in the sample, the data given in column 3 are obtained. The figure given for m/e 44 still contains the contribution of the fragment peak of acetaldehyde-d_1, which can be calculated on the basis of the assumption that the specific intensities of the parent ions of the various acetaldehyde species are the same.

Table II

Peak heights at masses 48—44 in the spectrum of the labelled acetaldehyde sample

m/e	Corrected for background and natural abundances of ^{13}C and ^{18}O	Corrected for fragmetns of aldehyde-d_2, -d_3 and -d_4	Peak heights of parent ions
48	~0.1	~0.1	~0.1
47	0.7	0.7	0.7
46	4.1	4.0	4.0
45	245	244	244
44	25	23.4	7.2

The sum of the peak heights[1] given in column 3 is 272.2 which compared with the peak height of 256 measured at mass 44 in the spectrum of CH_3CHO yields 16.2 for the required fragment ion intensity of acetaldehyde-d_1. Hence, the parent ion intensities (peak heights) given in the last column of Table II are derived.

[1] Peak heights were obtained from spectra taken at identical ion-source pressures of $6 \cdot 10^{-6}$ torr.

It has been shown by BRINTON and BLACET [3] that the parent peak intensities can be used as a measure of the relative abundance of the various acetaldehyde species present in the sample. With this postulate on the basis of results given in the last column of Table II the isotopic composition of the labelled aldehyde sample was obtained:

2.8% acetaldehyde-d_0	0.3% acetaldehyde-d_3
95.3% acetaldehyde-d_1	<0.1% acetaldehyde-d_4
1.6% acetaldehyde-d_2	

Regarding the position of the deuterium atom (or atoms) in the aldehyde molecule, a comparison of the heavy and light formyl ion intensities may supply information. At the electron bombardment of the labelled aldehyde sample, ions at m/e 30 are formed from formyl deuterated species by simple fission of the C—C bond. However, the situation is more involved regarding the formation of ions at mass 29. The presence of a peak at m/e 29 in the spectrum of CH_3CDO (see below) indicates that H—D exchange occurs before or simultaneously with fragmentation. Thus, ions of mass 29 are formed in case of the labelled aldehyde sample in two ways: by simple C—C spliting from aldehydes containing a CHO group, and by a process involving H—D exchange from aldehydes having a CDO functional group.

The ratio of the number of molecules with CHO and CDO groups can be estimated from the intensities (I) measured at m/e 29 and 30: (number of CHO groups)/(number of CDO groups)$=(I_{29}-0.072I_{30})/I_{30}$, where 0.072 is the intensity ratio at m/e 29 and 30 in the spectrum of pure CH_3CDO.

Using intensities obtained at m/e 29 and 30 with the labelled aldehyde sample, the value 0.027 for the ratio (number of CHO groups)/(number of CDO groups) can be calculated, which means that 2.6 per cent of the molecules contain undeuterated formyl groups. This value is equal, within the limits of experimental error, with the value found for the CH_3CHO content of the sample studied. Hence we conclude that the formyl group in heavy aldehyde molecules is virtually fully deuterated. Thus the composition of the labelled aldehyde sample may be given as

2.8% CH_3CHO	1.6% CH_2DCDO	<0.1% CD_3CDO
95.3% CH_3CDO	0.3% CHD_2CDO	

Mass spectrum of CH_3CDO. The spectra of the labelled acetaldehyde sample and of CH_3CHO are shown in columns 3 and 2, resp., of Table III. The peak heights given are corrected for the background and for the natural abundances of ^{13}C and ^{18}O isotopes.

In order to derive the spectrum of CH_3CDO from that of the labelled aldehyde sample, the contributions from isotopic species other than CH_3CDO have to be substracted. Since the amount of CD_3CDO and CHD_2CDO was found to be small, only the contributions of their parent ions (at mass 48 and 47) were taken into account. Correction for the presence of 1.6% CH_2DCDO was made on the basis of an assumed spectrum (relative intensities): 1000(m/e 46), 400(m/e 44), 1350(m/e 30), 300(m/e 17), and 400(m/e 16). Contributions from the 2.8 per cent of CH_3CHO were calculated by means of the measured spectrum of acetaldehyde. In this way the spectrum for pure CH_3CDO, given in columns 4 and 5 was obtained. For comparison, the last column of Table III contains the spectrum of CH_3CHO.

Table III

The mass spectrum of CH_3CDO

m/e	CH_3CHO (peak heights)	Labelled sample (peak heights)	CH_3CDO (peak heights)[a]	CH_3CDO (relative intensities)	CH_3CHO (relative intensities)
48		~0.1			
47		0.7			
46		4.1			
45		245	244	1000	
44	256	25	16	66	1000
43	138	99	95	389	539
42	34	27	26	107	133
41	14	10	9	37	55
30		333	328	1343	
29	330	33	24	97	1289
28	11	21	21	86	43
27	14	21	21	86	55
26	26	13	12	49	102
25	11	6	6	25	43
17	2	18	17	70	8
16	22	69	67	275	86
15	171	101	96	393	668
14	59	27	25	103	230
13	20	12	11	45	78
12	8	7	7	29	31

[a] For derivation see text.

A detailed study of the spectrum of CH_3CDO has been published by BRINTON and BLACET [3]. The spectra obtained by these authors and in the present work agree in the main features but some differences are to be pointed out. There are differences in two mass ranges of the spectra; these are the m/e range 30—27 and 17—13. In both ranges we find lower intensities relative to the parent ion intensity. Similar differences occur at m/e 29—28 and 16—13 in the spectrum of CH_3CHO reported by BRINTON and BLACET [3] and that obtained in the present work. It seems that the cause for this is related to the different experimental conditions rather than to the dissimilar isotopic purity of the samples investigated.

Fragmentation processes. The main fragmentation processes for both CH_3CDO and CH_3CHO are the formation of formyl-type ions by the simple split of the C—C bond of the molecules. However, these processes were found to be somewhat less important than suggested by BRINTON and BLACET [3]. The appearance of the CHO^+ ion in the spectrum of CH_3CDO clearly indicates that H—D exchange occurs between the methyl and formyl groups before or simultaneously with fragmentation. The ratio of probability of the C—C fission accompanied by H—D exchange to that of simple C—C fission was found to be 0.072 in good agreement with the value of 0.079 derived from the spectrum of BRINTON and BLACET.

Another question of importance is the formation of methane and methyl ions from CH_3CDO. Assuming that the contribution of OH^+ is the same in the case of CH_3CDO and CH_3CHO, a value of about 62 for the relative intensity of the CH_3D^+ ion can be estimated. High intensity is found at mass 16 in the spectrum

of CH_3CDO, which is not fully explained by the formation of O^+. Taking $O^+ < 86$ (from the spectrum of CH_3CHO) is obtained $CH_2D^+ > 189$, *i.e.* CH_2D^+ ions are formed from CH_3CDO with considerable probability. The deuterated methyl ion may be formed provided H—D exchange occurs before or simultaneously with the split of the C—C bond. (Note that H—D exchange also accompanies the C—C split yielding a formyl-type ion). Ions of mass 15 might be CH_3^+ and CHD^+, the relative probabilities of which are difficult to estimate. Thus we can give only the upper limit $CH_3^+ < 393$. Hence, $CH_2D^+/CH_3^+ > 0.5$, *i.e.* a considerable portion of the methyl radicals are formed in a process involving H—D exchange between the methyl and formyl groups.

Table IV

Relative probabilities for parent-, formyl-, and methyl-type ion formation

	Parent ion	Formyl-type ion	Methyl-type ion
CH_3CHO	1000	1289	668
CH_3CDO	1000	1440	580

Finally, in Table IV the probabilities of formation of formyl-type (CHO^+ and CDO^+) and methyl type (CH_3^+ and CH_2D^+) ions are given relative to that of the corresponding parent ions. Formyl formation is more probable from CH_3CDO than from CH_3CHO, while for the methyl formation the opposite seems to be true.

References

[1] *Neiman, M. B., D. Gál:* „The Kinetic Isotope Method and its Application", Elsevier Publ. Co., Amsterdam, 1971.
[2] *Bárdi, I., F. Márta:* Acta Phys. et Chem. Szeged **19**, 227 (1973).
[3] *Brinton, R. K., F. E. Blacet:* J. Chem. Phys. **17**, 797 (1949).
[4] *Leitch, L. C.:* Can. J. Chem. **33**, 400 (1955).

МАСС-СПЕКТРЫ CH_3CDO

И. Силади, Т. Берцеш, И. Барди

Синтезирована смесь дейтерированных ацетальдегидов с высоким содержанием CH_3CDO и проведено ее масс-спектрографическое изучение. С учетом необходимых поправок на вклады различных изотопных загрязнений, определен спектр чистого CH_3CDO и обсуждены наблюдавшиеся основные фрагментационные процессы.

ИССЛЕДОВАНИЕ СТРУКТУРЫ И СВОЙСТВ МЫЛ, I

Инфракрасный спектр лаурата кальция, полученного реакцией на границе раздела фаз эмульсионной системы

И. А. АНДОР

Институт общей и физической химии университета им. Аттилы Йожефа, Сегед

Я. КИШ

Кафедра органической химии университета им. Аттилы Йожефа, Сегед

(Поступило в редакцию 15 сентября 1975 г.)

Рассмотрен ИК-спектр лаурата кальция полученного методом реакции на границе раздела фаз динамической эмульсии (РГФ). На основании термогравиметрических, рентгеноструктурных и ИК данных установлено, что методом РГФ образуется моногидрат лаурата кальция с хорошо выраженной кристаллической структурой. Проведено отнесение основных характеристических частот поглощения лаурата кальция в сравнении со спектром лауриновой кислоты в твердой фазе. Обнаруженная серия полос в интервале частот от 1620 до 1520 $см^{-1}$, предлагается для характеристики структуры мыл и их гидратов.

В связи со значением и распространенностью применения различных мыл в современной технике, неудивительно то большое внимание, которое уделяется вопросам теории строения и практического применения мыл и различных сложных мыльных систем. Широко применяются различные мыла в нефтедобывающей, горно-рудной, металлообрабатывающей и в ряде других отраслей промышленности. Мыла металлов переменной валентности применяются также в качестве катализаторов различных жидкофазных химических процессов. Запросы техники требуют дальнейшее все более глубокое и детальное изучение структуры и свойств мыл и мыльных систем с целью разработки их теории, которая представила бы возможность нахождения теоретически обоснованных оптимальных решений различных практически важных проблем, вместо длительных эмпирических поисков приближенных решений.

Проведенное нами ранее изучение свойств трехкомпонентных систем кальциевых мыл жирных кислот, полученных методом непосредственной нейтрализации кислоты гидроокисью на границе раздела фаз эмульсии вода-масло [1, 2], и применение нами мыл металлов переменной валентности в сложных синтезах полимеров, побудило нас к проведению детального исследования структуры различных мыл. Выяснение особенностей структуры мыл должно способствовать получению возможности целеустремленных синтезов и управления свойствами различных мыльных систем.

Инфракрасная спектроскопия, позволяющая не только идентифицировать вещества, но дающая весьма ценную информацию о структуре молекул и

кристаллов широко применялась к изучению жирных кислот и их эфиров [3—6], в значительно меньшей мере к мылам щелочных металлов [7—10] и сравнительно мало данных относительно ИК-спектров мыл многовалентных металлов [11—14].

Задача данной работы заключалась в ИК-спектроскопическом анализе продукта нейтрализации лауриновой кислоты гидроокисью кальция на границе раздела фаз динамической эмульсии, в отнесении основных полос поглощения спектра, снятого в *KBr*-ных таблетках, и в поиске характерных полос поглощения в области обычно применяемых аналитических длин волн, которые могли бы быть использованы для выяснения структуры мыл и их гидратов.

Объекты и методы исследования

Лауриновая кислота *(HLr)* использовалась фирмы *Fluka* марки «*puriss*» с содержанием основного продукта выше 99,5%-ов. Ксилол и другие реактивы использовались фирмы *Reanal* аналитической степени чистоты.

Синтез лаурата кальция *($CaLr_2$)* производили следующим образом. Необходимое количество *$Ca(OH)_2$* суспендировали в дистиллированной воде. *HLr* в количестве несколько большем, чем эквивалентное к гидроокиси, растворяли в ксилоле. В реакционном сосуде, при сливании двух жидких фаз с помощью гомогенизатора типа *Mixer Unipan-309*, получали динамическую эмульсию воды в ксилоле. На границе раздела фаз эмульсии при температуре 25 °C за 20 минут практически полностью проходила реакция образования мыла, которое выделялось в виде твердой фазы, нерастворимой в воде и мало растворимой в ксилоле. После отделения жидких фаз, мыло многократно промывали водой, ксилолом и *n*-гексаном. Продукт сушили при комнатной температуре в вакууме при остаточном давлении 5 мм *Hg* ст. до постоянного веса.

Подробности синтеза и о материальном баллансе реакции на границе раздела фаз эмульсии мы докладывали ранее [15]. Исследуемые препараты *$CaLr_2$* не содержали остатков *$Ca(OH)_2$* и *HLr*.

ИК- спекры были сняты на двухлучевом приборе типа *Unicam SP 1000* с дифракционной решеткой. Чувствительность и ошибка измерений составляла не более ± 3 см$^{-1}$ в интервале 600—2000 см$^{-1}$ и ± 9 см$^{-1}$ при 2000—3800 см$^{-1}$. Частоты в максимумах полос поглощения указываются нами с точностью ± 5 см$^{-1}$. Ошибка в воспроизводимости интенсиности полос не превышала 5 %-ов. ИК- спектры образцов снимались в *KBr*-ных таблетках, наиболее пригодным методом для изучения кристаллогидратов [16, 17].

Термогравиметрический анализ производили с помощью дериватографа типа *MOM G-425* с автоматической записью результатов. Измерения производили в интервале температур 25—300 °C при скорости нагрева 3° в минуту.

Рентгеноструктурные данные образцов были получены на приборе типа *Mikrometa-2*, с применением железного катода. Дифракция рентгеновских лучей регистрировалась самописцем прибора.

В работе используются символы вида характеристических колебаний предложенные в монографии [18]:

$\nu(xy)$ — валентные колебания, (к.)
$\nu_s(xy_2)$, $\nu_{as}(xy_2)$ — симметричные и асимметричные валентные к. нелинейной группы, а так же группы XY_3,
$\beta(xy)$, $\gamma(xy)$ — деформационные к. в плоскости и вне плоскости,
$\delta(xy)$ — деформационные к.,
$\beta_s(xy_2)$, $\beta_{as}(xy_2)$ — симметричные и асимметричные деформационные к. в плоскости
$\gamma_s(xy_2)$, $\gamma_{as}(xy_2)$ — симметричные и асимметричные деформационные к. перпендикулярные к плоскости,
$\delta_s(xy_3)$, $\delta_{as}(xy_3)$ — симметричные и асимметричные деформационные к.

Экспериментальные данные

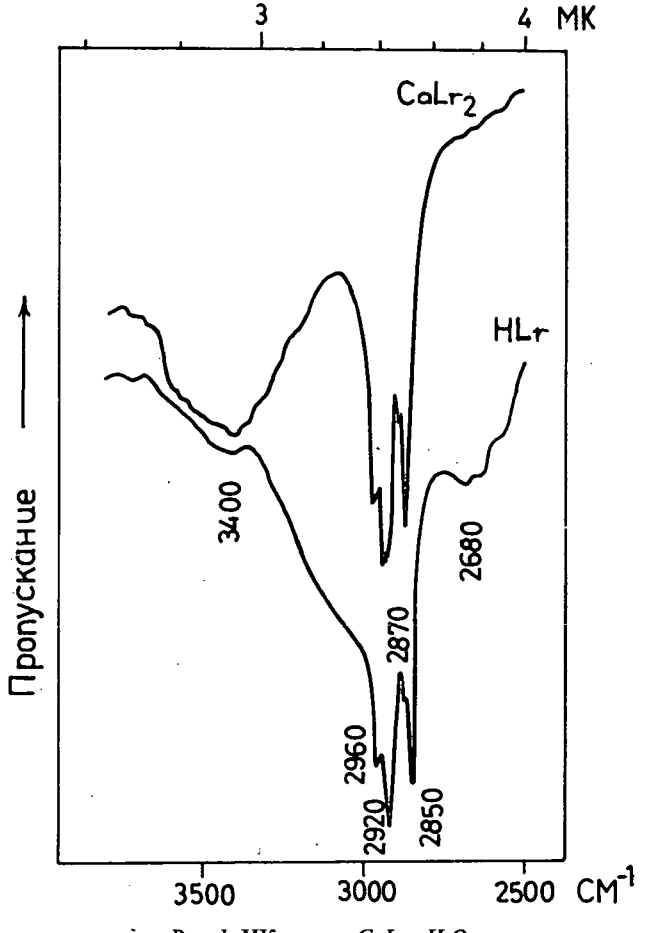

Рис. 1. ИК-спектр $CaLr_2 \cdot H_2O$ и *HLr* в интервале длин волн от 2,7 до 4,0 мк.

Из числа разных способов синтеза мыл многовалентных металлов [19—21], метод получения мыл реакцией на границе раздела фаз эмульсионной системы (РГФ) обладает рядом преимуществ по сравнению с другими методами. Из числа преимуществ метода РГФ прежде всего следует отметить известный факт, что мыла многовалентных металлов при температурах выше комнатных легко претерпевают полиморфные превращения [22—24], поэтому метод РГФ, позволяющий простое и быстрое получение металлических мыл без повышения температуры, представляет особый интерес при исследовании структуры мыл.

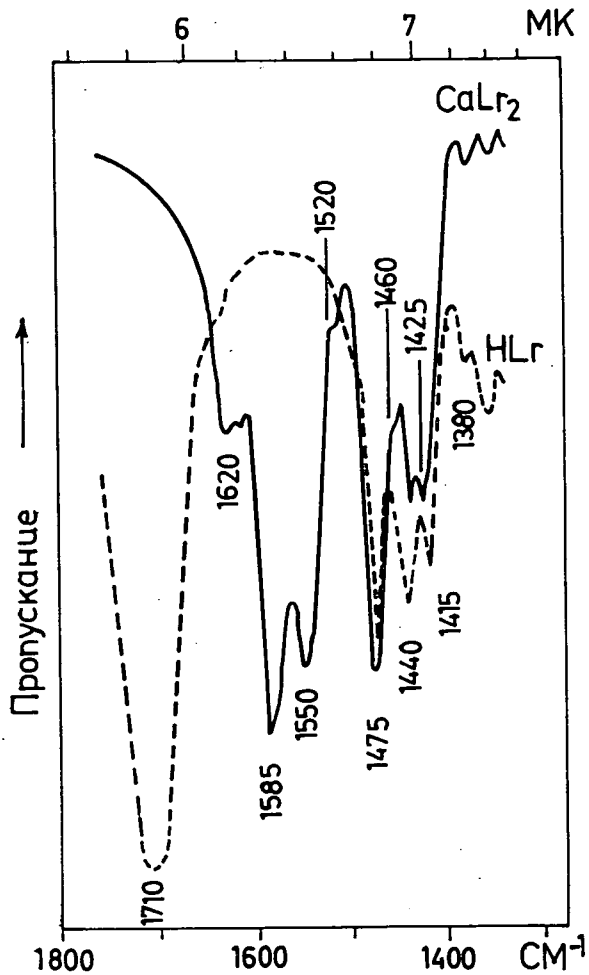

Рис. 2. ИК-спектр $CaLr_2 \cdot H_2O$ и *HLr* в интервале длин волн от 5,7 до 7,4 мк.

Метод РГФ представляет также возможность получения особо чистых продуктов в виду того, что непосредственное взаимодействие катиона металла с кислотой обеспечивает отсутствие одновалентных металлов в готовом продукте, попадающих при обменной реакции с солями щелочных металлов [21, 25]; а также обеспечивает отсутствие продуктов термического распада, образующихся при методе сплавления гидроокиси металлов с кислотами. Несмотря на ряд преимуществ метода РГФ в эмульсионных системах, в литературе мы не нашли данных по изучению структуры мыл полученных этим способом.

На рис. 1—4 представлены ИК-спектры $CaLr_2$ и применяемой для синтеза мыла *HLr*, перекристаллизованной при комнатной температуре из ксилольно-гексанового раствора, для обеспечения аналогичных условий формирования кристаллов кислоты с частицами мыла. Представленные данные по спектру

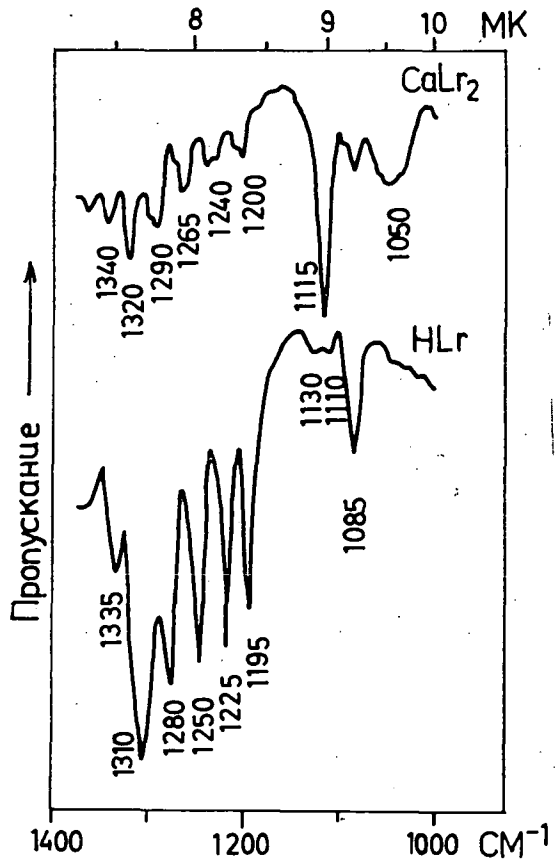

Рис. 3. ИК-спектр $CaLr_2 \cdot H_2O$ и *HLr* в интервале длин волн от 7,4 до 10 мк.

HLr преследуют цель, как обычно [12, 14], получения возможности более точного отнесения полос поглощения в спектре синтетизированного мыла.

На рис. 1—4 обозначены частоты соответствующие максимумам поглощения в спектре *HLr*, на спектрах же $CaLr_2$ максимумы обозначены только в тех случаях, когда получены отличающиеся от спектра кислоты значения. Отнесение полос к соответствующим колебаниям атомов и групп молекул изучаемых веществ проведено на основании общепринятых корреляций [5, 18,

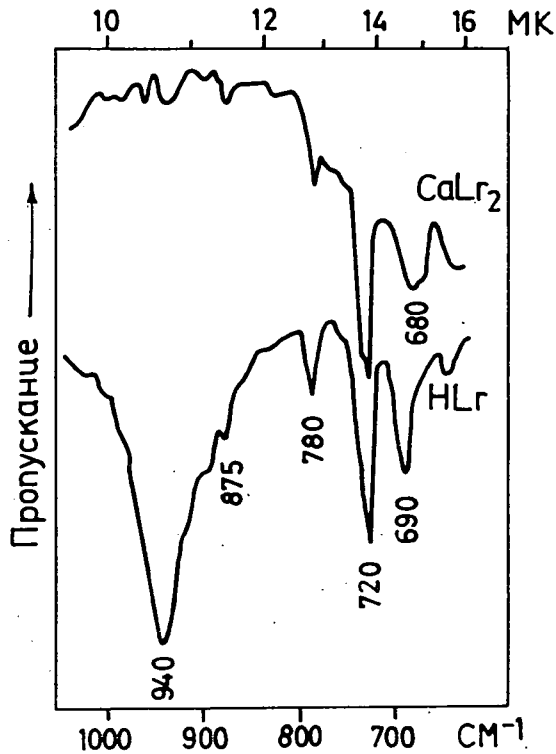

Рис. 4. ИК-спектр $CaLr_2 \cdot H_2O$ и *HLr* в интервале длин волн от 10 до 16 мк.

26—31] и имеющихся специальных литературных данных. Проведенное нами отнесение полос поглощения спектров к соответствующим колебаниям представлено в таблицах III—VI.

Экспериментальные данные термогравиметрического анализа представлены в таблице I. В интервале температур до 200 °C были проведены также контрольные визуальные наблюдения с помощью микронагревательного стола типа *Boëtius*.

Таблица I

Данные термогравиметрического анализа лаурата кальция

Содержание H_2O в образце, мг/100 мг	3,8
Температурный интервал удаления H_2O	85—110 °C
Установленный состав образца	$CaLr_2 \cdot H_2O$
Температура перехода в пластичную фазу	130 °C
Температура начала разложения в воздухе	180 °C

Данные рассчитанные на основании дифракции рентгеновских лучей представлены в таблице II.

Таблица II

Данные рентгеноструктурного анализа $CaLr_2 \cdot H_2O$

Расстояния идентичности по интенсивным пикам, Å $CaLr_2 \cdot H_2O$	4,4*	4,9	5,7	6,6	9,7	11,5*	17,1	34,2*
Параметры элементарной ячейки *HLr* [32], Å		4,98*(b)*			9,76*(a)*			36,9*(c)*

* — наиболее интенсивные полосы

Обсуждение результатов

Полосы поглощения валентных колебаний *OH*, обнаруживающиеся в спектрах воды в паровой фазе, находятся при частотах 3756 и 3652 $см^{-1}$. Эти частоты значительно снижены для воды, находящегося в кристаллах [33] и, в результате межмолекулярных водородных связей и резонансных взаимодействий, проявляется широкая диффузная полоса в области частот 3500—3400 $см^{-1}$ [29]. Из рис. 1 видно, что в спектре *HLr* имеется широкое плечо в этой области. Это свидетельствует о наличии влаги, которая могла попасть в образец в процессе таблетирования.

Спектр $CaLr_2$ в области длин волн от 2,7 до 4,0 мк, представленный на рис. 1, имеет интенсивную диффузную полосу поглощения с максимумом в области 3400 $см^{-1}$, свидетельствующую о наличии гидратной воды [33]. Так как образец перед измерениями подвергался вакуумсушке при комнатной температуре, полоса поглощения не могла возникнуть вследствие наличия поверхностно адсорбированной воды. Подтвержается это и данными работы [12], согласно которым полоса, обнаруживающаяся в области 3 мк (в спектрах фенилстеаратов кальция), относится к воде, которая не удаляется при вакуумировании образцов.

В спектрах *HLr* и $CaLr_2$ в равной мере четко выражены четыре полосы относящиеся к асимметричным и симметричным валентным колебаниям *C—H* связей метильных и метиленовых групп [3]. Эти полосы в спектре *HLr* накладываются на серию диффузных полос, характерных для колебаний *OH* в ассоциированных карбоксилах органических кислот [12, 14, 34, 35], обнаруживающихся обычно в интервале 3400—2400 $см^{-1}$.

Таблица III

Полосы поглощения в спектрах $CaLr_2 \cdot H_2O$ и HLr в интервале длин волн от 2,7 до 4,0 мк

Частота, $см^{-1}$		Отнесение частот к характеристическим колебаниям	
HLr	$CaLr_2 \cdot H_2O$	Символ	Примечание
3400		$\nu(OH)$	*OH* связан. водородн. связью, H_2O
3300—2400		$\nu(OH)$	Серия *OH* ассоц. кислот, широк. диффуз.
2960		$\nu_{as}(CH_3)$	В спектре кислоты узкие интенсивные полосы накладывающиеся на широкую диффузную серию полос *OH* колебаний
2920		$\nu_{as}(CH_2)$	
2870		$\nu_s(CH_3)$	
2850		$\nu_s(CH_2)$	
2680			Из серии полос 3300—2400 $см^{-1}$

На рис. 2 представлены спектры $CaLr_2$ и *HLr* в области длин волн от 5,7 до 7,4 мк. Для этой области характерны наиболее ярко выраженные различия между спектрами кислоты и ее кальциевой соли. Очень интенсивная полоса поглощения валентного колебания кислотного карбонила [3, 8, 12, 14, 35], находящаяся при 1710 $см^{-1}$, не появляется, как известно, в спектрах солей [7, 9, 29]. В работах авторов [9, 11, 36] было показано, что карбоксилатный ион, вследствие полного внутреннего резонанса, характеризуется колебаниями обычной нелинейной группы типа XY_2. Согласно данным работы [11], асимметричные валентные колебания CO_2^- группы проявляются в области 1600—1550 $см^{-1}$, симметричные в области 1400—1350 $см^{-1}$, а деформационные при 900—800 $см^{-1}$. В спектре $CaLr_2$, полученного нами, в области ожидаемой полосы поглощения $\nu_{as}(CO_2^-)$ как это видно из рис. 2, имеется серия полос: дублетная полоса с максимумами при 1585 и 1550 $см^{-1}$, имеющая с обеих сторон плечи при 1620 и 1520 $см^{-1}$. Из характера формы полос следует, что все они, по-видимому, являются сложными.

В литературе нет указаний относительно наличия такой серии полос в этой области. Для трихлорацетата кальция к $\nu_{as}(CO_2^-)$ отнесена полоса при 1586 $см^{-1}$ [9]. В спектре фенилстеарата кальция была найдена очень широкая интенсивная полоса, охватывающая область от 1620 до 1520 $см^{-1}$ с максимумом около 1560 $см^{-1}$ [12]. Автор этой работы указывает на несомненную сложность найденной им полосы. В ионизированных аминокислотах в твердой фазе к $\nu_{as}(CO_2^-)$ отнесена полоса находящаяся в области 1610—1570 $см^{-1}$ [37], а в суспензиях ряда солей к валентным колебаниям карбоксилата отнесены полосы при 1610 и 1570 $см^{-1}$ [38]. Для стеарата кобальта к $\nu_{as}(CO_2^-)$ отнесена частота 1532 $см^{-1}$ [14]. В работе [18] авторы предполагают появление полосы поглощения $\nu_{as}(CO_2^-)$ в интервале частот 1625—1500 $см^{-1}$.

В настоящее время уже нет сомнения в том, что точное значение частот валентных колебаний в карбоксилате должно зависеть от типа катиона и ряда других внутри- и межмолекулярных эффектов, изменяющих силу и поляризацию связей *C—O* в карбоксилате [7, 39]. На наш взгляд, по аналогии с наблюдавшимся расщеплением полос карбонильного поглощения у симметричных диацильных перекисей [40] и у фталевых кислот [41], механический резонанс между однотипными колебаниями карбоксилатных групп внутри молекул мыла приводит к расщеплению основной полосы поглощения колебания $\nu_{as}(CO_2^-)$. Поскольку в непосредственной связи с карбоксилатными группами находится и катион металла, его физические параметры (масса, радиус, заряд, электроотрицательность) должны отразиться на положении полос этой серии. Найденные нами полосы в спектре $CaLr_2$ располагаются с интервалом ± 30—35 $см^{-1}$ от наиболее интенсивной основной полосы 1585 $см^{-1}$. Необходимо, однако, еще раз подчеркнуть, что упомянутые полосы могут иметь тонкую структуру, которые с увеличением разрешающей способности прибора, очевидно, могут быть выявлены и анализированы в дальнейшем.

Особенно ярко проявляется сложный характер плеча при 1620 $см^{-1}$. Вероятно, здесь доминирующей является полоса деформационных колебаний воды (1595 $см^{-1}$ [33]), которая, например в работе [42] обнаруживала полосу поглощения при 1620 $см^{-1}$.

Таким образом, приведенные литературные данные и полученный нами результат дают достаточно оснований для предположения, что в интервале длин волн от 6,1 до 6,7 мк, состав спектра может быть пригодным для характеристики различных солей жирных кислот.

Весьма сложно надежное отнесение полос в интервале длин волн от 6,7 до 7,4 мк. В этом интервале следует ожидать поглощения $\nu_s(CO_2^-)$, однако, здесь же находятся характерные частоты поглощения деформационных колебаний метильных и метиленовых групп. Как видно из рис. 2, в спектрах *HLr* и $CaLr_2$ не наблюдается резкого различия в положении полос, только интенсивность полос в спектре $CaLr_2$ несколько больше. Кроме этого наблюдается смещение полосы 1415 $см^{-1}$ на $+10$ $см^{-1}$.

В этой области длин волн, по-видимому, весьма затруднительно или вообще нельзя установить принадлежносчь той или иной полосы поглощения к определенному простому типу колебаний в молекулах, не только вследствие появления гибридных колебаний, но и в результате перекрывания полос разного рода. В спектрах кристаллических парафинов авторы работы [43] отмечали наличие серий полос в области 1460 и 1380 $см^{-1}$, соответствующих деформационным колебаниям метильных и метиленовых групп. В спектре полиэтилена имеется интенсивный дублет полос 1470 и 1460 $см^{-1}$ деформационных колебаний метиленовых групп [44]. По-видиному, полосу поглощения при 1475 $см^{-1}$ и плечо при 1460 $см^{-1}$ необходимо отнести к деформационным колебаниям метильных и метиленовых групп алифатической цепи, обычно поглощающих в интервале частот от 1485 до 1445 $см^{-1}$ [18]. Полоса 1440 $см^{-1}$ должна быть отнесена к деформационным колебаниям метиленовой группы, находящейся в α-положении к карбоксилу [18, 45]. Однако, отметим, что автор работы [12] в спектре фенилстеарата кальция широкую интенсивную полосу с максимумом при 1440 $см^{-1}$ отнес к симметричным валентным колебаниям карбоксилата. Необходимо отметить также, что встречается взгляд в литературе [39] согласно

которому поглощение $\nu_s(CO_2^-)$ может проявиться при частоте 1550 $см^{-1}$. Большинство исследователей, однако, к симметричным валентным колебаниям относит полосу в области 1430—1410 $см^{-1}$ [7, 14, 37]. Следовательно, полоса при 1425 $см^{-1}$ в спектре $CaLr_2$ с наибольшей вероятностью может быть отнесена к колебаниям $\nu_s(CO_2^-)$.

Полоса при 1380 $см^{-1}$ соответствует симметричным деформационным колебаниям метильной группы. Таким образом, из вышеизложенного следует, что в интервале длин волн от 6,7 до 7,4 мк, вследствие перекрывания частот колебаний разных групп и меньшей интенсивности полос поглощения $\nu_s(CO_2^-)$, по сравнению с $\nu_{as}(CO_2^-)$ труднее выделить полосы, которые были бы пригодны для установления структуры различных мыл. Все же встречаем и другое мнение, например, в работе [46] авторы, изучая ряд солей амино-салициловой кислоты различных металлов, высказывали мнение, что соотношение интенсивностей полос 1470 и 1410 $см^{-1}$ может характеризовать различия в полярности связей кислород — металл. Эта мысль авторов в их работе не развивается подробно и мы не имеем достаточных оснований судить об их предположении.

Таблица IV

Полосы поглощения в спектрах $CaLr_2 \cdot H_2O$ и HLr в интервале длин волн от 5,7 до 7,4 мк

Частота, $см^{-1}$		Отнесение частот к характеристическим колебаниям	
HLr	$CaLr_2 \cdot H_2O$	Символ	Примечание
1710		$\nu(C=O)$	В *COOH* ассоц. кислот, очень интенсивная
	1620	$\beta(OH)$, $\nu_{as}(CO_2^-)$	Серия полос, которая может быть характерной для гидратов мыл разных металлов
	1585	$\nu_{as}(CO_2^-)$	
	1550		
	1520		
1475		$\beta_s(CH_2)$	Интенсивная, резкая
1460		$\delta_{as}(CH_3)$	Слабо выраженное плечо
1440		$\beta_s(\alpha - CH_2)$	
	1425	$\nu_s(CO_2^-)$	
1415		$\beta(OH) + \nu(C-O)$	Гибридная полоса ассоц. кислот
1380		$\delta_s(CH_3)$	Очень слабая

Область спектров в интервале длин волн от 7,4 до 10 мк, представленный на рис. 3, содержит в себе наиболее детально изученную рядом исследователей серию полос, располагающуюся от 7,4 до 8,5 мк [6, 43, 47, 48]. Полученные нами спектры соответствуют литературным данным, характеризующим ряд соединений с алифатической цепью, находящихся в кристаллическом состоянии. Мы отметим только, что в спектре $CaLr_2$ полосы несколько смещены в сторону больших частот по сравнению со спектром *HLr*. Хотя наблюдаемые смещения в спектре *CaLr* незначительны, все же возможно, что в спектрах мыл разных металлов эти смещения могут оказаться характерными, вследствие влияния природы концевых групп на расположение этих полос [47].

В интервале длин волн от 8,5 до 10 мк, в спектрах жирных кислот и их солей наблюдается серия полос слабой интенсивности, соответствующая *C—C* скелетным колебаниям, аналогично обычным парафинам. В спектрах *HLr* и $CaLr_2$ наблюдаем, однако, достаточно заметные различия в интенсивностях и расположении полос поглощения. Весьма слабый дублет полос 1130—1110 $см^{-1}$ у кислоты заменяется острой полосой поглощения средней интенсивности при 1115 $см^{-1}$ у соли. Эту полосу чаще всего относят и гибридным *C—C* скелетным колебаниям с концевыми группами [4]. Вероятно, ионизация карбоксильной группы обусловливает изменение интенсивности и некоторое смещение полосы. Однако, более определенное отнесение полос в интервале 1150—1050 $см^{-1}$ еще затруднительно.

Таблица V

Полосы поглощения в спектрах $CaLr_2 \cdot H_2O$ и HLr в интервале длин волн от 7,4 до 10 мк

Частота, $см^{-1}$		Отнесение частот к характеристическим колебаниям	
HLr	$CaLr_2 \cdot H_2O$	Символ	Примечание
1335	1340	$\gamma_{as}(CH_2)$	Характерная серия приближенно
1310	1320	+	эквидистантных полос для алифатических цепей
1280	1290	$\gamma_s(CH_2)$	связанных с полярными концевыми группами.
1250	1265	+	В кислоте накладывается
1225	1230	$C—C_{скел.}$	на интенсивную гибридную полосу
1195	1200		$\nu(C—O)+\beta(OH)$ при 1310 $см^{-1}$
1130, 1110		*C—C* ?	Очень слабый дублет
	1115	*C—C* ?	Резкая, средней интенсивности
1085		*C—C* ?	Резкая, слабая
	1050	*C—C* ?	Диффузная, слабая

В интервале длин волн от 10 до 16 мк (рис. 4) доминирующей полосой поглощения в спектре *HLr* является широкая интенсивная надежно установленная полоса, находящаяся при 940 $см^{-1}$, внеплоскостных деформационных колебаний *OH* группы в димерном кольце карбоксилов кислот [6, 14, 35, 45]. В спектре $CaLr_2$, естественно, отсутсвует эта полоса, а имеющаяся весьма слабая полоса при этой частоте была отнесена [12] к деформационным колебаниям карбоксилата. Так же слишком мало данных для более конкретного отнесения полос при 875 и 780 $см^{-1}$.

Характерная резкая средней интенсивности полоса маятниковых колебаний CH_2-групп алифатических цепей находится, как и следовало ожидать, в обоих спектрах при 720 $см^{-1}$ [6, 12, 14, 45]. Малой интенсивности, несколько диффузные полосы, находящиеся в области 680 $см^{-1}$, должны быть отнесены, вероятно, также к скелетным колебаниям алифатических цепей [40].

Данные термогравиметрического анализа, приведенные в табл. I подтверждают ряд вышеприведенных представлений о структуре и отнесении характеристических частот спектра $CaLr_2$, синтетизированного методом РГФ.

Содержание воды в продукте после вакуумсушки, согласно полученным термогравиметрическим данным, составляет 3,8%-ов, что с очень хорошим приближением соответствует составу моногидрата $CaLr_2$. В литературе име-

Таблица VI

Полосы поглощения в спектрах $CaLr_2 \cdot H_2O$ и HLr в интервале длин волн от 10 до 16 мк

Частота, $см^{-1}$		Отнесение частот к характеристическим колебаниям	
HLr	$CaLr_2 \cdot H_2O$	Символ	Примечание
940		$\gamma(OH)$	В *COOH* ассоц. кислот, широкая, интенсивная
	940	?	Очень слабая; $\beta(CO_2^-)$?
875		C—C ?	Очень слабая
780		?	Резкая слабая
720		$\beta_{as}(CH_2)$	Резкая, средней интенсивности, $(—CH_2—)_n$
690—670		C—C ?	
	680—670	C—C ?	

ются данные доказывающие возможность образования моногидратов пальмитата и стеарата кальция [22, 23]. Таким образом очевидно, что методом РГФ непосредственно образуется моногидрат кальциевого мыла, без необходимости применения повышенных температур для проведения гидратирования. Наличие полос поглощения в области 3400 и 1620 $см^{-1}$ свидетельствует о том, что вода расположена в кристаллической решетке $CaLr_2$ и связана относительно слабыми силами межмолекулярных взаимодействий. Это подтверждается также удалением воды в интервале температур 85—110 °С при нагревании. Микроскопически визуально улавливаемый фазовый переход наблюдался для исследуемого образца при 130 °С. Этой температуре соответствовал второй минимум (первый — разложению гидрата) на кривой ДТ. Другие фазовые переходы примененной нами методикой не были обнаружены.

В данной работе мы не преследовали цель детального рентгеноструктурного анализа полученных образцов $CaLr_2$. Однако, представлял интерес определить наличие или отсутствие кристаллической структуры в мыле полученного методом РГФ. В таблице II представлены рассчитанные расстояния идентичности по наиболее интенсивным полосам дифракции рентгеновских лучей и, наряду с тем, там же приведены литературные данные по параметрам элементарной ячейки *HLr*. Совокупность дифракционных пиков указывает на достаточно ярко выраженный кристаллический характер продукта, полученного методом РГФ. Об этом свидетельствует также ИК-спектр образца в области частот 1340—1190 $см^{-1}$. После нагревания до восково-пластичного состояния $CaLr_2$ и охлаждения до комнатной температуры, на рентгенограмме такого образца осталась единственная полоса, соответствующая наибольшему периоду идентичности (34,2 Å), который приблизительно соответствует длине молекул $CaLr_2$ [49].

Из всего вышеизложенного следует, что метод синтеза металлического мыла из $Ca(OH)_2$ и *HLr* методом РГФ при температуре 25 °С приводит к непосредственному получению моногидрата $CaLr_2$ с хорошо выраженной кристаллической структурой. Изучение ИК-спектра позволило идентифицировать полученный продукт, как гидратированную соль лауриновой кислоты. Обнаруженная серия полос в интервале частот 1620—1520 $см^{-1}$ представляется наиболее пригодной для установления структуры различных мыл и их гидратов.

Литература

[1] *Андор, И., Я. Балаж, С. В. Фельдман:* Acta Phys. et Chem. Szeged **20**, 157 (1974).
[2] *Андор, И., С. В. Фельдман, Балашине-А. Бенюш:* Acta Phys. et Chem. Szeged **20**, 427 (1974).
[3] *Sinclair, R. G., A. F. McKay, R. N. Jones:* J. Amer. Chem. Soc. **74**, 2570 (1952).
[4] *Jones, R. N.:* Canad. J. Chem. **40**, 301 (1962).
[5] *Bellamy, L. J.:* Ultrarot-Spektrum und Chemische Konstitution, Darmstadt, 1955.
[6] *Meiklejohn, R. A., R. J. Meyer, S. M. Aronovic, H. A. Schuette, V. W. Meloch:* Anal. Chem. **29**, 329 (1957).
[7] *Hummel, D.:* Identification and Analysis of Surface-Active Agent (Text Volume), Interscience Publ., 1962.
[8] *Klotz, J. M., D. M. Gruen:* J. Phys. Chem. **52**, 961 (1948).
[9] *Duval, Cl., J. Lecomte, F. Douvillé:* Bull. soc. chim. France **9**, 263 (1942).
[10] *Childers, G. W. Struthers:* Anal. Chem. **27**, 737 (1955).
[11] *Duval, Cl., J. Lecomte, F. Douvillé:* Ann. Phys. **17**, 5 (1942).
[12] *Kagarise, R. E.,* J. Phys. Chem. **59**, 271 (1955).
[13] *Büsch G.:* Untersuchung Über Mehrwertige Metallseifen Als W/Ö-Emulgatoren, Diss. Der Univers. Hamburg, 1973.
[14] *Kambe, H., I. Mita:* Bull. Chem. Soc. Japan **34**, 1798 (1961).
[15] *Andor, J., Balázs J., Nagy E.:* XII. (Колористический симпозиум), Győr, 1975. 3 old.
[16] *Baker, A. W.:* J. Phys. Chem. **61**, 450 (1957).
[17] *Карякин, А. В., Г. М. Мурадова:* Ж. физ. хим. **42**, 2735 (1968).
[18] *Holly, S., Sohár P.:* Infravörös spektroszkópia. (Инфракрасная спектроскопия) Műszaki Könyvkiadó, Budapest, 1968.
[19] *Kambe, H.:* Bull. Chem. Soc. Japan **34**, 1786 (1961).
[20] *Birdsall, D. H., B. B. Farrington:* J. Phys. Chem. **52**, 1415 (1948).
[21] *Трапезников, А. А., Е. М. Шлосберг:* Колл. ж. **8**, 421 (1946).
[22] *Hattiangdi, G. S., M. J. Vold, R. D. Vold:* Ind. Eng. Chem. **41**, 2320 (1949).
[23] *Виноградов, Г. В.:* Успехи хим. **20**, 533 (1951).
[24] *Тулупов, В. А., Д. А. Кивилис, А. Г. Капышев:* Ж. физ. хим. **38**, 2415 (1964).
[25] *Солнышкин, В. И.:* Колл. ж. **19**, 736 (1957).
[26] *Szymanski, H. A.:* Progress in Infrared Spectroscopy, Vol. 1, Plenum Press. New York, 1962.
[27] *Szymanski, H. A.:* Progress in Infrared Spectroscopy, Vol. 2, Plenum Press. New York, 1964.
[28] *Szymanski, H. A.:* Interpreted Infrared Spectra, Vol. 1, Plenum Press. New York, 1964.
[29] *Наканиси, К.:* Инфракрасные спектры и строение органических соединений, „Мир", Москва, 1965.
[30] *Szymanski, H. A.:* Interpreted Infrared Spectra, Vol. 3, Plenum Press. New York, 1967.
[31] *Kiss—Erdős, K.:* Az infravörös spektroszkópia analitikai alkalmazása, (Аналитическое применение инфракрасной спектроскопии) Műszaki Könyvkiadó, Budapest, 1974.
[32] Справочник химика, том I. „Химия" Москва, 1966. ст. 534.
[33] *Mitra, S. S., P. J. Gielisse:* in [27] p. 74.
[34] *Тихонов, В. П., С. С. Тодосиенко, Г. И. Фукс:* Колл. ж. **36**, 76 (1974).
[35] *Shreve, O. D., M. R. Heether, H. B. Knight, D. Swern:* Anal. Chem. **22**, 1498 (1950).
[36] *Davies, M. M., G. B. B. M. Sutherland:* J. Chem. Phys. **6**, 755 (1938).
[37] *Салимов, М. А., В. А. Пчелин, А. В. Керимбеков:* Ж. физ. хим. **37**, 2285 (1963).
[38] *Масленникова, И. С.:* Ж. физ. хим. **44**, 2509 (1970).
[39] *Ferrao, J. R.:* in [26] p. 35.
[40] *Иванчев, С. С., А. И. Юрженко, Ю. Н. Анисимов:* Ж. физ. хим. **39**, 1900 (1965).
[41] *Луцкий, А. Е., А. К. Кульчицкая:* Ж. физ. хим. **41**, 983 (1967).
[42] *Ефименко, Л. В., Г. Д. Чукин, Л. А. Игнатьева, Л. В. Левшин, Б. В. Смирнов:* Ж. физ. хим. **49**, 212 (1975).
[43] *Brown, J. K., N. Sheppard:* Trans. Faraday Soc. **50**, 535 (1954).
[44] *Angell, C. L.:* in [27] p. 1.
[45] *Jones, R. N.:* Canad. J. Chem. **40**, 321 (1962).
[46] *Шейнкер, Ю. Н., Ю. И. Померанцев:* Ж. физ. хим. **33**, 1819 (1959).
[47] *Jones, R. N., A. F. McKay, R. G. Sinclair:* J. Amer. Chem. Soc. **74**, 2575 (1952).
[48] *Susi, H.:* Anal. Chem. **31**, 910 (1959).
[49] *Hückel, W.:* Theoretische Grundlagen der Organischen Chemie, 2 Band, 8 Auflage, Leipzig, 1957. s. 367.

INVESTIGATION OF THE STRUCTURE AND CHARACTERISTICS OF LONG-CHAIN FATTY ACID SALTS, I

IR Spectrum of Calcium Dodecanate Obtained by Interfacial Reaction of an Emulsion System

J. A. Andor and J. Kiss

The IR spectrum of calcium dodecanate obtained by the interfacial reaction (IFR) of dynamic emulsion has been investigated. Based upon data of TG, X-ray and IR investigations, it could be assumed that, in the case of IFR, calcium laurate monohydrate formed in well-defined crystal-structure. The IR spectrum of calcium dodecanate was compared with the solid-phase IR spectrum of dodecanoic acid and the bands were assigned. A set of bands in the region 1620—1520 cm^{-1} seems to be characteristic for the structure of long-chain fatty acid salts and of their hydrates.

CHEMISTRY OF TWISTANE SYSTEM AND ITS USE IN STEREOCHEMISTRY*

By

M. TICHÝ

Institute of Organic Chemistry and Biochemistry, Czechoslovak Academy of Sciences, Prague

(Received October 10, 1975)

The aim of the present review is to show the chemistry of twistane system and the various ways in which it can be used as a stereochemical model of great utility. Many of the stereochemical applications mentioned are the result of investigations made in the author's Laboratory.

Twistane — tricyclo(4,4,0,$0^{3,8}$)decane (**I**) — belongs to the great family of adamantane isomers** of the formula $C_{10}H_{16}$. It is composed solely of six-membered rings, twisted in the same sense. The parent hydrocarbon has three two-fold rotational axes of symmetry (D_2) and exists in two enantiomeric forms which differ in the sense of twist: according to the CAHN—INGOLD—PRELOG nomenclature [11] the enantiomer (**Ia**) has *P*-helicity whereas the other (**Ib**) *M*-helicity.

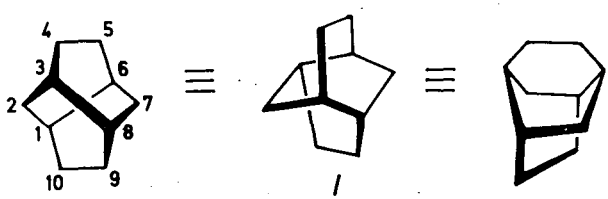

I

Ia *Ib*

* This review is based on a lecture presented at A. József University, Szeged, and on the review in Chem. Listy **69**, 45 (1975).

** For reviews on adamantane chemistry see [1—3], adamantane isomers other than twistane are studied e.g. in ref. [4—10].

There are three groups of sterically analogous carbon atoms in this system: carbons 1,3,6,8, carbons 4,5,9,10 and carbons 2 and 7. Whereas the two bonds at $C_{(2)}$ and $C_{(7)}$ in the parent hydrocarbon are sterically equivalent, the bonds in positions 4,5,9 and 10 are non-equivalent and therefore substitution in these positions affords two diastereoisomeric (monosubstituted) derivatives (Formulae **A** and **B**).

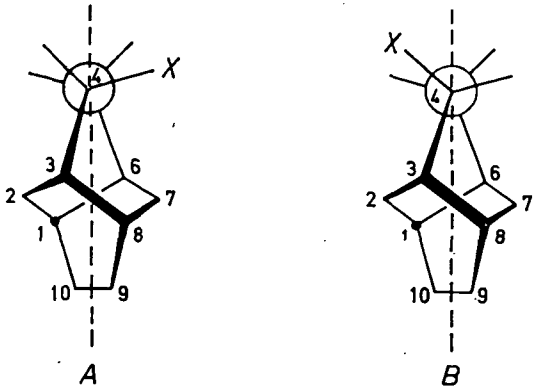

It has been suggested [12] to denote the isomers according to the position of the substituent relative to the carbon $C_{(1)}$: if the substituent is on the same side of the molecule as the carbon $C_{(1)}$ the configuration of the epimer is *endo*. Another alternative was suggested by MUSSO [13].

A generally applicable, though somewhat cumbersome, way of description is the use of the R—S nomenclature [11]. Thus, the isomer **A** (*exo*-4-X-twistane) would be called rel(1S, 3S, 4S, 6S, 8S)-4-X-tricyclo(4,4,0,$0^{3,8}$)decane (under assumption that the substituent X has higher priority than the carbon atom in the sense of the Sequence rule).

Preparation and Formation of Twistane System

Twistane was first synthesized by WHITLOCK and SIEFKEN [14, 15] in 1962 (Scheme 1). This synthesis started from *endo*-bicyclo(2,2,2)oct-5-ene-2-carboxylic acid (**II**) and its crucial step was the cyclization of the keto mesylate (**III**) to 2-twistanone (**IV**).

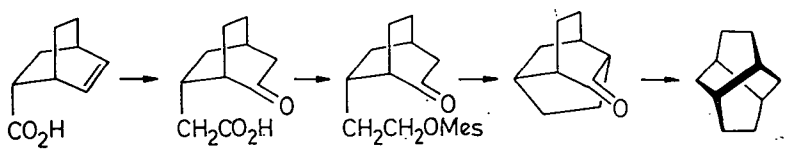

II *III* *IV* *I*

Another synthesis, carried out by DESLONGCHAMPS [16] and his co-workers, is substantially simpler and allows to prepare 4,5-vicinally disubstituted twistane derivatives *(vide infra)*. The starting compound is *cis*-decalin-2,7-dione (V) (Scheme 2).

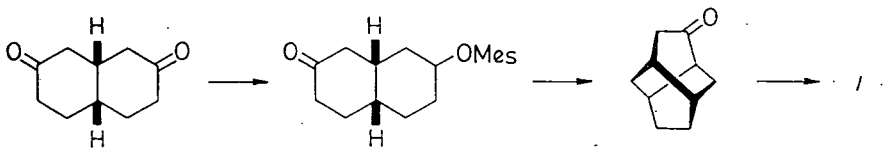

Later, this synthesis was shortened [17] practically to one step (Scheme 3).

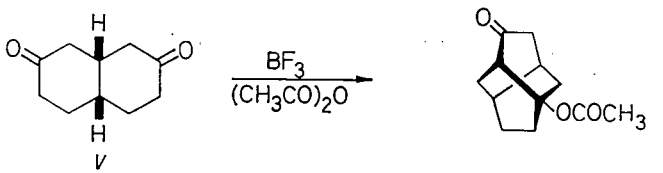

TICHÝ and SICHER [18, 19] devised also a simple synthetic approach which was used in the synthesis of twistene (**IX**) and which allows to synthesize also optically active derivatives. The reaction sequence is depicted in Scheme 4, the starting compound being dimethyl *endo*, *endo*-bicyclo(2,2,2)octane-2,5-dicarboxylate (**VII**) (Scheme 4).

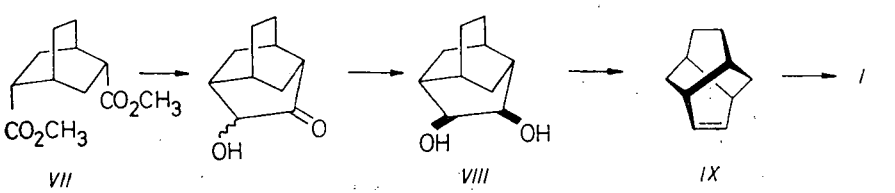

Also the possibility of hydrogenolysis of the tetracyclic ketone **X** over palladium was studied [18] (Scheme 5). This treatment, however, afforded only about 12% of 4-twistanone (**VI**), the principal product being the isomeric ketone (**XI**). This method was, neverthless, very useful in an optical correlation *(vide infra)*.

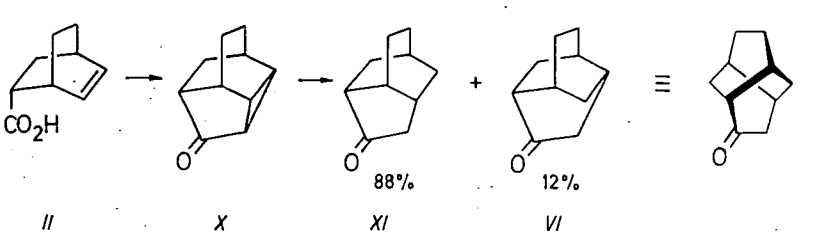

Another reaction leading to substituted twistane derivatives was described by GREUTER and SCHMID [20] (Scheme 6.)

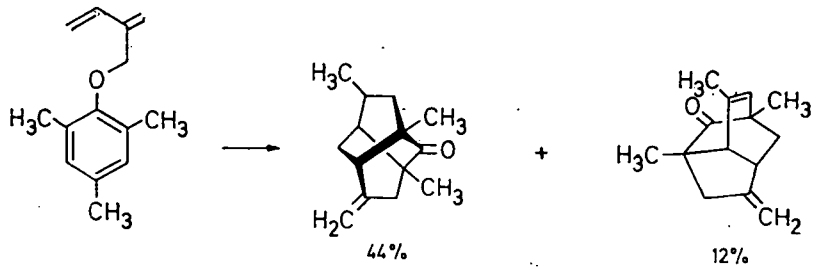

Hydrogenation of basketane (**XII**) and its derivatives [13, 21] affords also twistane or its derivatives as principal products (Scheme 7).

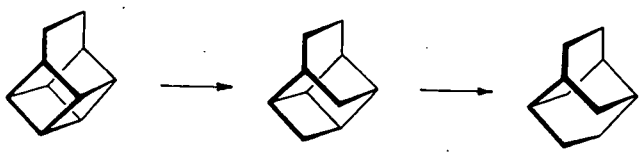

XII

Small quantities of twistyl products are formed in the solvolysis of 2- and 10-protoadamantyl tosylates [6, 22] (**XIII** and **XIV**, Scheme 8).

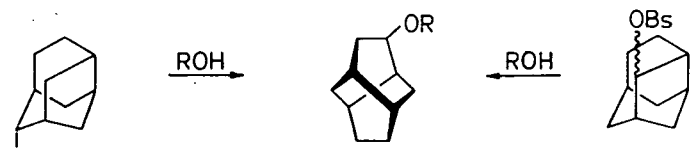

XIII *XIV*

Many synthetic pathways leading to twistane system were invented by artificial intelligence [24], including the actually used synthetic approaches.

Twistane as Stereochemical Model

Thanks to the twist of the whole molecule, the torsion angles between the bonds in positions 4 and 5 are about 30°, 90° and 150° (Formula C). All these are angles which are difficult to achieve in the common conformationally fixed systems. It is therefore possible to use the system as a model for studying the dependence of the reactivity (or interactions) of vicinal substituents on the torsion angle between the vicinal bonds. The knowledge of such dependence is of primary importance

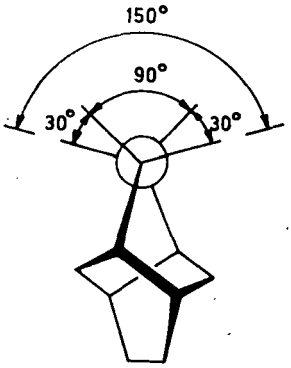

C

in the assessment of the reactivity or the energy of a given conformational situation. For such investigations it is necessary to have some rigid "standards" with defined torsion angles. The choice of the simple systems which served as yet as such standards was very meagre and the twistane system with its angles 30°, 90° and 150° fills very

Table I

Systems Used as Standards with Fixed Torsion Angles

System	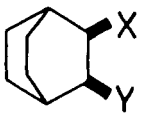	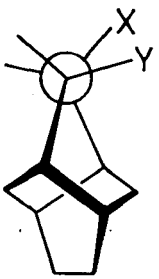	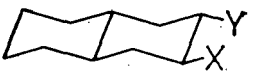	
Torsion angle	0–10°	30°	60°	
System	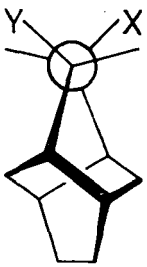	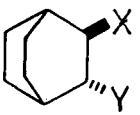	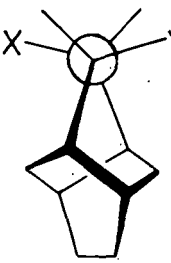	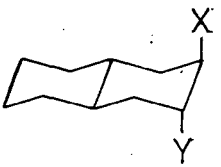
Torsion angle	90°	120°	150°	180°

well the gaps in the present "scale" (Table I). Particularly the 90° angle is very interesting since for many reactions involving two vicinal substituents it represents an arrangement with the smallest overlap of orbitals.

For the study of the dependence of reactivity and vicinal interactions on the torsion angle, some 4,5-disubstituted twistane derivatives were prepared [12, 25].

Equilibration studies [12] of epimeric 4-hydroxy-5-methyltwistanes showed the magnitude of the repulsive interactions between OH and CH_3 groups in the isomers with 30° torsion angle. From Table II, where also values for other torsion angles are listed, the dependence on the torsion angle is clearly to be seen.

Table II

Vicinal OH/CH_3 *Interactions,* ΔG_{vic}, *in Various Systems with Fixed Torsion Angles*

Model	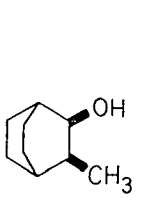	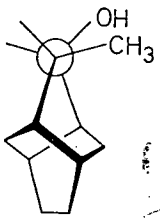	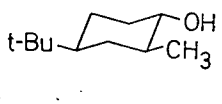
Torsion angle	0–10°.	30°	60°
ΔG_{vic} (kcal/mol)	3.6	2.0	0.4

Concerning the attractive interactions, the hydrogen bond in vicinal amino-alcohols, dimethylamino alcohols and hydroxy esters was studied [25]. Here again the twistane derivatives filled the gaps in the present scale of models. Thus, it was found that the $\Delta\nu$ value for the torsion angle of about 30° is surprisingly similar to the value for the eclipsed conformation with an approximately zero torsion angle.

Of particular interest is the fact that the twistane aminoalcohol with the torsion angle 90° exhibits hydrogen bonding, even though the $\Delta\nu$ value is very small. The enthalpy of this hydrogen bond was estimated [25] to be about 1.5 kcal/mol. Also the corresponding hydroxy ester has a weak hydrogen bond.

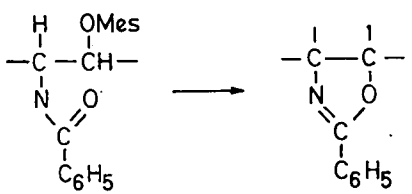

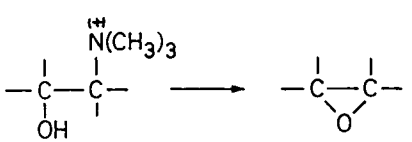

The relation between torsion angle and reactivity was studied [26] using two reactions: cyclisation of N-benzoyl O-methanesulphonyl derivatives of 2-amino-alcohols to Δ^2-oxazolines and epoxide formation from quaternary hydroxides derived from 2-amino alcohols (Scheme 9). It was found (Table III) that the twistane derivative with the torsion angle 90° still predominantly gives the five-membered oxazoline ring, whereas the geometrically more demanding cyclisation to the three-membered epoxide does not occur at all.

Table III

Cyclisation of Vicinal Benzamido Methanesulphonates and Quaternary Bases in Various Systems with Fixed Torsion Angles

Angle	System	Benzamido Mesylates		Quaternary Bases[a]	
		Cyclisation	Solvolysis	Epoxide	Ketone
0°		—	100%	—	100%
30°	Twistane	—	100%	—	100%
90°	Twistane	72%	28%	No non-basic products	
120°		100%	—	35%	65%
150°	Twistane	Skeletal rearrangement		92%	8%
180°	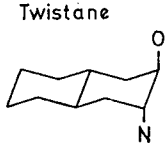	100%	—	100%	—

[a]Percentage based on non basic products.

Reactivity of the Twistane System

Strong Lewis acids, such as antimony pentachloride or aluminium tribromide, convert twistane into adamantane without any detectable intermediate [15]. Twistane is separated from adamantane (**XV**) by only one structure — protoadamantane (**XVI**) — and the isomerisation to adamantane goes energetically downhill [15, 27].

In contrast to the undiscriminative generation of carbonium ions by Lewis acids, leading to adamantane, the solvolysis of tosylates gives different products depending on the initial position of the tosyloxy group. Solvolysis of 1-twistyl tosylate gives solely 1-twistyl derivative, without any rearrangement [28]. On the contrary, 2-twistyl tosylate affords a mixture of about eight compounds, none of them being adamantyl acetate or 2-twistyl derivative [15].

We studied the solvolysis of the two epimeric 4-twistyl tosylates [22, 23] (**XVIIa** and **XVIIb**). The *exo*-epimer (**XVIIa**) reacts by about three orders of magnitude faster than the *endo*-epimer (**XVIIb**), this large difference being indicative of an anchimeric assistance in the former isomer. Both isomers give approximately the same mixture of compounds in which the predominating product is 10-protoadamantyl derivative (**XVIII**; X=OH, CH_3COO—), the 4-twistyl derivative representing only a minor component (20—40%, acording to the solvent) (Scheme 10).

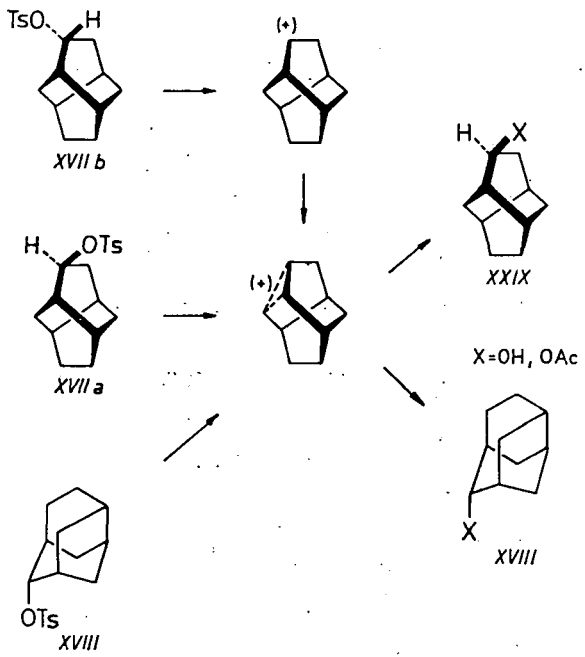

Adamantane derivatives were not found at all. The solvolysis of *exo*-10-protoadamantyl tosylate (**XVIII**; *X*=OTs) affords exactly the same mixture of products as *exo*-4-twistyl tosylate (**XVIIa**). The stereospecificity of the reaction is remarkable: both *exo*-4-twistyl and *exo*-10-protoadamantyl tosylate afforded only products of *exo*-configuration. Using detailed stereochemical study and deuterium labelling it was possible to explain the mechanism of these rearrangements [22, 23]. In all probability the common intermediate of the solvolysis of 4-twistyl as well as 10-protoadamantyl tosylates is a bridged carbonium ion which is then stereospecifically opened by the solvent (Scheme 10). Similar reaction course was observed also on heterotwistane derivatives, substituted in the analogous position [29, 30].

Since the reaction proceeds via a common intermediate, it was possible to calculate the energy difference between the twistane and protoadamantane system using the GOERING—SCHEWENE free-energy diagram [31]. The 10-protoadamantyl derivative (**XVIII**) was thus found to be by 4.4 kcal/mol more stable than the *exo*-4-twistyl derivative (**XVIIa**). According to calculations of SCHLEYER [32], protoadamantane should be by about 7.8 kcal/mol more stable than twistane.

Optically Active System

As already mentioned above, the twistane system is chiral and it can exist in two enantiomeric forms (**Ia** and **Ib**). The same holds also for heterotwistanes (see p. 166). Twistane is a very suitable (if not fundamental) model for the study of the so-called permolecular chirality, i.e. chirality which is due to the asymmetry of the molecule as a whole.

The first attempt to prepare optically active twistane derivatives and to determine their absolute configuration was made by ADACHI [33] and co-workers. These authors prepared optically active (+)-twistane ((+)-**I**) from the optically active keto acid (−)-**XIX** via 2-twistanone (+)-**IV** (Scheme 11). TICHÝ and SICHER [19, 34] prepared (+)-twistane and (+)-twistene according to Scheme 12.

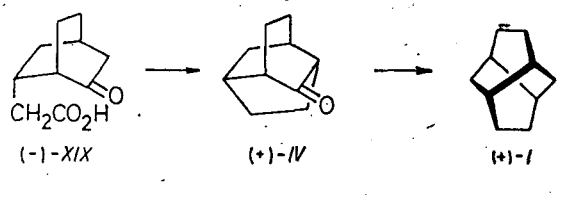

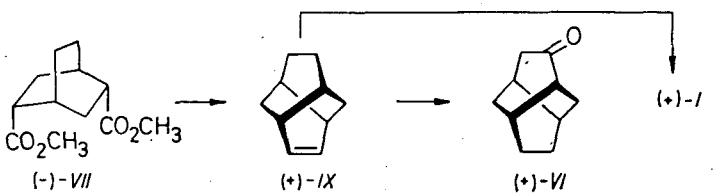

Absolute configuration was assigned [33] to (+)-**IV** on the basis of ORD studies, using the KLYNE—DJERASSI rule [35]. The same absolute configuration was deduced later from the optical properties of (+)-4-twistanone [19]. Also the application of the SCOTT—WRIXON rule [36] to (+)-twistene led to identical result [34].

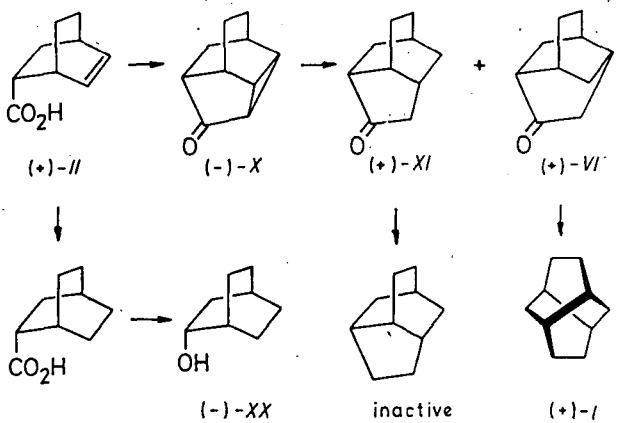

Because these assignments were made only on the basis of empirical optical methods, it was necessary to determine the absolute configuration by an unequivocal chemical correlation. The crucial compound was the optically active (+)-*endo*-bicyclo (2,2,2)oct-5-ene-2-carboxylic acid, (+)-**II**, (Scheme 13) which was correlated on the one hand with (−)-bicyclo(2,2,2)octan-2-ol ((−)-**XX**) of known absolute configuration [37—40] and on the other hand with (+)-twistane by two independent series of reactions [34].

Surprisingly, both these correlations revealed that the absolute configuration is opposite to that derived from the optical measurements. Further studies have shown that some of the rules, applied to optically active twistane derivatives, are valid, whereas other rules are not, (*cf.* [41]). The decisive factor in this system is in some cases evidently not the chromophore itself (ketone, double bond, etc.) but the permolecular chirality of the molecule.

This view is also supported by the fact that all the known optically active derivatives of twistane and heterotwistanes with the same helicity have the same sign of optical rotation (Table IV).

Table IV

Specific Rotation Values for Various Systems of Twistane Type

Compound	Formula		Ref.
(M)-Twistane	**Ib**	+434°(+355°)[a]	[34]
(M)-Twistene	(+)-**IX**	+417°	[34]
(M)-2,7-Dioxatwistane	(+)-**XXVIa**	+217°	[44]
(M)-4-Azatwistane	(+)-**XXIII**	+423°	[51]

[a] Calculated by BREWSTER [24].

It is worth notice that the rotation of (M)-twistane calculated [42] by the BREWSTER Helical Conductor Model [43] gives $[\alpha]_D$+355° which is in a good agreement with the found value (Table V). On the contrary, calculations [33] using the Conformation Disymmetry Model [45] give a low value and even a wrong sign of rotation.

Heterotwistanes

Systems containing one or two atoms of oxygen, nitrogen or sulphur were also studied. 1-Azatwistane (**XXI**) was prepared independently by several authors [46—49] (Scheme 14). A recent synthesis of a 4-azatwistane derivative (**XXII**) is reported [50]. Also 4-azatwistane (**XXIII**) itself was synthesized, both in the racemic and optically active form [51] (Scheme 15). Its derivative, 4-azatwistan-5-one (**XXIV**), was exploited as a valuable model of a twisted amide group with a defined angle of twist [52, 53] (Scheme 15). Also the oxygen analogue, 4-oxatwistan-5-one (**XXV**), prepared by LEE [54] (cf. [55, 56]), should be a promising model (Scheme 16).

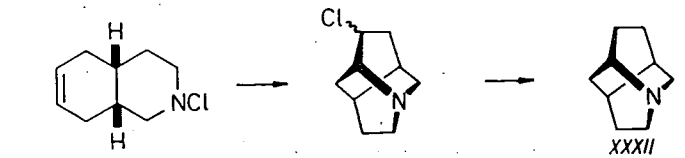

XXXII ref. [46]

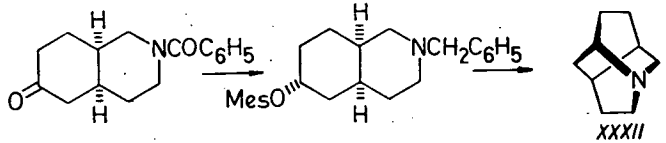

XXXII ref. [47]

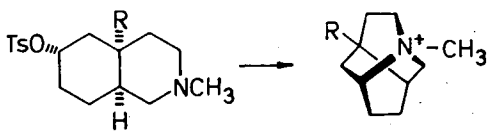

ref. [48,49]

R=H or CH_3

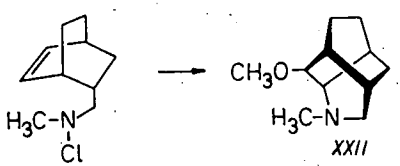

XXII

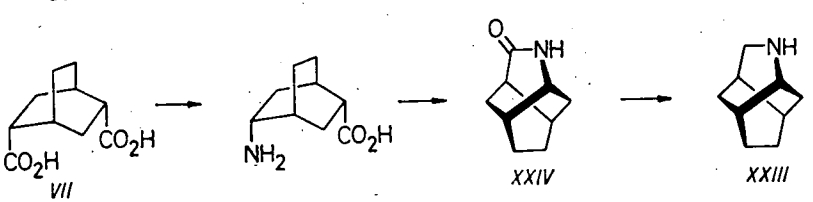

VII *XXIV* *XXIII*

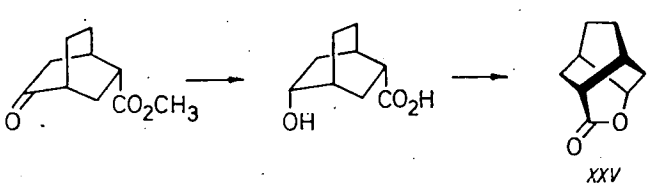

XXV

Systems with two hetero atoms in the twistane skeleton were investigated by GANTER and collaborators [57, 58]. A whole series of compounds of the type **XXVI**

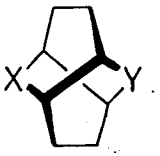

XXVI

a, X = O, Y = O ref. [30,44,58,59]
b, X = S, Y = O ref. [60]
c, X = SO_2, Y = O ref. [61]
d, X = NH, Y = O ref. [62]

was prepared [30, 44, 59—63]. Cyclooctadiene was used as starting material in all these syntheses (Scheme 17). Compound **XXVIa** was prepared also in the optically active form and its absolute configuration was determined [44].

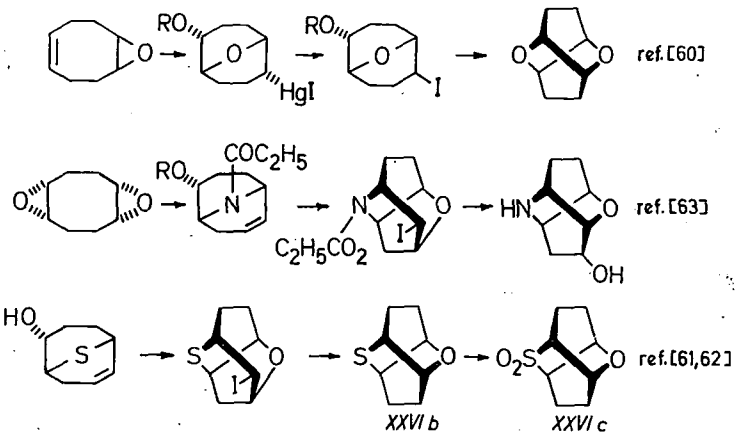

The reactions of heterotwistane derivatives are similar to that of the carbocyclic system. Halides and tosylates with the reacting group in position 4 are solvolysed under partial or complete rearrangement to the corresponding heteroprotoadamantane derivatives [30, 57]. Unsaturated 2,7-dioxatwistene (**XXVII**) and doubly unsaturated 2,7-dioxatwistadiene (**XXVIII**) were also synthesized [64] (Scheme 18) whereas the carbocyclic analogue of **XXVIII** is still unknown.

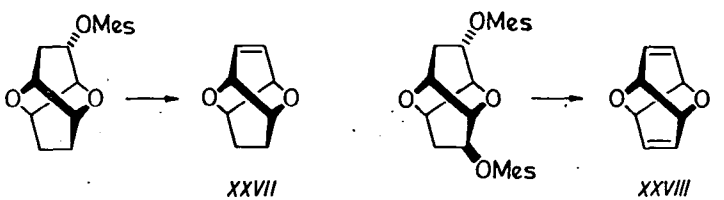

Conclusion

As has been shown, the twistane system is a suitable model for the study of permolecular chirality and its relation to other forms of chirality. The twist of the molecule allows studies of steric situations caused by the uncommon torsion angles 30°, 90° and 150°. The six-membered rings of which the system is formed can serve as models of the usually elusive twist-boat form. Also, the rearrangements of the system are not without interest.

Recently, it was found that some twistane derivatives also exhibit antiviral activity [65, 66]. It is therefore evident that twistane system can be useful in more than one way and that the possibilities of its exploitation are far from being exhausted.

References

[1] *Fort, R. C., P.v.R. Schleyer:* Chem. Rev. **64**, 277 (1964).
[2] *Bingham, R. C., P. v. R. Schleyer, :* Fortschr. Chem. Forsch. **18**, 1 (1971).
[3] *Sevostjanova, V. V., M. M. Krajuškin, A. G. Jurčenko, G. A.:* Usp. Khim. **39**, 1721 (1970).
[4] *Lenoir, D., P. Mison, E. Hyson, P.v.R. Schleyer, M. Saunders, P. Vogel, L. A. Telkowski:* J. Amer. Chem. Soc. **96**, 2157 (1974).
[5] *Cupas, C., W. Schumann, W. E. Heyd:* J. Amer. Chem. Soc. **92**, 3237 (1970).
[6] *Spurlock, L. A., K. P. Clark:* J. Amer. Chem. Soc. **94**, 5349 (1972).
[7] *Corey, E. J., R. S. Glass:* J. Amer. Chem. Soc. **89**, 2600 (1967).
[8] *Jacobson, I. T.:* Acta Chem. Scand. **21**, 2235 (1967).
[9] *Paquette, L. A., G. V. Meehan, S. L. Marshall.:* J. Amer. Chem. Soc. **91**, 6779 (1969).
[10] *Pozdnikina, S. G., O. E. Morozova, A. A. Petrov.:* Neftekhimiya **13**, 21 (1973).
[11] *Cahn, R. S., C. K. Ingold, V. Prelog:* Angew. Chem. Int. Ed. **5**, 385 (1966).
[12] *Tichý, M., L. Kniežo:* Coll. Czechoslov. Chem. Commun. **38**, 1537 (1973).
[13] *Musso, H.:* Chem. Ber. **108**, 337 (1975).
[14] *Whitlock, H. W. Jr.:* J. Amer. Chem. Soc. **84**, 3412 (1962).
[15] *Whitlock, H. W. Jr., M. W. Siefken:* J. Amer. Chem. Soc. **90**, 4929 (1968).
[16] *Gauthier, J., P. Deslongchamps:* Can. J. Chem. **45**, 297 (1967).
[17] *Bélanger, A., Y. Lambert, P. Deslongchamps:* Can. J. Chem. **47**, 795 (1969).
[18] *Tichý, M., J. Sicher:* Coll. Czechoslov. Chem. Commun. **37**, 3106 (1972).
[19] *Tichý, M., J. Sicher:* Tetrahedron Lett. **1969**, 4609.
[20] *Greuter H., H. Schmid:* Helv. Chim. Acta **55**, 2382 (1972).
[21] *Osawa, E., P.v.R. Schleyer, L. W. K. Chang, V. V. Kane:* Tetrahedron Lett. **1974**, 4189.
[22] *Tichý, M., L. Kniežo, J. Hapala:* Tetrahedron Lett. **1972**, 699.
[23] *Tichý, M., L. Kniežo, J. Hapala:* Coll. Czechoslov. Chem. Commun., **40** 3862 (1975).
[24] *Gelernter, H., N. S. Sridharan, A. J. Hart, S. C. Yen, F. W. Fowler, H. J. Shue:* Fortschr. Chem. Forsch. 41, **113** (1973).
[25] *Tichý, M., L. Kniežo, S. Vašíčková:* Coll. Czechoslov. Chem. Commun. **39**, 555 (1974).
[26] *Kniežo, L.:* Dissertation, Prague 1972.
[27] *Engler, E. M., M. Farcasiu, A. Sevin, J. M. Cense, P.v.R. Schleyer:* J. Amer. Chem. Soc. **95**, 5769 (1973).
[28] *Bingham, R. C., P.v.R. Schleyer, Y. Lambert, P. Deslongchamps:* Can. J. Chem. **48**, 3739 (1970).
[29] *Teufel, H., E. F. Jenny, K. Heusler:* Tetrahedron Lett. **1973**, 3413, 3421, 3425.
[30] *Wicker, K., P. Ackermann, C. Ganter:* Helv. Chim. Acta **55**, 2744 (1972).
[31] *Goering, H. L., C. B. Schewene:* J. Amer. Chem. Soc. **87**, 3516 (1965).
[32] *Engler, E. M., J. D. Andose, P.v.R. Schleyer:* J. Amer. Chem. Soc. **95**, 8005 (1973).
[33] *Adachi, K., K., Naemura, M. Nakazaki:* Tetrahedron Lett. **1968**, 5467.
[34] *Tichý, M.;* Coll. Czechoslov. Chem. Commun. **39**, 2673 (1974).
[35] *Djerassi, K., W. Klyne:* Proc. Nat. Acad. Sci. U.S.A. **48**, 1093 (1962).
[36] *Scott, A. I., A. D. Wrixon:* J. Chem. Soc. D, **1969**, 1182, 1184.
[37] *Berson, J. A., R. T. Luibrand, N. G. Kundu, D. G. Morris,:* J. Amer. Chem. Soc. **93**, 3075 (1971).
[38] *Berson, J. A., D. Willner:* J. Amer. Chem. Soc. **84**, 675 (1962).

[39] *Mislow, K., J. G. Berger:* J. Amer. Chem. Soc. **84**, 1956 (1962).
[40] *Walborski, H. M., M. E. Baum, A. A. Yousseff:* J. Amer. Chem. Soc. **83**, 988 (1961).
[41] *Snatzke, G., F. Werner-Zamojska:* Tetrahedron Lett. **1972**, 4275.
[42] *Brewster, J. H.:* Tetrahedron Lett. **1972**, 4355.
[43] *Brewster, J. H.* in „Topics in Stereochemistry" Vol. 2., p. 1, Interscience, London 1967.
[44] *Ackermann, P., H. Tobler, C. Ganter:* Helv. Chim. Acta **55**, 2731 (1972).
[45] *Brewster, J. H.:* J. Amer. Chem. Soc. **81**, 5475, 5483, 5493 (1959).
[46] *Heusler, K.:* Tetrahedron Lett. **1970**, 97.
[47] *Dubé, S., P. Deslongchamps:* Tetrahedron Lett. **1970**, 101.
[48] *Perelman, D., S. Sicsic, Z. Welvart:* Tetrahedron Lett. **1970**, 103.
[49] *Sicsic, S., N. T. Luong-thi:* Tetrahedron Lett. **1973**, 169.
[50] *Lockhart, R. W., K. Hanaya, F. W. B. Einstein, Y. L. Chow:* Chem. Commun. **1975**, 344.
[51] *Tichý, M., E. Dušková:* Unpublished results.
[52] *Tichý, M., M. Dušková, K. Bláha:* Tetrahedron Lett. **1974**, 237.
[53] *Smoliková, J., M. Tichý, K. Bláha:* Coll. Czechoslov. Chem. Commun. (in press).
[54] *Lee, R. A.:* Tetrahedron Lett. **1973**, 3333.
[55] *Moriarty, R. M., T. Adams:* J. Amer. Chem. Soc. **95**, 4071 (1973).
[56] *Storm, D. R., D. E. Jr. Koshland:* J. Amer. Chem. Soc. **94**, 5815 (1972).
[57] *Ganter, C.:* Chimia **25**, 418 (1971).
[58] *Canter, C.:* Chimia **27**, 18 (1973).
[59] *Ganter, C., K. Wicker:* Helv. Chim. Acta **53**, 1693 (1970).
[60] *Ganter, C., W. Zwahlen:* Helv. Chim. Acta **54**, 2628 (1971).
[61] *Wigger, N., C. Ganter:* Helv. Chim. Acta **55**, 2769 (1972).
[62] *Wigger, N., N. Stückeli, H. Czepanski, C. Ganter:* Helv. Chim. Acta **55**, 2791 (1972).
[63] *Portmann, R. E., C. Ganter:* Helv. Chim. Acta **56**, 1991 (1973).
[64] *Ackermann, P., C. Ganter:* Helv. Chim. Acta **56**, 3054 (1973).
[65] *Deslongchamps, P.:* U.S. Patent 3,845,124; Chem. Abstr. **83**, 9327h (1975).
[66] *Schaffner, K., A. Storni, A. Meisels:* Swiss Patent Appl. 4261/73; Chem. Abstr. **82**, 124910j (1975).

ХИМИЯ ТВИСТАНОВ И ИХ ПРИМЕНЕНИЕ В СТЕРЕОХИМИИ

M. Тихи

В данном обзоре автор преследовал цель отражения химии твистанов и различные возможности их применения в качестве стереохимических моделей. Многие из упоминаемых в этой статье стереохимических применений являются результатом исследований проведенных в лаборатории автора.

ХИМИЯ 1,3-БИФУНКЦИОНАЛЬНЫХ СИСТЕМ, XIX
ТИОЛИЗ 1,3-ДИОКСАЦИКЛАНОВ

Д. Л. РАХМАНКУЛОВ, Н. Е. МАКСИМОВА, Е. А. КАНТОР,
Р. А. КАРАХАНОВ*, М. БАРТОК**.
Уфимский нефтяной институт, Уфа, СССР

(Поступило в редакцию 2-го февраля 1975 г.)

В работе сообщается о кислотно-катализируемых превращениях циклических ацеталей под действием серусодержащих соединений. Установлено, что рассматриваемое взаимодействие характерно для всех циклических 1,3-диоксаструктур и при этом образуются тиали и гликоли с высокими выходами. Показано, что шестичленные ацетали обладают большей устойчивостью к действию меркаптанов, чем пяти— и семичленные, что, очевидно, связано с различной напряженностью циклов. Установлено, что электронодонорные заместители при втором атоме углерода облегчают разрыв СО-связей кольца.

В литературе содержится мало сведений о действии серусодержащих соединений на 1,3-диоксацикланы (ДЦ). Имеется лишь единственное сообщение *М. Ф. Шостаковского* с сотр. [1], в котором указывается на возможность получения линейных 3,5-дитиоалканов тиолизом ацеталей. Между тем, эта реакция позволяет уточнить механизм кислотно-катализируемых превращений ДЦ, так как характер образующихся продуктов однозначно отмечает место разрыва связей исходной молекулы, и приводит к весьма ценным монои- и полифункциональным структурам.

Результаты и обсуждение.

Нашими исследованиями установлено, что рассматриваемое взаимодействие характерно для всех циклических 1,3-диоксаструктур. Образование тиоацеталей сопровождается при этом выделением эквимолекулярных количеств известных своим значением гликолей или продуктов их дегидратации:

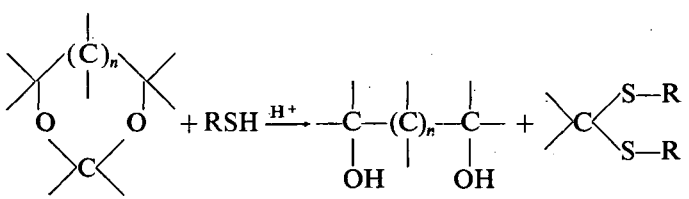

I II III IV

$n = 0, 1, 2$

* Институт органической химии им. Н. Д. Зелинского АН СССР, Москва.
** Кафедра органической химии университета им. Аттилы Йожефа, Сегед.

Наличие экстремума функции выхода (III) и (IV) от режимных параметров (рис. 1,2) свидетельствует о возможности первоначального перехода (I) в неустойчивое промежуточное соединение (Б):

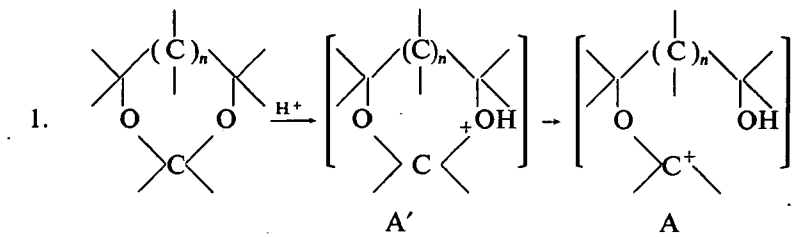

A′ A

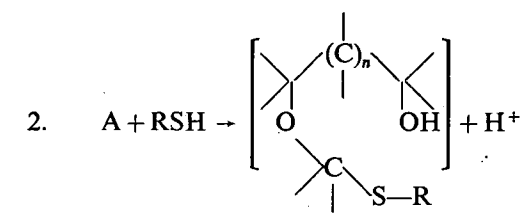

Б

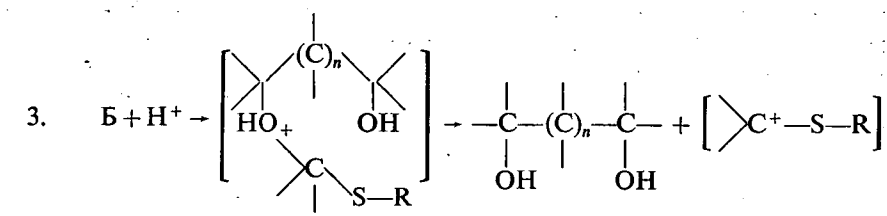

В

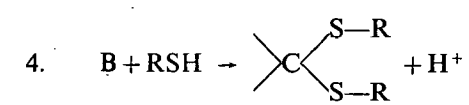

Квантово-химические расчеты σ-электронной плотности (рис. 3) были осуществлены с использованием метода Дель Ре [2], который не требует знания геометрии молекул и предполагает локализацию σ-связей с учетом взаимного влияния атомов посредством индуктивных параметров. Принцип расчета основан на адаптации простого метода МО ЛКАО [3]. Результаты расчетов, выполненных нами на ЭЦВМ «Минск-32», показывают, что наименьший отрицательный заряд имеет атом кислорода в молекуле 1,3-диоксолана. Поэтому можно утверждать, что скорость образования иона (A′) для пятич-

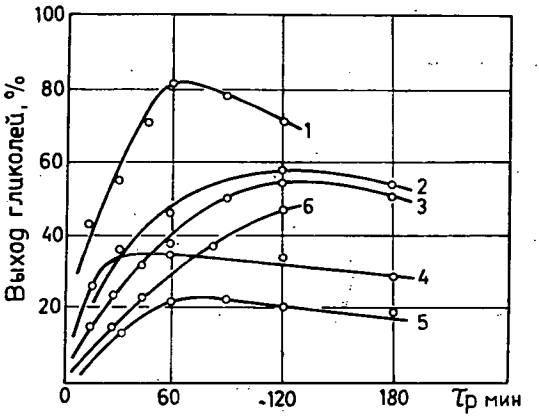

Рис. 1. Влияние продолжительности реакции на выход гликолей и тетрагидрофурана при тиолизе 1,3-диоксацикланов. 1. Пропандиол-1,3 из 1,3-диоксана. 2. Бутандиол-1, 3 из 2,4-диметил-1,3-диоксана. 3. Пропандиол-1,3 из 2-метил-1,3-диоксана. 4. Бутандиол-1,4 из 1,3-диоксепана. 5. Этиленгликоль из 1,3-диоксолана. 6. Тетрагидрофуран. *Условия:* температура 80 °С, продолжительность реакции 3 часа, количество катионита КУ-2 25 г/моль ацеталя.

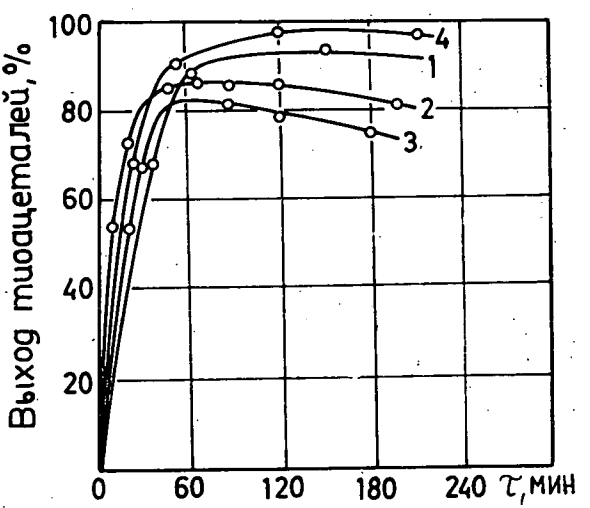

Рис. 2. Влияние продолжительности реакции на выход тиалей при тиолизе 1,3-диоксацикланов. 1. 3,5-Дитиагептан из 1,3-диоксана. 2. 3,5-Дитиагептан из 1,3-диоксолана. 3. 3,5-Дитиагептан из 1,3-диоксепана. 4. 4-Метил-3,5-дитиагептан из 2-метил-1,3-диоксана. *Условия:* температура 80 °С, количество катионита КУ-2 25 г/моль 1,3-диоксациклана.

ленных ацеталей ниже, чем для шестичленных. В то же время, судя по конверсии (рис. 4) наибольшей устойчивостью обладают 1,3-диоксаны. Это обстоятельство указывает на то, что стадия присоединения протона не является лимитирующей.

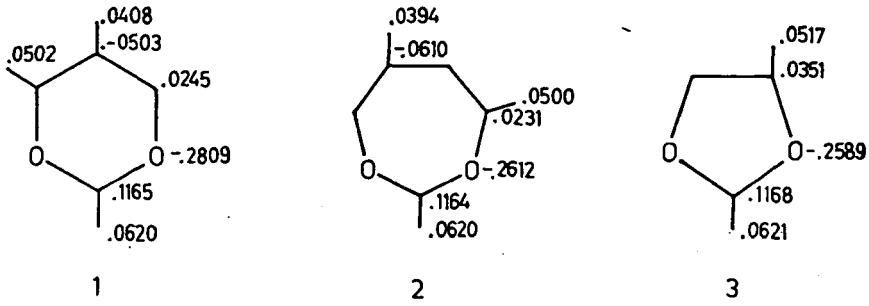

Рис. 3. Молекулярные диаграммы 1,3-диоксацикланов. 1. 1,3-Диоксан. 2. 1,3-Диоксепан. 3. 1,3-Диоксолан.

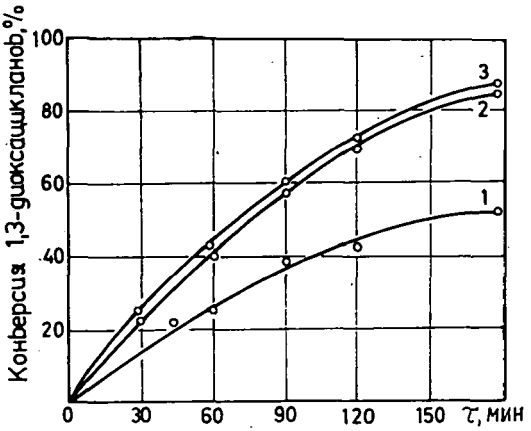

Рис. 4. Влияние продолжительности реакции на конверсию 1,3-диоксацикланов при тиолизе этилмеркаптаном. 1. 1,3-Диоксан. 2. 1,3-Диоксепан. 3. 1,3-Диоксолан. Условия: температура 80 °С, количество КУ-2 25 г/моль формаля, мольное отношение формаль: тиоспирт 1:2.

По-видимому, 1,3-диоксан, как и циклогексан [3] имеет наименее напряженный цикл. Следствием этого и является повышенная стойкость к действию тиолов у шестичленных ацеталей.

Следует отметить, что для любого ДЦ электроннодонорные заместители при $C_{(2)}$ облегчают разрыв С—О-связей кольца. Подобные группы при других атомах повышают селективность процесса. Величина последней по (IV)

для всех исходных систем может быть доведена до 95—98%. Выход же (III) лишь в отдельных случаях приближается к 80—85%. Это связано, очевидно, со склонностью гликолей к дегидратации. Так, образующийся при тиолизе 1,3-диоксепана 1,4-бутандиол при повышенных температурах отщепляет молекулу воды с переходом в тетрагидрофуран (рис 1.).

Экспериментальная часть

Опыты проводились в непрерывно встряхиваемой металлической ампуле (емкостью 50 см^3), снабженной устройством для отбора проб для хроматографического анализа в ходе эксперимента, и помещенной в термостат. В качестве катализатора использовались КУ-2 и *p*-толуолсульфокислота, а гомогенизирующим агентом служил 1,4-диоксан. Продукты реакции выделялись перегонкой в вакууме и очищались на препаративном хроматографе.

Физико-химические свойства их приведены в таблице. Стуктура выделенных соединений доказывалась общепринятыми способами, включая встречный синтез [4].

Таблица I

Соединение	Т. кип. °С (мм *Hg*)	n_D^{20}	d_4^{20}
3,5-Дитиагептан	77,5—78,5 (16)	1,5048	1,0009
Этиленгликоль	194,6—195,0	1,4320	1,1079
Пропандиол-1,3	109,0—110,0 (15)	1,4397	1,0530
Бутандиол-1,3	114,0—116,0 (15)	1,4391	1,0069
Тетрагидрофуран	64,0—65,0	1,4042	0,8878

Литература

[1] *Шостаковский, М. Ф., А. С. Атавин и др.:* Изв. АН СССР, сер. хим. **9**, 1686 (1964).
[2] Del Re, I.: J. Chem Soc., **40**, 4031 (1958).
[3] *Кругляк, Ю. А. и др.:* Методы расчета электронной структуры и спектров молекул, Киев, 1969.
[4] *Илиел, З. Л.:* Основы стереохимии, Москва, 1971.
[5] *Кулиев, А. М. и др.:* Присадки к смазочным маслам, Баку, 1967.

CHEMISTRY OF 1,3-DIFUNCTIONAL SYSTEMS, XIX THIOLYSIS OF 1,3-DIOXACYCLOALKANES

D. L. Rakhmankulov, N. E. Maksimova, E. A. Kantor, R. A. Karakhanov and M. Bartók

The present paper deals with acid-catalysed thiolysis of 5-, 6- and 7-membered 1,3-dioxacycloalkanes under the influence of thioalcohols. Diols, thioacetals and thioketals are formed with good yields in the course of the thiolysis. Conclusions concerning the mechanism of the process were drawn on the basis of the experimental data.

ХИМИЯ 1,3-БИФУНКЦИОНАЛЬНЫХ СИСТЕМ, XX
СИНТЕЗ И ТИОЛИЗ СЕРУСОДЕРЖАЩИХ 1,3-ДИОКСАЦИКЛАНОВ

Д. Л. РАХМАНКУЛОВ, Н. Е. МАКСИМОВА, Р. А. КАРАХАНОВ*,
Е. А. КАНТОР, М. БАРТОК**, С. С. ЗЛОТСКИЙ

Уфимский нефтяной институт, Уфа

(Поступило в редакцию 12 февраля 1975 г.)

2-Винил-1,3-диоксацикланы взаимодействуют с этантиолом с образованием продуктов присоединения. Реакцию катализируют Na_2CO_3, элементарная сера, катионит КУ-2. В присутствии КУ-2 наряду с присоединением в результате тиолиза с заметной селективностью образуются соответствующие гликоли и алкилтиотиоацетали.

В литературе практически отсутствуют сведения о серусодержащих 1,3-диоксацикланах, хотя соединения подобного типа представляют несомненный интерес как биологически активные и лекарственные препараты, растворители, добавки к полимерным и каучукообразным материалам.

Синтез серусодержащих 1,3-диоксацикланов был осуществлен нами тремя методами:

1. Ацеталированием гликолей 4-тиагексаналом, полученным на основе акролеина и этантиола:

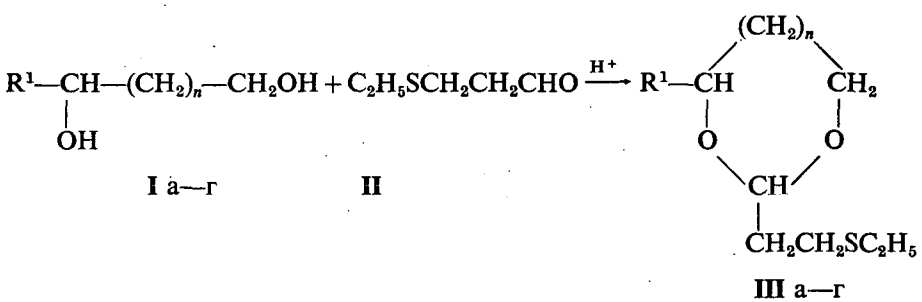

I а—г II III а—г

2. Присоединением этантиола по двойной связи 2-винил-1,3-диоксацикланов:

*Институт органической химии им. Н. Д. Зелинского, Москва
**Университет им. Йожефа Аттилы, Сегед

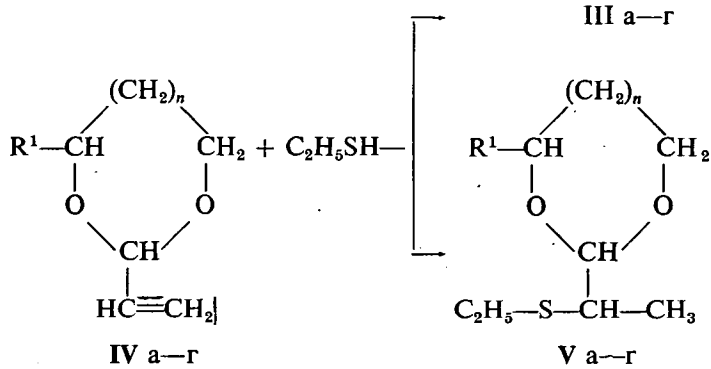

3. Из глиоксаля, этантиола и гликоля в две стадии:

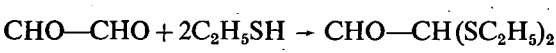

VI

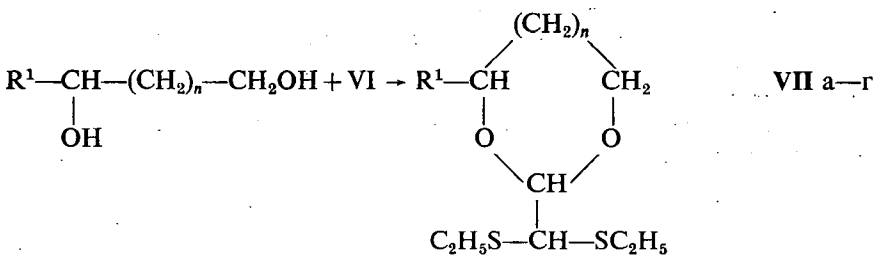

$R^1 = H$; $n = 0$ (Ia, IIIa, IVa, Va, VIIa)
$R^1 = H$; $n = 1$ (Iб, IIIб, IVб, Vб, VIIб)
$R^1 = CH_3$; $n = 0$ (Iв, IIIв, IVв, Vв, VIIв)
$R^1 = CH_3$; $n = 1$ (Iг, IIIг, IVг, Vг, VIIг)

Свойства полученных и некоторых исходных соединений приведены в таблице 1.

Ранее нами было показано, что тиолиз 1,3-диоксацикланов, являющихся доступными продуктами нефтехимического синтеза, приводит к соответствующим тиоацеталям и гликолям [1—2], которые могут найти применение как пластификаторы, ингибиторы коррозии, а также в качестве полупродуктов в ряде синтезов.

Таблица I

Физико-химические характеристики синтезированных соединений

Соединения	Брутто-формула	Т кип. °С (мм Hg)	n_D^{20}	d_4^{20}
Iа	$C_2H_6O_2$	197—198	1,4320	1,1136
Iб	$C_3H_8O_2$	109—110 (15)	1,4397	1,0526
Iв	$C_3H_8O_2$	188—189	1,4295	1,0408
Iг	$C_4H_{10}O_2$	141—146 (15)	1,4391	1,0069
IIIа	$C_7H_{14}SO_2$	122—123 (15)	1,4755	1,0653
IIIб	$C_8H_{16}SO_2$	132—133 (22)	1,4822	1,0483
IIIв	$C_8H_{16}SO_2$	125—130 (28)	1,4698	1,0189
IIIг	$C_9H_{18}SO_2$	142—144 (32)	1,4755	1,0088
IVа	$C_5H_8O_2$	150 (50)	1,4571	0,9581
IVб	$C_6H_{10}O_2$	60 (30)	1,4432	1,0427
IVв	$C_6H_{10}O_2$	35 (8)	1,4242	0,9063
IVг	$C_7H_{12}O_2$	42—43 (15)	1,4389	0,9523
Vа	$C_7H_{14}SO_2$	121 (19)	1,4875	1,0388
Vб	$C_8H_{16}SO_2$	123—125 (18)	1,4859	1,1281
Vв	$C_8H_{16}SO_2$	125—130 (28)	1,4698	1,0108
Vг	$C_9H_{18}SO_2$	143 (29)	1,4803	1,0110
VI	$C_6H_{12}S_2O$	121—123 (20)	1,5279	1,0862
VIIа	$C_8H_{16}S_2O_2$	156—159 (20)	1,5544	1,1891
VIIб	$C_9H_{18}S_2O_2$	206—215 (25)	1,5449	1,1608
VIIв	$C_9H_{18}S_2O_2$	182—185 (20)	1,5612	1,1503
VIIг	$C_{10}H_{20}S_2O_2$	208—212 (18)	1,5509	1,1593
VIII	$C_9H_{20}S_3$	139—142 (5)	1,5270	1,0221
IX	$C_9H_{20}S_3$	176—179 (24)	1,5173	1,0226
X	$C_{10}H_{22}S_4$	197—199 (25)	1,5573	1,0885

Интересно отметить, что наличие двух функциональных групп в 2-винил-1,3-диоксацикланах предопределяет их двойственную реакционную способность. Так, помимо присоединения этантиола по двойной связи, в продуктах реакции при определенных условиях в значительных количествах присутствуют соединения, являющиеся результатом тиолиза промежуточного серусодержащего 1,3-диоксациклана. Относительное содержание продуктов фрагментации цикла в первую очередь определяется выбором катализатора.

Так, например, элементарная сера и Na_2CO_3 являются селективными, но малоактивными катализаторами присоединения. Степень превращения диоксациклана в этом случае не превышает 10—25%.

Кислотные катализаторы (H_2SO_4, катионит КУ-2) обладают более высокой активностью, но селективность их несколько ниже (табл. 2.).

Тиолизу были подвергнуты все три типа серусодержащих 1,3-диоксацикланов (**III, V, VII**), при этом наряду с гликолями (**I а—г**) получены серусодержащие тиоацетали следующего строения:

$C_2H_5SCH_2CH_2CH(SC_2H_5)_2$; **VIII**

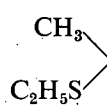

IX

$(C_2H_5S)_2CH—CH(SC_2H_5)_2$

X

Таблица II

Результаты взаимодействия 2-винил-1,3-диоксацикланов с этантиолом
Условия: температура 100 °С; продолжительность реакции 10 час.

Исходное соединение	Катализатор	Выход продуктов присоединения, %		Выход продуктов расщепления, %		
				Гликоль		Тиоацеталь
IVа	Na_2CO_3	Va	16,3	Ia	—	—
	элементарная сера		8,4		—	—
	КУ-2		23,9		33,6	48,7
IVб	Na_2CO_3	Vб	18,2	Iб	—	—
	элементарная сера		12,6		—	—
	КУ-2		26,2		38,3	49,3
IVв	Na_2CO_3	Vв	19,1	Iв	—	—
	элементарная сера		11,8		—	—
	КУ-2		26,9		36,4	51,2
IVг	Na_2CO_3	Vг	19,4	Iг	—	—
	элементарная сера		12,3		—	—
	КУ-2		32,6		36,8	49,5

Экспериментальная часть

1. Синтез серусодержащих 1,3-диоксацикланов из гликолей и 4-тиогексаналя осуществлялся по описанной методике [3].

2. В металлическую ампулу вносили 2-винил-1,3-диоксациклан и этантиол в мольном отношении 1:0,5:1 и катализатор. Ампулу помещали в термостат и при непрерывном встряхивании выдерживали в течении 8—12 часов. Анализ продуктов реакции проводили на хроматографе «Цвет-4» с детектором по теплопроводности (1,2,3-трис-β-цианэтоксипропан на хроматоне N—AW, газ-носитель—водород 3—5 л/час; температура колонки 80—150 °С).

Выделение продуктов реакции проводили на препаративном хроматографе ПАХВ-05 (аниезон L на хроматоне, газ-носитель—гелий, температура колонки 120—160 °С) после отделения реакционной массы от катализатора (нейтрализация и фильтрование) и отгонки исходных реагентов.

3. Тиолиз 1,3-диоксацикланов проводился по описанной ранее методике [2].

Литература

[1] *Рахманкулов, Д. Л., Н. Е. Максимова, В. Р. Меликян, В. И. Исагулянц:* ЖПХ, **47**, 233 (1974).

[2] *Рахманкулов, Д. Л., Н. Е. Максимова, В. Р. Меликян, В. И. Исагулянц:* ЖПХ, **47**, 469 (1974).

[3] *Апьок, Й. М. Барток, Р. А. Караханов, Н. И. Шуйкин:* Изв. АН СССР, сер. хим **10**, 2354 (1968).

CHEMISTRY OF 1,3-DIFUNCTIONAL SYSTEMS, XX
SYNTHESIS AND THIOLYSIS OF 1,3-DIOXACYCLOALKANES CONTAINING SULPHUR

D. L. Rakhmankulov, N. E. Maksimova, R. A. Karakhanov, E. A. Kantor, M. Bartók and S. S. Zlotskii

2-Vinyl-1,3-dioxacycloalkanes undergo with ethyl mercaptan in an addition reaction. The reaction is catalysed by sodium carbonate, sulphur, synthetic resin of KU-2 type. In the presence of the latter, not only addition but also thiolysis occurs yielding glycols and alkylthio-thioacetals.

REARRANGEMENTS OF STEROIDS, IX

Schmidt Reactions and Beckmann Rearrangements of Bile Acid Ketones and Ketoximes*

By

B. MATKOVICS, GY. BALÁZS and L. BALÁSPIRI

Biochemical Group, Department of Animal Physiology, Attila József University, Szeged

(Received September 8, 1975)

Various O-acetyl-protected 3-keto, 6-keto, 7-keto- and 12-keto-cholanic acid methyl esters were subjected to Schmidt rearrangement, and the resulting homo-lactams were compared with the homo-lactams isolated in the Beckmann rearrangement of the corresponding ketoximes. In addition, the structures of the homo-lactams formed were confirmed by Hofmann degradation from the side of the amine formed after hydrolysis of the homo-lactam, by pyrolysis and in several cases by subsequent Oppenauer oxidation, *via* the structures of the substances isolated.

Comparatively few publications deal with the rearrangements of bile acid ketones and ketoximes [1—3]. We have primarily regarded the bile acid ketones and ketoximes as the simplest and most easily accessible coprostane skeleton model for the comparative study of the mechanisms of the Schmidt reaction and Beckmann rearrangement [4, 5].

Bile acid derivatives were dealt with earlier in another respect [6—8], and thus their investigation, preparation and isolation did not cause any particular difficulty.

The following bile acid ketones and ketoximes (**I—VIII**) were prepared and subjected to rearrangement.

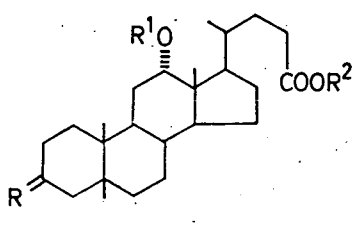

I: R=O; R^1=Ac; R^2=CH_3

II: R=NOH; R^1=Ac; R^2=CH_3

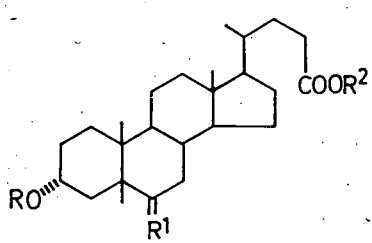

III: R=Ac; R^1=O; R^2=CH_3

IV: R=Ac; R^1=NOH; R^2=CH_3

* Lecture delivered at the Conference of the Hungarian Chemical Society in Szeged on 22 August, 1969.

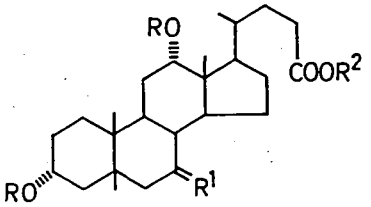

V : R=Ac ; R^1=O; R =CH_3

VI: R=Ac; R^1=NOH; R^2=CH_3

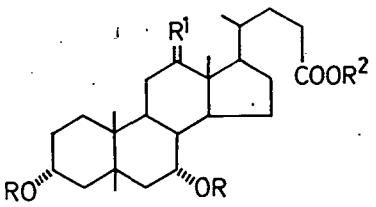

VII : R=Ac ; R^1=O; R^2=CH_3

VIII : R=Ac; R^1=NOH; R^2=CH_3

The rearrangements of **I** and **II** lead to two A-homo-lactams with different structures, which are formed side by side. It was necessary to determine the structures of these products (**IX—X**).

HARA [3] carried out the Schmidt reactions of 3-keto-A-nor-methylcholanate and 3-keto-methylcholanate in chloroform in the presence of sulphuric acid, and the Beckmann rearrangements of the oximes, and isolated both lactams and homo-lactams formed in the rearrangements. Thus, in our case, too, the formation of both homo-lactams was to be expected in both rearrangements. Infact, in the Schmidt reaction of 3-keto-methylcholanate a third homo-lactam was found; as regards its physical constants, this differed from the other homo-lactams, and we assume it to be a derivative containing a free carboxyl group. HARA observed that one lactam and homo-lactam are produced only in low amounts, whereas the yield of the main product is much more significant.

In the rearrangements of 12α-acetoxy-3-keto-methylcholanate (**I**) and its oxime (**II**) we similarly expected, and did isolate two homo-lactams (**IX, X**). Interestingly, however, the rearrangements of **I** and **II** led to the lactams **IX** and **X**, respectively, in almost pure states. The structures of the homo-lactams were established by

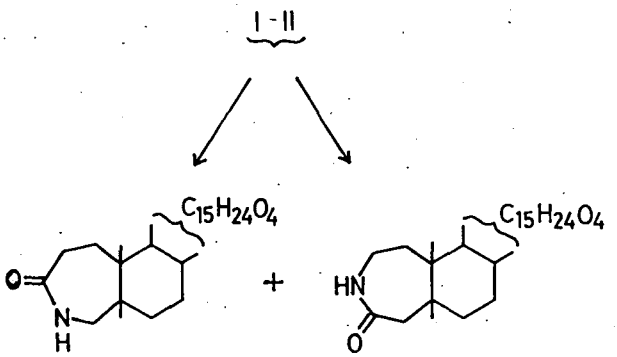

IX X

Hofmann exhaustive methylation following hydrolysis, and by study of the infrared spectra, of various physical constants, and other properties of the products of various structures (**XI—XVI**) produced on pyrolysis.

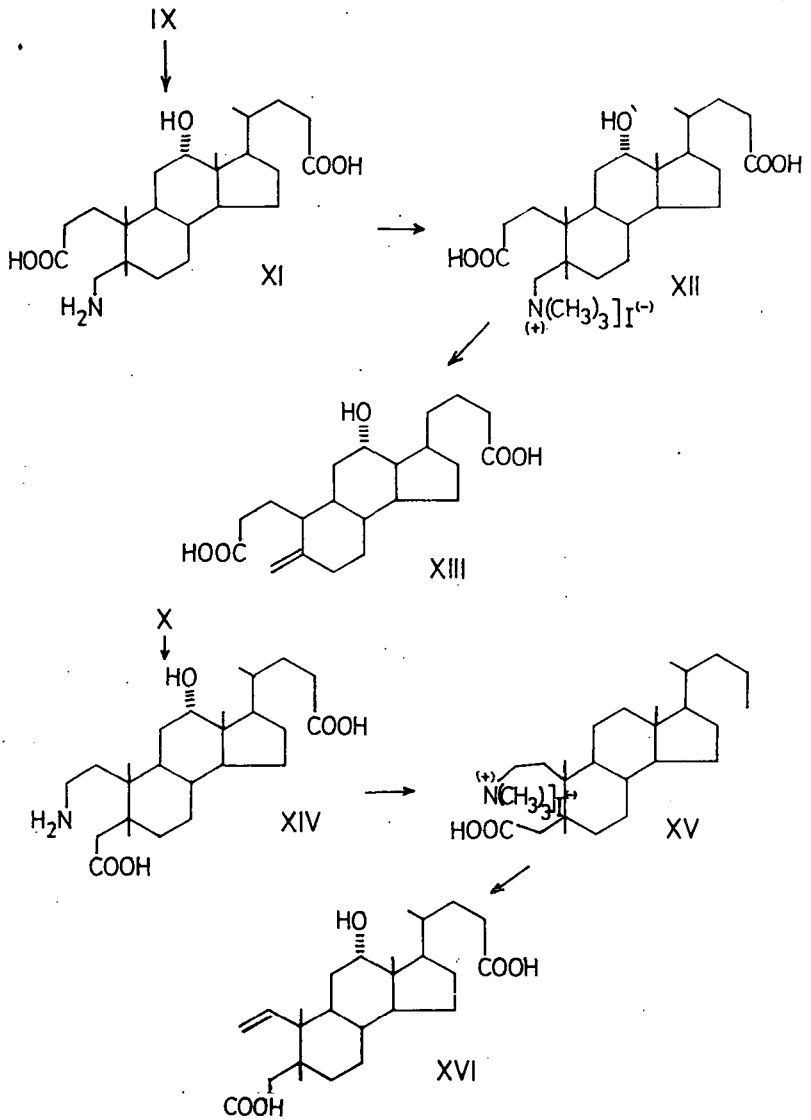

Compound **XIII** displays a methylene vibration in the infrared spectrum, while **XVI** is found to contain an isolated double-bond.

Rearrangement of 3α-acetoxy-6-keto-methylcholanate (**III**) and its oxime (**IV**) gave the homo-lactam **XVII**:

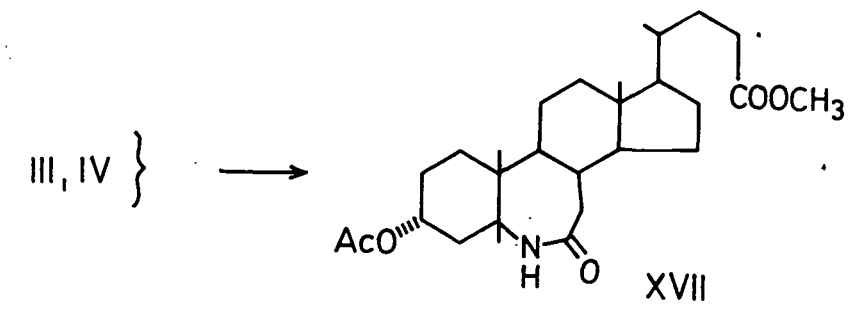

This was hydrolysed, and then pyrolysed after quaternary salt formation under alkaline conditions. The pyrolysis here was followed by Oppenauer oxidation [10]: (**XVIII—XXI**)

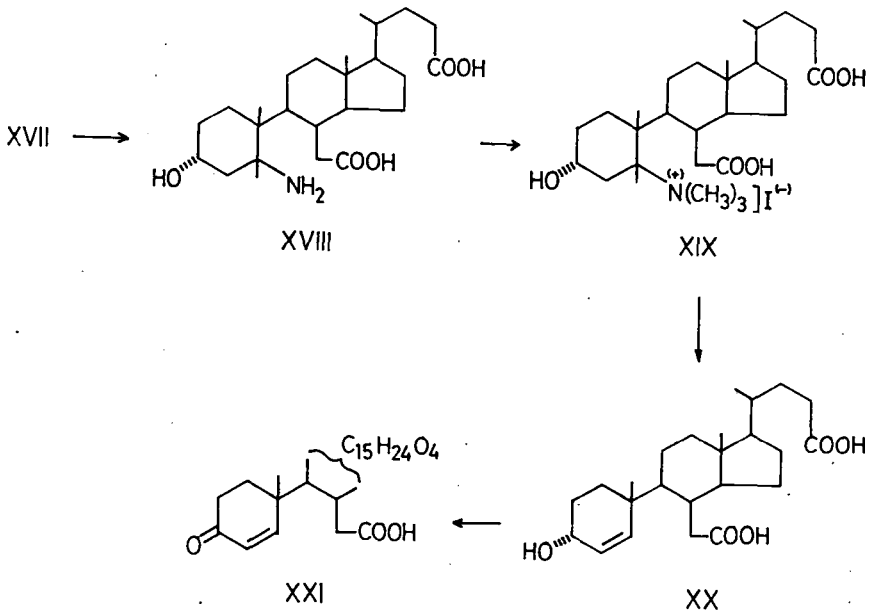

The end-product of the Oppenauer oxidation was compound **XXI**; the characteristic infrared spectrum of this is due to the conjugated ketone structure of ring A.

Under the normal conditions of the Schmidt reactions [11] and Beckmann rearrangements, the same homo-lactam (**XXII**) was isolated from 3α,12α-diacetoxy--7-ketomethylcholanate (**V**) and its oxime (**VI**):

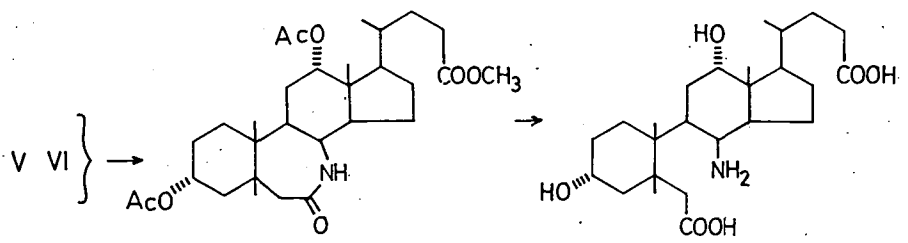

XXII XXIII

This was subsequently hydrolyzed, and the structure of the product was established by Oppenauer oxidation, similarly as for the homo-lactam isolated in the rearrangement of 6-ketone (**XXIV—XXVI**):

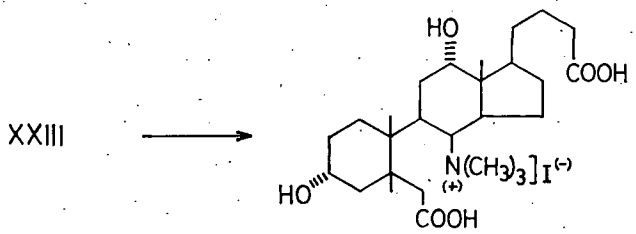

XXIV

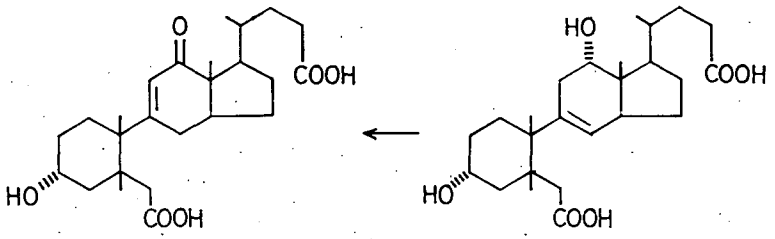

XXVI XXV

Thus, a conjugated ketone structure developed in ring C of the seco-steroid skeleton on Oppenauer oxidation. This made it easier to follow the events.

After hydrolysis of the homo-lactam the presence of the two carboxylic acid groups was proved by microtitration [7].

Finally, 3α,7α-diacetoxy-12-keto-methylcholanate (**VII**) and its oxime (**VIII**) were subjected to the Schmidt reaction and the Beckmann rearrangement, and again one homo-lactam was obtained. The structure of this was determined as before, with hydrolysis, quaternary salt formation and pyrolysis, resulting in a methylene group at C_{18}.

The characteristics of the methylene structure, and of the compounds produced in general (**XXVII—XXX**), are described in the experimental part.

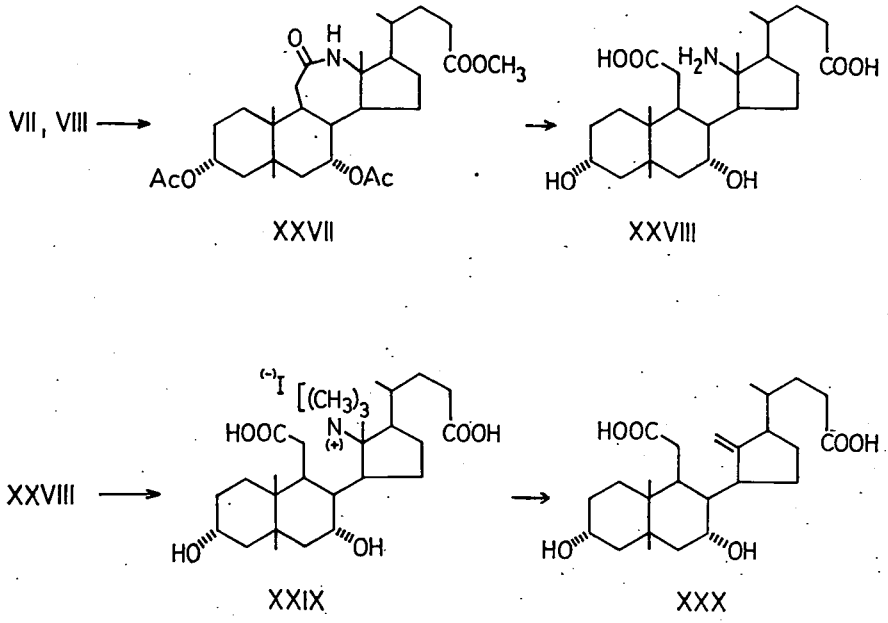

Experimental

Details of the experimental conditions were published earlier [7, 11—13], while details on the TLC are to be found in [6] and [14].

3α,12α-Dihydroxycholanic acid (deoxycholic acid)

This was a gift of the Gedeon Richter Pharmaceutical Works (Budapest). After repeated recrystallization, m.p.: 176—177 °C (literature m.p.: 176—177 °C [15]). This was used to prepare 3α,12α-dihydroxy-methylcholanate with conc. hydrochloric acid in methanol. M.p.: 79—81 °C (lit. m.p.: 80—81 °C [15]).

The methyl compound was acetylated with acetic anhydride in pyridine to give 3α,12α-diacetoxy-methylcholanate. Partial hydrolysis of the 3α-acetoxy group at room temperature with methanolic hydrochloric acid led to 3α-hydroxy-12α-acetoxy-methylcholanate. Repeated attempts were made to recrystallize this from aqueous methanol, without success. The same partial deacetylation was carried out with K_2CO_3 in aqueous methanol, but this did not give a crystalline end-product either [16]. The material was subsequently treated with diazomethane in ether for the methyl ester to be taken further quantitatively.

3-Keto-12α-acetoxy-methylcholanate (**I**) [15]

Prepared from 3α-hydroxy-12α-acetoxy-methylcholanate by CrO_3 oxidation in glacial acetic acid at room temperature. The product was recrystallized several times from ether. M.p.: 121—122 °C; $[\alpha]_D = +83 \pm 2°$ (c=2.15; acetone) [16].

$C_{27}H_{42}O_5$ (446.64). Calcd.: $C_{27}H_{42}O_5$ C 72.61; H 9.43. Found: C 72.64; H 9.48%. ν_{max}^{KBr} 1730, 1700 (C=O), 1260 (C—O acetate) cm^{-1}.

12α-Acetoxy-3-ketoxime-methylcholanate (**II**)

Prepared from **I** in pyridine with hydroxylamine hydrochloride. Recrystallized repeatedly from methanol. M.p.: 74—75 °C; $[\alpha]_D = +99 \pm 2°$ (c=1.0; $CHCl_3$);

$C_{27}H_{42}O_5$=(461.65). Anal.: Calcd.: $C_{27}H_{43}O_5N$ C 70.25; H 9.39; N 3.03. Found: C 70.29; H 9.42; N 3.18%. ν_{max}^{KBr} 3450 (OH), 1720 (C=O), 1650 (C=N), 1250 (C—O acetate) cm^{-1}.

12α-Acetoxy-3-ketoxime-methylcholanate: Beckmann rearrangement

The Beckmann rearrangement of **II** was carried out in pyridine in the presence of *p*-acetylamino-benzenesulfonic acid chloride (PAABSCl) at room temperature, or in dioxane with thionyl chloride at 10 °C. The material obtained by ether extraction was chromatographed on a neutral alumina/activity grade II (n. Al_2O_3/II) column after evaporation of the solvent. The lactam could be eluted from the column only with chloroform. The isolated lactam, the structure of which is given on the basis of the reconstruction of further structural examinations, is 3-keto-3a-aza-12α-acetoxy-A-homo-methylcholanate (**IX**), M.p.: 60—62 °C; $[\alpha]_D = +63 \pm 2°$ (c=1.0; $CHCl_3$);

$C_{27}H_{42}O_5$ (446.64). Calcd: for M.w., molecular formula and calculated values, of C, H and N see **II**). Found: C 70.24; H 9.24; N 3.25%.
ν_{max}^{KBr} 3350, 3300 (NH), 1730, 1670 (C=O), 1250 (C—O ester) cm^{-1}. (Similar rearrangement of **II** is described in [2] and [17].)

3-Keto-12α-acetoxy-methylcholanate: Schmidt reaction

The Schmidt reaction was carried out in polyphosphoric acid (PP) [12], and thus the homo-lactam **X** was obtained in addition to the lactam **IX**.

3-Aza-3a-keto-12α-acetoxy-A-homo-methylcholanate

M.p.: 91—92 °C; $[\alpha]_D = +31 \pm 2°$ (c=1.0; $CHCl_3$);

$C_{27}H_{42}O_5$ (446.64). Cald: for M.w., *etc.* see **II**). Found: C 70.26; H 9.38; N 3.10%. ν_{max}^{KBr} 3350, 3200, 3100 (NH), 1720, 1670 (C=O), 1250 (C—O acetate) cm^{-1}.

3α-Acetoxy-6-keto-methylcholanate (**III**)

Prepared from 3α-acetoxy-6α-hydroxy-methylcholanate. First the methyl ester was prepared from 3α,6α-dihydroxycholanic acid with diazomethane, and this was used to prepare 3α-acetoxy-6α-hydroxy-methylcholanate [7, 18], which was oxidized to **III** with CrO_3 by the method of HOEHN *et al.* [19]; the product was repeatedly

recrystallized from aqueous methanol. M.p.: 156—157 °C; $[\alpha]_D = -19 \pm 2°$ (c=1.0; dioxane); M.w.: 446.63. (Lit. M.p.: 155—157 °C; $[\alpha]_D^{23} = -18.8 \pm 3°$ (dioxane) [19].)

$C_{27}H_{42}O_5$ (446.64). Calcd.: $C_{27}H_{42}O_5$ C 72.61; H 9.48. Found: C 72.65; H 9.52%. ν_{max}^{KBr} 1720, 1700 (C=O), 1250 (C—O acetate) cm^{-1}.

3α-Hydroxy-6-keto-cholanic acid [19]

The method of HOEHN *et al.* [19] can also be used to prepare the deacetylated bile acid 6-ketone. It was recrystallized from aqueous methanol. M.p.: 138—140 °C; $[\alpha]_D = -42 \pm 2°$ (c=1.0; $CHCl_3$); M.w.: 374.57. (Lit. m.p.: 138—140 °C; $[\alpha]_D^{27} = -41.5 \pm 3°$ (dioxane) [19].)

$C_{27}H_{42}O_5$ (446.64). Calcd.: $C_{24}H_{38}O_4$ C 73.81; H 9.80. Found: C 73.94; H 9.86%. ν_{max}^{KBr} 3500 (OH), 1710, 1690 (C=O) cm^{-1}.

3α-Acetoxy-6-ketoxime-methylcholanate (**IV**) [19]

Prepared from **III** in pyridine with hydroxylamine hydrochloride as before. Repeatedly recrystallized from aqueous methanol. M.p.: 161—163 °C; $[\alpha]_D = -18 \pm 2°$ (c=1.0; $CHCl_3$); M.w.: 461.55 (Lit. m.p.: 162—163 °C; $[\alpha]_D^{25} = -17.6 \pm 3°$ (benzene));

$C_{27}H_{42}O_5$ (446.64). Calcd.: $C_{27}H_{43}O_5N$; C 70.25; H 9.39; N 3.04. Found: C 70.26; H 9.41; N 3.10%. ν_{max}^{KBr} 3360 (OH), 1720, 1690 (C=O), 1640 (C=N), 1240 (C—O acetate) cm^{-1}.

3α-Hydroxy-6-ketoxime-cholanic acid

Similarly prepared in pyridine with hydroxylamine hydrochloride. The isolated material was repeatedly recrystallized from aqueous methanol. M.p.: 110—112 °C; $[\alpha]_D = +15 \pm 2°$ (c=1.0; $CHCl_3$); M.w.: 405.58.

$C_{27}H_{42}O_5$ (446.64). Calcd.: $C_{24}H_{39}O_4N$; C 71.08; H 9.69; N 3.45. Found: C 71.12; H 9.73; N 3.43%. ν_{max}^{KBr} 3450 (OH), 1700 (C=O), 1630 (C=N) cm^{-1}.

3α-Acetoxy-6-ketoxime-methylcholanate: Beckmann rearrangement

A solution of 4.61 g of **IV** in 150 ml anhydrous dioxane was added dropwise at room temperature to 8 ml thionyl chloride. The solution was allowed to stand at room temperature for an hour, and then poured onto ice. The product formed was extracted with ether, the extract was washed with distilled water, 5% $NaHCO_3$ solution, and distilled water. The extract was dried and evaporated to dryness. leaving a residue of 3.95 g. The residue consisted of 3.95 g brown crystalline material. The crude product was chromatographed on a silica gel column. Data of 3α-acetoxy-6-aza-6a-keto-B-homo-methylcholanate (**XVII**): m.p.: 82—84 °C; $[\alpha]_D = +72 \pm 2°$ (c=1.0; methanol); M.w.: 461.55.

$C_{27}H_{42}O_5$ (446.64). Calcd: For molecular formula and calculated C, H and N values see **IV**.) Found: C 70.22; H 9.43 N 3.15%. ν_{max}^{KBr} 3420 (NH), 1730, 1660 (O=C.NH), 1350 (C—O acetate) cm^{-1}.

3α-Acetoxy-6-keto-methylcholanate: Schmidt reaction

The Schmidt reaction was carried out by two methods:

a) 4.46 g (0.01 mole) **III** was dissolved in 100 ml dry benzene, and 8.3 ml conc. sulphuric acid was layered under it. 0.62 g (0.015 mole) hydrazoic acid in benzene was added dropwise at room temperature. After stirring for an hour, the mixture was poured onto ice. The benzene phase was separated, washed with 2*N* NaOH and dried. This phase contained 1.02 g material. When the aqueous fraction was extracted with ethyl acetate, a further 2.53 g material was isolated. The two portions of solid were combined, and 1.88 g pure **XVII** was obtained by column chromatography. The calculated physical data for the material are the same as described earlier. Found: C 70.20; H 9.35; N 3.20%.

b) Under the Schmidt reaction conditions employed with **I**, besides the starting substance and **XVII** the lactam of the deacetylated free acid was obtained. See also: 3α-hydroxy-6-ketoximecholanic acid and its Beckmann rearrangement.

3α-Hydroxy-6-ketoxime-cholanic acid: Beckmann rearrangement

When the Beckmann rearrangement of the above oxime was carried out in the manner described, with thionyl chloride and the reaction mixture was poured onto ice, the deacetylated form of the homo-lactam **XVII** was isolated. Physical constants: m.p.: 88—90 °C; $[\alpha]_D = +54 \pm 2°$ (c=1.0; $CHCl_3$).

$C_{27}H_{42}O_5$ (446.64). Calcd: M.w.: 389.58. (For the calculated data, see the oxime.) Found. C 74.03; H 10.12; N 3.75%. ν_{max}^{KBr} 3400 (OH), 1730, 1650 (O=C.NH) cm^{-1}.

3α,12α-Diacetoxy-7-keto-methylcholanate (**V**)

Prepared from the methyl ester of cholic acid by the method of COREY [20]. This is first oxidized with N-bromosuccinimide to 3α,12α-dihydroxy-7-keto-methylcholanate, which is transformed to 3α,12α-diacetoxy-7-keto-methylcholanate with a mixture of acetic acid and acetic anhydride. Physical characteristics: m.p.: 117—118 °C; $[\alpha]_D = +48 \pm 2°$ (c=1.0; $CHCl_3$). M.w.: 504.67.

$C_{27}H_{42}O_5$ (446.64). Calcd.: $C_{29}H_{44}O_7$ C 69.02; H 8.78. Found: C 69.51; H 8.96%. ν_{max}^{KBr} 1725 (C=O), 1250, 1030 (C—O acetate) cm^{-1}.

3α,12α-Diacetoxy-7-ketoxime-methylcholanate (**VI**)

Formed on reaction of **V** with hydroxylamine hydrochloride in ethanol in the presence of anhydrous sodium acetate. The product was repeatedly recrystallized from aqueous methanol. Physical data: m.p.: 99—100 °C; $[\alpha]_D = +8 \pm 2°$ (c=1.0; $CHCl_3$); M.w.: 519.69.

$C_{27}H_{24}O_5$ (446.64). Calcd.: $C_{29}H_{45}O_7N$ C 67.02; H 8.73; N 2.70. Found: C 67.07; H 8.76; N 2.82%. ν_{max}^{KBr} 3500 (OH), 1720 (C=O), 1650 (C=N), 1240 (C—O acetate) cm^{-1}.

3α,12α-Diacetoxy-7-ketoxime-methylcholanate: Beckmann rearrangement

2.48 g (0.005 mole) **VI** was dissolved in pyridine and subjected to rearrangement in the presence of PAABSCl at room temperature. The lactam isolated after chromatography on Al_2O_3/II was 3α,12α-diacetoxy-7-keto-7a-aza-B-homo-methylcholanate (**XXII**). M.p.: 88—90 °C; $[\alpha]_D = +55 \pm 2°$ (c=1.0; $CHCl_3$).

$C_{27}H_{42}O_5$ (446.64). For calcd. m.w., *etc.*, see **VI**). Found: C 67.04; H 8.75; N 2.85%. ν_{max}^{KBr} 3450 (NH), 1720, 1660 (O=C.NH), 1250 (C—O acetate) cm^{-1}.

3α,12α-Diacetoxy-7-keto-methylcholanate: Schmidt reaction

The Schmidt reaction was carried out on **V** in PP. The chloroform extract obtained after neutralization was evaporated to give a yellow-brown oil; this was chromatographed and the lactam **XXII** was isolated. Its physical data were the same as those of the lactam obtained in the Beckmann rearrangement. M.p.: 89—91 °C. Found: C 67.04; H 8.70; N 2.79%. (The IR spectrum, too, coincided with the earlier one.)

3α,7α-Diacetoxy-12-keto-methylcholanate (**VII**) [21, 22]

VII was prepared from 3α,7α,12α-trihydroxycholanic acid methyl ester. 3α,7α-Diacetoxy-12α-hydroxy-methylcholanate was oxidized with Kiliani solution. The isolated material was repeatedly recrystallized from methanol. M.p.: 179—180 °C; $[\alpha]_D = +71 \pm 2°$ (c=1.0; $CHCl_3$); (for M.w. and calcd. values, see **V**). (lit. m.p.: 178—179 °C; $[\alpha]_D^{20} = +73.5°$ (dioxane) [21].)

$C_{27}H_{42}O_5$ (446.64). Found: C 68.78; H 8.81%. ν_{max}^{KBr} 1720, 1690 (C=O), 1250, 1030 (C—O acetate) cm^{-1}.

3α,7α-Diacetoxy-12-ketoxime-methylcholanate (**VIII**)

The oxime was prepared from **VII** in ethanol with hydroxylamine hydrochloride in the presence of anhydrous sodium acetate. The isolated material was repeatedly recrystallized from methanol. M.p.: 99—100 °C; $[\alpha]_D = +160 \pm 2°$ (c=1.0; $CHCl_3$).

$C_{27}H_{42}O_5$ (446.64). (for M.w., *etc.*, see **VI**). Found: C 66.97; H 8.69%. ν_{max}^{KBr} 3450 (OH), 1720 (C=O), 1630 (C=N), 1250, 1030 (C—O acetate) cm^{-1}.

3α,7α-Diacetoxy-12-ketoxime-methylcholanate: Beckmann rearrangement

Rearrangement of 0.005 mole **VIII** was carried out at room temperature in pyridine in the presence of PAABSCl; after evaporation of the extract to dryness 2.2 g crude product was obtained. Column chromatography finally led to a substance with m.p. 93—95 °C; $[\alpha]_D = +37 \pm 2°$ (c=1.0; $CHCl_3$); (for M.w. *etc.*, see **VII**). The lactam is 3α,7α-diacetoxy-12-keto-12a-aza-C-homo-methylcholanate (**XXVII**).

$C_{27}H_{42}O_5$ (446.64). Found: C 67.05; H 8.71; N 2.75%. ν_{max}^{KBr} 3450 (NH), 1720, 1650 (O=C.NH), 1250 (C—O acetate) cm^{-1}.

3α,7α-Diacetoxy-12-keto-methylcholanate: Schmidt reaction

2.87 g (0.005 mole) **VII** was dissolved in 20 ml dry benzene, and 2.5 ml conc. sulphuric acid was layered under it, as described earlier. The calculated amount of hydrazoic acid was added in benzene solution, with constanst stirring, and stirring was continued for further 1 hr at room temperature. The mixture was then poured onto ice, and the product was isolated in the usual manner; a yellow-brown oil was obtained. This was chromatographed, and yielded a lactam with the same physical properties as the homo-lactam **XXVII**. M.p.: 93—95 °C. Found: C 67.04; H 8.78; N 2.88%. (The IR spectrum was the same as that of the C-homo-lactam isolated in the Beckmann rearrangement.)

3,3a-Seco-3a-amino-12α-hydroxycholane-dicarboxylic acid (**XI**)

IX was refluxed for 5 hrs with 5% methanolic KOH and yielded the seco-amino-dicarboxylic acid **XI**. The presence of the primary amine was confirmed by the positive iodine-azide test, and that of the dicarboxylic acid by the microtitration used in the study of the bile acids [7]. (Both methods were used later, for structural determinations, too, and in the following will be mentioned only of their positive or negative nature.) The product was repeatedly recrystallized from methanol. M.p.: 240—244 °C; $[\alpha]_D = +40 \pm 2°$ (c=0.5; methanol);

Calcd.: $C_{24}H_{41}O_5N$ (423,6). C 68.05; H 9.75; N 3.30. Found: C 68.08; H 9.72; N 3.40%. ν_{max}^{KBr} 3500 (OH, NH_2), 1700, 1670 (C=O) cm^{-1}.

3,3a-Seco-3a-amino-12α-hydroxy-dimethylcholanate

XI was dissolved in a few ml methanol. Ether was then added, the mixture was cooled, and an excess of diazomethane was added. The mixture was allowed to stand at room temperature for several hours, filtered and evaporated to dryness in vacuum. The residue was a yellow mastic, which was used to prepare the quaternary compound without further purification.

3,3a-Seco-12α-hydroxy-dimethylcholanate-3a-trimethylammonium iodide (**XII**)

XII was prepared from the former seco-dimethylcholanate by the method of HEUSSER *et al.* [9, 10]. M.p.: 136-138 °C; $[\alpha]_D = -107 \pm 2°$ (c=0.75; methanol);

M.w.: 621.65. Calcd.: $C_{29}H_{52}O_5NI$ C 56.03; H 8.43; N 2.25; I^- 20.41. Found: C 56.05; H 8.17; N 2.31; I^- 20.64%. ν_{max}^{KBr} 3420 (OH), 1720 (C=O), 1440 (C—O-alkyl) cm^{-1}.

Hofmann decomposition of **XII**

Hofmann decomposition is described in the articles of HEUSSER *et al.* [9, 10], in aqueous ethylene glycol in the presence of a base. In the isolation, the reaction mixture was acidified after reaction. The material separating out from the neutral aqueous solution was filtered off and crystallized from methanol. The physical

constants of compound **XIII**: m.p.: 186—188 °C; $[\alpha]_D = +42 \pm 2°$ (c=0.25; $CHCl_3$); M.w.: 406.56. Calc.: $C_{24}H_{38}O_5$ C 70.91; H 9.42. Found: C 71.05; H 9.39%. ν_{max}^{KBr} 3350 (OH), 1730 (C=O), 1620 (C=C) cm^{-1}.

3,3a-Seco-3-amino-12α-hydroxycholane-dicarboxylic acid[3,24] (**XIV**)

X was hydrolyzed, similarly to **IX**, in methanolic KOH, and the end-product was isolated. The hydrolysis was followed by neutralization, and the precipitate was filtered off and recrystallized from methanol. M.p.: 268—270 °C; $[\alpha]_D = +50 \pm 2°$ (c=1.0; $CHCl_3$); (for M.w.: and other calcd. data, see **XI**). Found C 68.10; H 9.72; N 3.22%. ν_{max}^{KBr} 3350, 3250 (OH, HN_2), 1620 (C=O) cm^{-1}.

3,3a-Seco-3-amino-12α-hydroxy-dimethylcholanate

Similarly as above, with an excess of diazomethane in ether, and used after evaporation of the solvent.

3,3a-Seco-12α-hydroxy-dimethylcholanate-3-trimethylammonium iodide (**XV**)

It was prepared by the method of HEUSSER *et al.* [9, 10]. M.p.: 123—125 °C; $[\alpha]_D = -23 \pm 2°$ (c=0.7; methanol); (for M.w. and calculated C, H, N and I^- data see **XII**). Found: C 55.98; H 8.25; N 2.31; I^- 20.64%. ν_{max}^{KBr} 3400 (OH), 1710 (C=O), 1440 (C—O-alkyl) cm^{-1}.

Hofmann decomposition of **XV**

The Hofmann decomposition of **XV** was carried out by the method described above, and **XVI** was isolated. M.p.: 160—162 °C; $[\alpha]_D = 55.5 \pm 2°$ (c=0.25; methanol); M.w.: 406.56 (for the other calcd. data, see **XIII**). Found: C 70.86; H 9.55%. ν_{max}^{KBr} 3420 (OH), 1700 (C=O), 1630 (C=C) cm^{-1}.

6,6a-Seco-5-amino-3α-hydroxycholanedicarboxylic acid[6,24] (**XVIII**)

The lactam **XVII** was hydrolyzed to **XVIII** by refluxing it with 5% methanolic KOH. The substance gives a positive iodine-azide test, and the new carboxylic acid group can be demonstrated by microtitration. M.p.: 168—170 °C; $[\alpha]_D = +6.5 \pm 2°$ (c=1.0; methanol); (M.w. and calculated data: as for **XIV**); Found: C 68.02; H 9.70; N 3.35%. ν_{max}^{KBr} 3300, 3220 (OH, NH_2), 1680, 1630 (C=O) cm^{-1}.

6,6a-Seco-5-amino-3α-hydroxy-dimethylcholanate

was prepared from **XVIII** with diazomethane in ethanol, and used without preliminary identification for preparation of the quaternary salt.

6,6a-Seco-3α-hydroxy-dimethylcholanate-5-trimethylammonium iodide (**XIX**)

Prepared from the former substance by the method of HEUSSER *et al.* [9, 10]. M.p.: 145—148 °C; $[\alpha]_D = +67 \pm 2°$ (c=0.28; methanol). (for M.w., *etc.*, see **XII**). Found: C 55.96; H 8.48; N 2.30; I^- 20.60%. ν_{max}^{KBr} 3350 (OH), 1700, 1630 (C=O), 1460 (C—O-methyl) cm^{-1}.

Hofmann decomposition of **XIX**

The Hofmann decomposition was carried out as above, and **XX** was isolated. M.p.: 204—206 °C; $[\alpha]_D + 36 \pm 2°$ (c=0.01; $CHCl_3$); M.w.: 406.57. Calcd.: $C_{24}H_{38}O_5$ C 70.91; H 9.42. Found: C 71.06; H 9.45%. ν_{max}^{KBr} 3440 (OH), 1720 (C=O), 1640 (C=C) cm^{-1}.

5,6a-Seco-3-ketochol-4-ene-dicarboxylic acid (**XXI**)

The Oppenauer oxidation of **XX** was carried out by the method of ANLIKER *et al.* [10]. In our case the ether extraction was preceded by acidification with 1:1 hydrochloric acid. The substance was recrystallized from acetone. M.p.: 183—185 °C; $[\alpha]_D = +85 \pm 2°$ (c=0.01; methanol); M.w.: 404.55. Calcd.: $C_{24}H_{36}O_5$ C 71.26; H 8.97. Found: C 71.45; H 9.01%. ν_{max}^{KBr} 3400 (OH), 1700, 1650 (C=CH=C=O) cm^{-1}.

7,7a-Seco-8-amino-3α,12α-dihydroxycholane-dicarboxylic acid[7,24] (**XXIII**)

Alkaline hydrolysis of **XXII** led to **XXIII**. M.p.: >350 °C; $[\alpha]_D = +50 \pm 2°$ (c=1.0; methanol); M.w.: 439.60. Calcd.: $C_{24}H_{41}O_6N$ C 65.57; H 9.40; N 3.18. Found: C 65.61; H 9.44; N 3.26%. ν_{max}^{KBr} 3400, 3280 (OH, HN_2), 1700, 1650, 1620 (C=O) cm^{-1}.

7,7a-Seco-8-amino-3α,12α-dihydroxy-dimethylcholanate

Prepared from **XXIII** with diazomethane in ether, and used without purification

7,7a-Seco-3α,12α-dihydroxy-dimethylcholanate-8-trimethylammonium iodide (**XXIV**)

Prepared by the earlier method. M.p.: 208 °C; $[\alpha]_D = +200 \pm 2°$ (c=0.2; $CHCl_3$); M.w.: 637.65 Calcd.: $C_{29}H_{52}O_6NI$ C 54.62; H 8.22; N 2.19; I^- 19.43. Found: C 54.73; H 8.45; N 2.22; I^- 19.38.% ν_{max}^{KBr} 3450 (OH), 1735, 1650 (C=O), 1480 (C—O -methyl) cm^{-1}.

Hofmann decomposition of **XXIV**

The Hofmann decomposition was carried out as above and led to isolation of an unsaturated-seco-dicarboxylic acid (**XXV**). M.p.: 106—108 °C; $[\alpha]_D = +57 \pm 2°$ (c=0.07; methanol); M.w.: 422.57. Calcd.: $C_{24}H_{38}O_6$ C 68.22; H 9.06. Found: C 68.32; H 9.42%. ν_{max}^{KBr} 3450. (OH), 1710) C=O), 1640 (CH_2=CH) cm^{-1}.

7,8-Seco-3α-hydroxy-12-ketochol-9(11)-ene-dicarboxylic acid (**XXVI**)

Prepared from **XXV** by Oppenauer oxidation as previously. M.p.: 142—144 °C; $[\alpha]_D = +92 \pm 2°$ (c=0.25; $CHCl_3$); M.w.: 420.55. Calcd.: $C_{24}H_{36}O_6$ C 68.55; H 8.62. Found: C 68.64; H 8.60%. ν_{max}^{KBr} 3420 (OH), 1710, 1680 (C=CH−C=O) cm^{-1}.

12,12a-Seco-13-amino-3α,7α-dihydroxycholane-dicarboxylic acid[12,24] (**XXVIII**)

Prepared by hydrolysis of **XXVII** with methanolic KOH. The substance gave a positive iodine-azide test, and the two carboxylic acid groups were detected by microtitration. M.p.: 260—263 °C; $[\alpha]_D = -39 \pm 2°$ (c=1.0; $CHCl_3$); (for M.w., *etc.*, see **XXIII**). Found: C 65.68; H 9.43; N 3.45%. ν_{max}^{KBr} 3400, 3300 (OH, HN_2), 1690, 1600 (C=O) cm^{-1}.

12,12a-seco-13-amino-3α,7α-dihydroxy-dimethylcholanate

Prepared from **XXVIII** with diazomethane in ether, and used in the following step.

12,12a-Seco-3α,7α-dihydroxy-dimethylcholanate-13-trimethylammonium iodide (**XXIX**)

Prepared as previously. M.p.: 145—150 °C; $[\alpha]_D = +12 \pm 2°$ (c=0.7; $CHCl_3$); (for M.w. and other calcd. data, see **XXIV**). Found: C 54.66; H 8.26; N 2.35; I^- 20.20%. ν_{max}^{KBr} 3450 (OH), 1730, 1640 (C=O), 1470 (C—O-methyl) cm^{-1}.

Hofmann decomposition of **XXIX**

The Hofmann decomposition was carried out as earlier, and resulted in **XXX**. M.p.: 168—170 °C; $[\alpha]_D = +71 \pm 2°$ (c=0.07; methanol); M.w.: 422.57. Calcd.: $C_{24}H_{38}O_6$ C 68.22; H 9.06. Found: C 68.34; H 9.42%. ν_{max}^{KBr} 3450, 3350 (OH), 1710 (C=O), 1620, 1520 (CH_2=CH), 770 (CH_2=CH) cm^{-1}.

References

[1] *Schenck, M.:* Z. angew. Chem. **42**, 61 (1929).
[2] *Singh, H., V. V., Parashar, S. Padmanabhan:* J. Sci. Industr. Res. **25**, 200 (1966).
[3] *Hara, S.: Chem. Pharm. Bull. Japan* **3**, 209 (1955).
[4] *Matkovics, B., Gy. Gõndõs,:* Kémiai Közlemények (Budapest) **31**, 287 (1969).
[5] *Matkovics, B., Zs. Tegyey,:* Lecture delivered at the Conference of the Hungarian Chemical Society, 21—23 August, 1969, Szeged.
[6] *Matkovics, B., Zs. Tegyey:* Microchem. J. **13**, 174 (1968).
[7] *Matkovics, B., Zs. Tegyey:* Magy. Kém. Foly. **73**, 431 (1967).
[8] *Matkovics, B.:* C. Sc. Thesis. Szeged, 1964.
[9] *Heusser, H., J. Wohlfahrt, M. Müller, R. Anliker:* Helv. Chim. Acta **38**, 1399 (1955).
[10] *Anliker, R., M. J. Müller, Wohlfahrt, H. Heusser:* Helv. Chim. Acta **38**, 1404 (1955).
[11] *Matkovics, B., Gy. Gõndõs, Zs. Tegyey:* Magy. Kém. Foly. **72**, 304 (1966).
[12] *Matkovics, B., Gy. Gõndõs, B. Taródi, Zs. Tegyey:* Magy. Kém. Foly. **75**, 236 (1969).
[13] *Matkovics, B., Zs. Tegyey, M. Resch, F. Sirokmán, E: Boga:* Acta Chim. Hung., (in press).
[14] *Matkovics, B., Zs. Tegyey:* Magy. Kém. Foly. **74**, 516 (1968).

[15] *Reichstein, T., M. Sorkin:* Helv. Chim. Acta **25**, 797 (1942).
[16] *Burckhardt, V., T. Reichstein:* Helv. Chim. Acta **25**, 821 (1942).
[17] *Hara, S.:* Pharm. Bull. Japan **3**, 297 (1955).
[18] *Matkovics, B., Zs. Tegyey, Gy. Göndös:* Steroids **5**, 117 (1965).
[19] *Hoehn, W. M., J. Linsk, R. B. Moffett:* J. Am. Chem. Soc. **68**, 1855 (1946).
[20] *Corey, E. J.:* J. Am. Chem. Soc. **76**, 175 (1954).
[21] *Sato, Y., N. Ikekawa:* J. Org. Chem. **24**, 1367 (1959).
[22] *Hofmann, A. P.:* Acta Chem. Scand. **17**, 173 (1963).

ПЕРЕГРУППИРОВКИ СТЕРОИДОВ, IX

Перегруппировки Шмидта и Бекмана кетонов и кетоксимов желчной кислоты

Б. Маткович, Дь. Балаж, Л. Балашпири

Различные метиловые эфиры 3-кето, 6-кето, 7-кето и 12-кето-желчной кислоты, защищенные О-ацетильной группой подвергались перегруппировке Шмидта и образовавшиеся гомолактамы были сравнены с образующимися из соответствующих кетоксимов Бекмановской перегруппировкой гомо-лактамами. Структуру полученных гомо-лактамов, кроме вышеуказанного сравнения, доказывали деструкцией Гофмана, проведенной со стороны образовавшегося амина, пиролизом и, в некоторых случаях, структурой соединений, которые могли быть выделены из последующей реакции окисления Опенауэра.

A kiadásért felelős: Dr. Tandori Károly
1975
A kézirat nyomdába érkezett: 1975 október. Megjelenés 1976 február
Példányszám: 550. Ábrák száma: 30 Terjedelem: 10,15 (A/5) ív
Készült monószedéssel, íves magasnyomással, az MNOSZ 5601—50 A szabványok szerint
75-4887 — Szegedi Nyomda

TOMI PRIORES

Acta Chemica, Mineralogica et Physica	Tom.	I,	Fasc.	1—2,	1028—29.
Acta Chemica, Mineralogica et Physica	Tom.	II,	Fasc.	1—2,	1932.
Acta Chemica, Mineralogica et Physica	Tom.	III,	Fasc.	1—3,	1934.
Acta Chemica, Mineralogica et Physica	Tom.	IV,	Fasc.	1—3,	1934.
Acta Chemica, Mineralogica et Physica	Tom.	V,	Fasc.	1—3,	1937.
Acta Chemica, Mineralogica et Physica	Tom.	VI,	Fasc.	1—3,	1938.
Acta Chemica, Mineralogica et Physica	Tom.	VII,	Fasc.	1—3,	1939.
Acta Chemica et Physica	Tom.	I,	Fasc.	1—2,	1942.
Acta Chemica et Physica	Tom.	II,	Fasc.	1—6,	1948—50.
Acta Physica et Chemica, Nova series	Tom.	I,	Fasc.	1—4,	1955.
Acta Physica et Chemica, Nova series	Tom.	II,	Fasc.	1—4,	1956.
Acta Physica et Chemica, Nova series	Tom.	III,	Fasc.	1—5,	1957.
Acta Physica et Chemica, Nova series	Tom.	IV,	Fasc.	1—2,	1958.
Acta Physica et Chemica, Nova series	Tom.	IV,	Fasc.	3—4,	1958.
Acta Physica et Chemica, Nova series	Tom.	V,	Fasc.	1—2,	1959.
Acta Physica et Chemica, Nova series	Tom.	V,	Fasc.	3—4,	1959.
Acta Physica et Chemica, Nova series	Tom.	VI,	Fasc.	1—4,	1960.
Acta Physica et Chemica, Nova series	Tom.	VII,	Fasc.	1—2,	1961.
Acta Physica et Chemica, Nova series	Tom.	VII,	Fasc.	3—4,	1961.
Acta Physica et Chemica, Nova series	Tom.	VIII,	Fasc.	1—2,	1962.
Acta Physica et Chemica, Nova series	Tom.	VIII,	Fasc.	3—4,	1962.
Acta Physica et Chemica, Nova series	Tom.	IX,	Fasc.	1—2,	1963.
Acta Physica et Chemica, Nova series	Tom.	IX,	Fasc.	3—4,	1963.
Acta Physica et Chemica, Nova series	Tom.	X,	Fasc.	1—2,	1964.
Acta Physica et Chemica, Nova series	Tom.	X,	Fasc.	3—4,	1964.
Acta Physica et Chemica, Nova series	Tom.	XI,	Fasc.	1—2,	1965.
Acta Physica et Chemica, Nova series	Tom.	XI,	Fasc.	3—4,	1965.
Acta Physica et Chemica, Nova series	Tom.	XII,	Fasc.	1—2,	1966.
Acta Physica et Chemica, Nova series	Tom.	XII,	Fasc.	3—4,	1966.
Acta Physica et Chemica, Nova series	Tom.	XIII,	Fasc.	1—2,	1967.
Acta Physica et Chemica, Nova series	Tom.	XIII,	Fasc.	3—4,	1967.
Acta Physica et Chemica, Nova series	Tom.	XIV,	Fasc.	1—2,	1968.
Acta Physica et Chemica, Nova series	Tom.	XIV,	Fasc.	3—4,	1968.
Acta Physica et Chemica, Nova series	Tom.	XV,	Fasc.	1—2,	1969.
Acta Physica et Chemica, Nova series	Tom.	XV,	Fasc.	3—4,	1969.
Acta Physica et Chemica, Nova series	Tom.	XVI,	Fasc.	1—2,	1970.
Acta Physica et Chemica, Nova series	Tom.	XVI,	Fasc.	3—4,	1970.
Acta Physica et Chemica, Nova series	Tom.	XVII,	Fasc.	1—2,	1971.
Acta Physica et Chemica, Nova series	Tom.	XVII,	Fasc.	3—4,	1971.
Acta Physica et Chemica, Nova series	Tom.	XVIII,	Fasc.	1—2,	1972.
Acta Physica et Chemica, Nova series	Tom.	XVIII,	Fasc.	3—4,	1972.
Acta Physica et Chemica, Nova series	Tom.	XIX,	Fasc.	1—2,	1973.
Acta Physica et Chemica, Nova series	Tom.	XIX,	Fasc.	3,	1973.
Acta Physica et Chemica, Nova series	Tom.	XIX,	Fasc.	4,	1973.
Acta Physica et Chemica, Nova series	Tom.	XX,	Fasc.	1—2,	1974.
Acta Physica et Chemica, Nova series	Tom.	XX,	Fasc.	3,	1974.
Acta Physica et Chemica, Nova series	Tom.	XX,	Fasc.	4,	1974.
Acta Physica et Chemica, Nova series	Tom.	XXI,	Fasc.	1—2.	1975.

INDEX